國立臺灣大學工學院化學工程學系

碩士論文

Department of Chemical Engineering

College of Engineering

National Taiwan University

Master Thesis

PBS 反應器之類神經網路模擬與模型預測控制器設計

The Simulation of a Polybutylene Succinate (PBS) Reactor with a Neural Network Model Based Predictive Controller

劉宇浩

Takorn Plengsangsri

指導教授：吳哲夫　博士

Advisor: Jeffrey D. Ward, Ph.D.

共同指導教授：Paisan Kittisupakorn 博士

Co-Advisor: Paisan Kittisupakorn, Ph.D.

中華民國 112 年 6 月

June, 2023

doi:10.6342/NTU202302309

國立臺灣大學碩士學位論文
口試委員會審定書

PBS 反應器之類神經網路模擬與模型預測控制器設計

The Simulation of a Polybutylene Succinate (PBS) Reactor with a Neural Network Model Based Predictive Controller

本論文係 Takorn Plengsangsri 君（學號 R10524141）在國立臺灣大學化學工程學系完成之碩士學位論文，於民國 112 年 6 月 30 日承下列考試委員審查通過及口試及格，特此證明

口試委員：

Jeffrey Ward （簽名）

（指導教授）

Parisom Kittisupakorn

李

郭文生

系主任、所長 廖英志（簽名）

（是否須簽章依各院系所規定）

ACKNOWLEDGEMENTS

I am grateful for the collaboration between Chulalongkorn University (CU) and National Taiwan University (NTU) in completing this thesis. Special thanks to Professor Dr. Paisan Kittisupakorn (CU advisor), and Professor Dr. Jeffrey D. Ward (NTU advisor) for their guidance, expertise, and continuous support throughout this research journey and for expanding my knowledge in the field. I also appreciate the valuable suggestions and concepts provided by the thesis examination committee and the faculty members of CU and NTU involved. I sincerely hope that this research will contribute to the advancement of control techniques. It is my aspiration that the findings and insights presented in this thesis will be beneficial in the development of advanced control strategies and make a meaningful impact on the field.

I would like to take this opportunity to express my gratitude to Mr. Kris Prasopsanti, who supported and taught me to write MPC in Python, as well as providing deep knowledge about neural networks. I would also like to thank Psalm and Hope for the advice, and all those who contributed to the completion of this thesis. Lastly, I am deeply thankful to my friends and family for their unwavering support and for letting the Master's degree period in Thailand and Taiwan become an incredibly joyful moment that will remain in my memory forever.

doi:10.6342/NTU202302309

中文摘要

聚丁二酸丁二醇酯 (PBS) 是一種可生物降解的塑料，以其在各種應用中的強度和多功能性而聞名。 本研究提出了一種數據驅動的方法來模擬聚合過程中半間歇反應器中的溫度控制，並將所提出方法的性能與傳統控制器（包括 PID 控制和第一原理模型 MPC 控制）進行了比較。 該研究使用 Python 和 Tensorflow 開發了基於神經網絡模型的預測控制 (NNMPC) 和基於多重神經網絡模型的預測控制 (Multi-NNMPC)。 通過使用隱藏層中具有不同數量的神經元的廣泛動態數據來訓練神經網絡模型，以研究不同模型複雜性下的過程動態。 在標稱條件下，50 神經元 NNMPC 表現出測試結構中最有效的複雜性，絕對誤差積分 (IAE) 值為 2,104.77，20 神經元多 NNMPC 的性能略有改善，IAE 降低至 2,030.52，且控制動作呈重複趨勢。 MPC 控制。 這些方法解決了 PID 控制失敗的問題，該失敗導致超調和低效的設定點跟踪。 PID 控制導致聚合物超規格，分子量幾乎達到 14,000，IAE 值為 3,271.83。 相比之下，50 神經元 NNMPC 的最佳溫度控制方法可以執行嚴格的溫度控制並產生所需的聚合物性能，顯著優於 PID 控制。 這項研究還考慮了不確定條件，包括白噪聲的干擾和模型失配，所有控制方法都成功地處理了噪聲並保持溫度等溫，50 神經元 NNMPC 表現出比 PID 控制更小的閥門運動，增強了控製作用並提高了魯棒性 並減少公用事業消耗。 當引入模型失配來表示反應器結垢時，總傳熱係數降低了 30%，與其他控制器相比，50 個神經元 NNMPC 實現了控制變量更快地收斂到設定值。 它產生的 IAE 為 2,892.41，而 MPC 顯示的 IAE 為 3,009.59。 此外，神經網絡模型展示了高效學習高度非線性動力學的能力，與使用順序最小二乘規劃 (SLSQP) 方法的數學模型相比，預測最

doi:10.6342/NTU202302309

佳操縱變量的速度最高可達 5 至 20 倍。

關鍵字：模型預測控制、 分程 PID 控制、 機器學習、人工神經網絡、 聚丁二酸丁二醇酯

doi:10.6342/NTU202302309

ABSTRACT

Polybutylene succinate (PBS) is a biodegradable plastic known for its strength and versatility in various applications. This research presents a data-driven approach to simulate temperature control in a semi-batch reactor during polymerization, the performance of the proposed approaches was compared against conventional controllers, including PID control and first-principles model MPC control. The study developed neural network model-based predictive control (NNMPC) and multiple neural network model-based predictive control (Multi-NNMPC), using Python and Tensorflow. Neural network models were trained by using a wide range of dynamic data with varying numbers of neurons in hidden layers to investigate the process dynamics under different model complexities. Under nominal conditions, 50 neuron NNMPC demonstrated the most efficient complexity among the tested structures, exhibiting an Integral of Absolute Error (IAE) value of 2,104.77, 20 neuron Multi-NNMPC provided slightly improved performance as IAE reduced to 2,030.52 and the control action trended duplicating MPC control. These approaches addressed the failure of PID control, which caused overshoot and inefficient setpoint tracking. The PID control resulted in polymer over-specification, with the molecular weight reaching almost 14,000 and an IAE value of 3,271.83. In contrast, the optimal temperature control approach of the 50 neuron NNMPC could perform tight temperature control and yield the desired properties of the polymer, significantly outperforming PID control. This research also considers uncertain conditions, including the interference of white noise and model mismatch, all control approaches successfully handled the noise and maintained temperature isothermally, the 50 neuron NNMPC exhibited less aggressive valve movement than PID control,

doi:10.6342/NTU202302309

enhancing control action and leading to increased robustness and reduced utility consumption. When model mismatch was introduced to represent reactor fouling, reducing the overall heat transfer coefficient by 30%, the 50 neuron NNMPC achieved faster convergence of control variable to setpoints compared to other controllers. It yielded an IAE of 2,892.41, while MPC showed an IAE of 3,009.59. Moreover, the neural network model demonstrated the ability to learn highly nonlinear dynamics efficiently, enabling the prediction of optimal manipulated variables up to 5 to 20 times faster than a mathematical model using the Sequential Least Squares Programming (SLSQP) method.

Keywords：Model Predictive Control; Split Range PID control; Machine Learning; Artificial Neural Networks; Polybutylene Succinate

doi:10.6342/NTU202302309

CONTENTS

doi:10.6342/NTU202302309

doi:10.6342/NTU202302309

doi:10.6342/NTU202302309

LIST OF FIGURES

doi:10.6342/NTU202302309

doi:10.6342/NTU202302309

doi:10.6342/NTU202302309

doi:10.6342/NTU202302309

doi:10.6342/NTU202302309

doi:10.6342/NTU202302309

doi:10.6342/NTU202302309

doi:10.6342/NTU202302309

doi:10.6342/NTU202302309

doi:10.6342/NTU202302309

doi:10.6342/NTU202302309

doi:10.6342/NTU202302309

doi:10.6342/NTU202302309

doi:10.6342/NTU202302309

LIST OF TABLES

doi:10.6342/NTU202302309

doi:10.6342/NTU202302309

Chapter 1 Introduction

1.1 Overview

In the past decade, there has been an enormous amount of plastic usage globally and the trend of usage also continues to grow rapidly because of its remarkable properties. However, conventional plastics from fossil fuels cannot be degraded or decomposed in the soil or marine environment leading to plastic pollution which is an inevitable environmental issue that impacts every country around the world [1].

Polybutylene succinate (PBS) is a biodegradable plastic that has received attention due to its sufficient strength and versatility in a variety of applications. It is 100% biodegradable in the natural environment [2]. The synthesis of polybutylene succinate requires esterification reaction which proceeds in a jacketed semi-batch reactor where oligomers are generated as a function of time and the polycondensation reaction takes place in a jacketed semi-batch reactor with vacuum environment that creates a longer chain of the polymer[3, 4]. Both of the reactions have a similar crucial factor in the control which is temperature leads to obtaining the polymer with desired average molecular weight and intrinsic viscosity that impacts the quality of the product [4].

The rise of data-driven technologies has been a significant development in industry recently and has poised for the upcoming transition to industry 5.0 [5]. The advancement of technology coupled with the availability of data has enabled data-driven solutions to be integrated into various applications in industries including chemical process control, the aspect is implementing data analytic technique of machine learning to the work field that could assist the operators to optimize the performance of chemical processes [6] and this method leverages the power of data in the control systems to achieve highly efficient control to improve final product quality and reduce energy usage [7, 8].

doi:10.6342/NTU202302309

This research emphasizes on neural network model-based predictive control strategy (NNMPC) implemented in the polybutylene succinate polymerization process, to regulate the temperature within the reactor through precise manipulation of heating and cooling oil flow rates. The temperature of both reactor and jacket, molecular specie profiles of polymer as a function of time are simulated. The polymerization in batch process has high complexity of multivariable process and non-linearity [9], it is challenging to practically develop a high-accuracy mathematical model for the chemical process operation. Furthermore, when the process encounters a large deviation from the model after a long time of operation [10], adjusting the model's accuracy becomes challenging since some of the critical parameters are difficult to measure. Neural network model can be a powerful approach to be utilized in approximating nonlinear functions of complex system by using training data [11]. However, the quality and quantity of training data are crucial factors that determine the neural network model's predictive efficiency [12].

One distinct advantage of using a neural network model in process control is the speed of optimization performed at each time step. Compared to solving a complex mathematical optimization problem of the conventional model-based predictive control [13], the optimization process in neural network models is much faster [14]. Therefore, deploying a neural network model in process control can lead to more efficient control actions in non-linear and fast dynamic processes.

Replacing the mathematics model with the neural network model has more advantages because the operator can adjust the model easily after the actual process deviates from the model by recollecting the data from the sensors of the process and retraining the neural network model by using a machine learning library such as Tensor flow which is an open source and it is a user-friendly library in order to generate the new neural network model that could describe the process more efficiently than the previous

doi:10.6342/NTU202302309

one thus it is evident that the model could be fixed easily and economically than the mathematic model that is very complex as its nature so it takes a long period of time to modify the deviated model to become efficient again.

The research shows the simulation results under NNMPC, MPC, and split range PID control for both esterification and polycondensation reactions that proceed in the reactors are analyzed and discussed the control performance by comparing IAE criteria and simulation time.

1.2 Literature Review

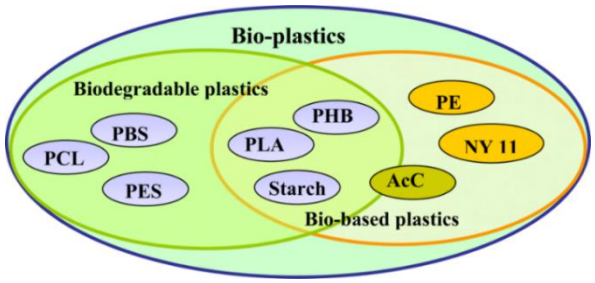

Figure 1-1 Type of Bio-plastics [15]

The various kind of bio-plastics have been developed under the development of chemistry knowledge that aims to completely substitute the usage of fossil fuel-based plastics and become an alternative way to reduce the accumulated amount of plastics that are waiting to be eliminated in landfills. Bio-plastics can be divided into 2 kinds: biodegradable and non-biodegradable plastics as shown in Figure 1-1. For instance, polyethylene (PE) and Nylon 11 (NY 11) are non-biodegradable plastics but it produced from biomass resources. On the other hand, biodegradable plastics can be provided by biomass or even using petroleum feedstock but their molecular structure is suitable to be degraded naturally including Polyhydroxybutyrate (PHB), Polylactic Acid (PLA), and strach which are bio-based plastic and can be degraded. Polyethersulfone (PES), Polycaprolactone (PCL), and Polybutylene succinate (PBS) are biodegradable plastic

doi:10.6342/NTU202302309

even though these are fossil fuels-based polymers [15].

Those biodegradable plastics have to be chosen to apply in appropriate applications because the degree of decomposable affects their properties [16] therefore they could have low strength as Polycaprolactone (PCL) cannot withstand moderate to high external force and vice-versa Polyhydroxybutyrate (PHB) can be degraded in only suitable environment but it is not decomposed in landfill or ocean. Polybutylene succinate (PBS) and Polylactic Acid (PLA), both are commercially produced and they have a high effort in research and development due to their sufficient strength and both are 100% degradable in the natural environment. The synthesis of polybutylene succinate occurs when succinic acid and butylene glycol or (1,4-butanediol) are reacted, the acid can be provided by sugar fermentation while butylene glycol could be obtained from biomass carbohydrates that passed through an enzymatic reaction leads to 100% biopath to obtain the PBS however butylene glycol manufacturing can be done by using fossil fuel feedstock which is 50% biopath [1].

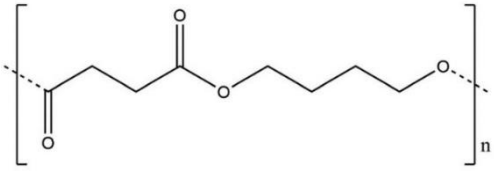

Figure 1-2 The molecular structure of polybutylene succinate (PBS) [17]

Polybutylene succinate (PBS) polymer chain consists of polymerized units of butylene succinate ($C_8H_{12}O_4$)) as illustrated in Figure 1-2. It has gained attention during the past two decades because of its degradable ability in nature to substitute conventional plastic usage with the intention to reduce accumulated plastic waste. PBS has outstanding properties of the transparent surface and rigid structure to withstand external force allowing it to be compatible with wide applications including packaging, composable bags, agricultural mulching films, textiles, and catering goods [2]. The performance

doi:10.6342/NTU202302309

limitation of PBS is the low melting temperature (114°C) compared to PLA with Tm over 160°C that restricted in food application however the reinforced nanofiller could enhance the properties [17]. In the PBS grade of FZ91PM from PTT public company limited (Thailand) has a melt flow index (MFI) at 190°C of 5g/ 10 min with a density of 1.26 g/cm3 and glass transition temperature (Tg) and melting temperature (Tm) at 78°C and 115°C, respectively. In the mechanical property view, the tensile strength is 20 MPa and the tensile modulus is 450 MPa [2].

The molecular weight plays a crucial role in shaping the crystal morphology and influencing the mechanical properties of polybutylene succinate (PBS). As illustrated in Figure 1-3, it becomes evident that an increase in the polymer's molecular weight yields a greater abundance of spherulites, while simultaneously leading to smaller sizes due to heightened nucleation density. PBS with higher molecular weight exhibits a remarkably denser branching texture, resulting in a more intricate morphology with internal birefringence patterns [18].

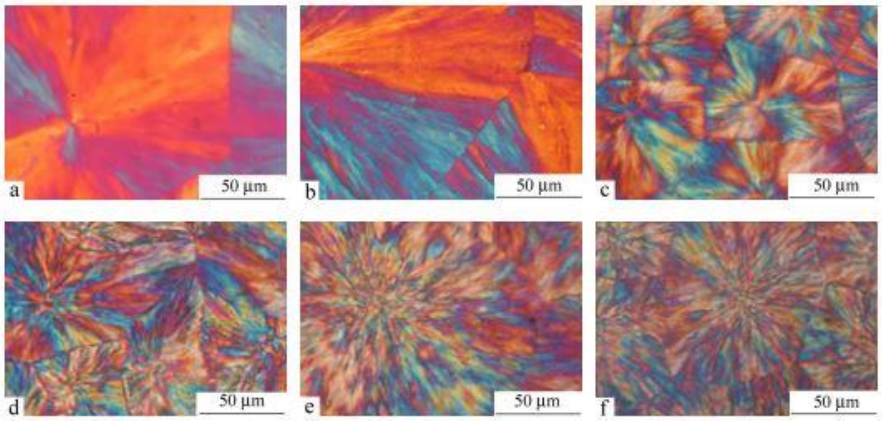

Figure 1-3 The morphology of PBS crystallized for different molecular weight: (a) 2.1 $\times 10^4$, (b) 2.9$\times$ 10^4, (c) 3.3$\times 10^4$, (d) 4.1$\times 10^4$, (e) 5.0$\times 10^4$ and (f) 6.3$\times 10^4$ [18]

Upon reaching a molecular weight of 40,000, it is observed that the modulus, yield strength, and elongation at break of PBS exhibit a diminishing trend as the molecular weight continues to increase. Thus, it becomes evident that the highest degree of

doi:10.6342/NTU202302309

crystallinity and the highest molecular weight does not singularly determine the optimal mechanical properties. Instead, the key lies in balancing between these factors. However, for industrial applications, molecular weights ranging from approximately 20,000 to 70,000 prove to be sufficiently high [18].

To attain a high molecular weight PBS through the condensation polymerization process is costly because it requires a long operating time in a high vacuum reactor [19]. However, one of the alternative methods is chain extension. Within this approach, an additional step is implemented during the melt condensation process, as depicted in Figure 1-4, utilizing a chain extender such as hexamethylene diisocyanate (HMDI), isocyanate, oxazoline, silazane, epoxy compound or anhydride to merge polymer chains that significantly contribute augment molecular weight of PBS [20]. A study has revealed the effectiveness of employing the HMDI chain extender, enabling PBS to reach molecular weight up to 200,000 g/mol [21].

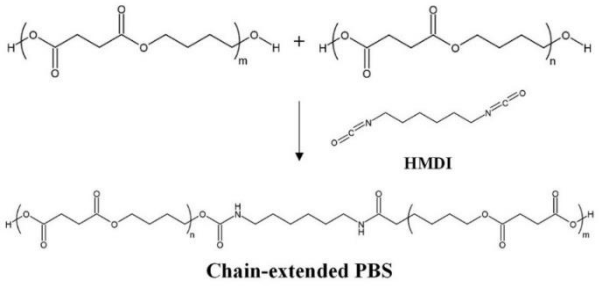

Figure 1-4 The molecular structure of polybutylene succinate (PBS) [17]

In the section on process control, there are many control techniques are adopted in chemical plants. The proportional-integral-derivative (PID) control is general and well-known technique because it is simple and provides good robustness and could gain sufficient control performance [22]. PID requires tuning for desired control action, Ziegler-Nichole tuning relation is widely used however the minimizing integral of time-weighted absolute error (ITAE) could be used as a tuning criterion to calculate the tuning

doi:10.6342/NTU202302309

parameters that provide better dynamic responses in temperature and concentration control of non-isothermal CSTR [22]. MPC is an advanced controller with online optimization that can control multi input multi output system (MIMO), and handle constraints with better response in minimizing the overshoot of the process in a continuous stirred tank reactor (CSTR) that is a nonlinear system MPC could drive process variable to the set point effectively under disturbance with small fluctuation of the controller output which is better than PID with automatic tuning [23].

The artificial neural network is one of the methods in artificial intelligence (AI) applications and it is a mathematically based model using the same concept as human brain work to process the data through several layers of neurons. Recently, the neural network plays a big role in various fields such as economics, financial forecast, medical diagnosis, etc. in order to assist humans with ease and efficient decision-making. The neural network model can perform certain tasks including character pattern recognition, time series prediction, clustering, and control.

Pattern recognition is usually found in the application of image processing and voice analysis. Converting handwriting to text on a smartphone (character recognition) is a notable example that implemented the neural network as the fundamental working principle. A thousand of human handwriting data are collected for model training to learn the pattern and similarity of a pixel arrangement of each handwritten alphabet and number leading to efficiently recognizing the alphabet [24].

Time series prediction is efficiently performed in this field including stock price forecasting, and product market price forecasting. The stock markets have very high volatility and the stock price changes every second, the historical stock prices are inputted into the neural network for building the model as beneficial to investors to forecast the change in the stock price [25].

doi:10.6342/NTU202302309

Control is the main point focused in this research, the neural network learns the chemical process dynamic data in order to directly command the final control element (control valve) to reach the desired point, this method is called direct control [26] while the neural network model-based control is used the model along with the calculation of manipulated variable. Not only chemical process control but also automotive and robotic control uses the neural network model as the fundamental of the control [27].

The feedforward neural network (FFNN) and recurrent neural network (RNN) have weights, and biases on each neuron consisting in the structure as shown in Figure 1-5. RNN is a recursive neural network structure, in which inputs are influenced by the previous output that is connected back to the initial nodes with a tapped delay line (TDL). While the output of FFNN is only influenced by the inputs as a signal flowing in forward direction [28].

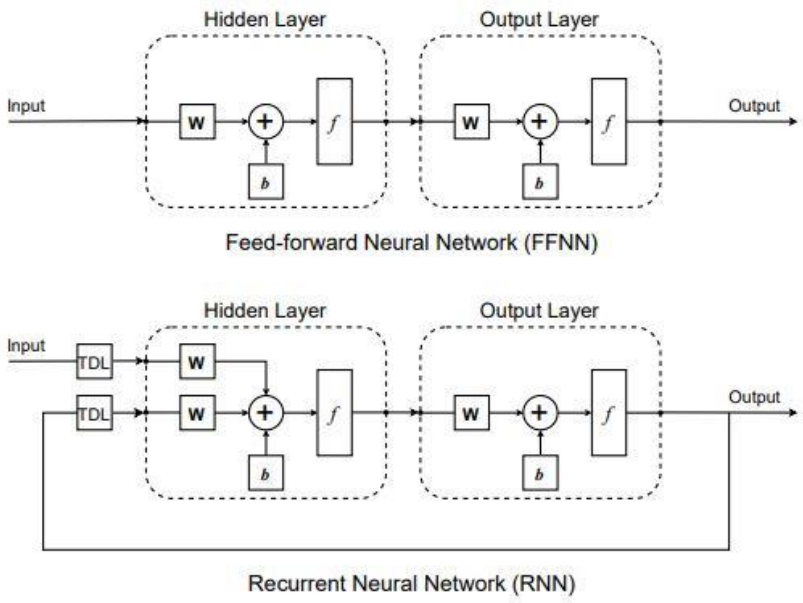

Figure 1-5 Feed forward and recurrent neural network structures[28]

The model predictive controller provides an optimal manipulated variable by doing optimization using the prediction model. To predict the future state of a system for all time step in the operation through a model that describing the system can be achieved by

doi:10.6342/NTU202302309

having all initial states of a minimum set of variables xi(t) where i ranges from 1 to n, and the system inputs for all t ≥ t0 [29]. Therefore, the FFNN is more appropriate to be utilized in model predictive controller because the output is based on only current state and it is not influenced by the previous state. The multilayered feed-forward neural network model used in model predictive control, the data is flow through the NN model as a sequence in the prediction horizon as shown in Figure 1-6.

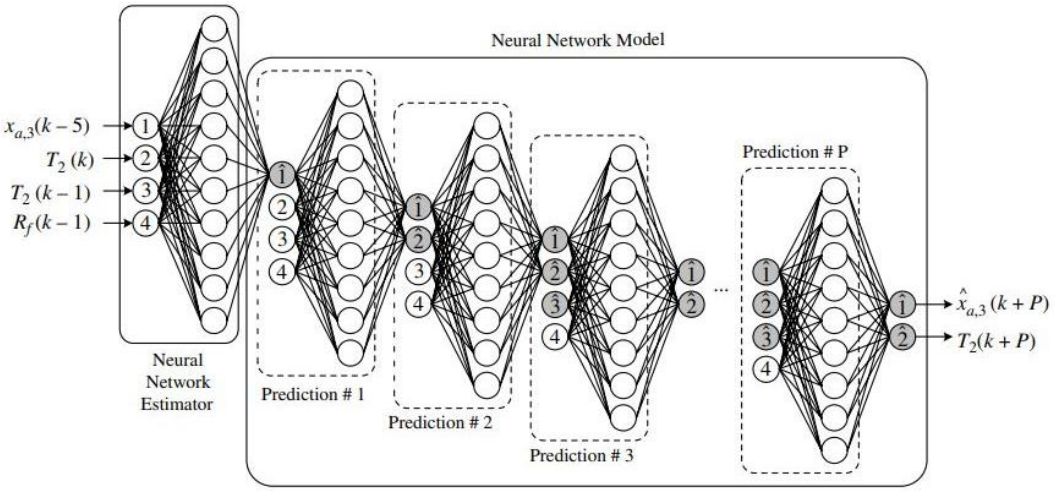

Figure 1-6 Feedforward neural network in NNMPC with neural network estimator[30]

Model-based control methods require a process model of a system to determine the control action, all states and model parameters are required. However, in most processes, there are numerous states and parameters that cannot be precisely measured such as heat and composition. Therefore, online estimation techniques are utilized to approximate the unknown states and parameters. Arpornwichanop et al [31] performed the temperature control in batch reactor by using extended Kalman filter incorporated with model predictive control (MPC), an extended Kalman filter is a state estimation technique that was utilized to estimate the heat released from the reactions. It is obvious that the application of extended Kalman filter provided outstanding state estimation resulting MPC showed high robustness and good control performance.

doi:10.6342/NTU202302309

The state estimation by using extended Kalman filter, the plant model has to be simplified for deploying the model in MPC [31]. The exact plant model contains numerous parameters and states, and some of them are unmeasurable. If the exact model was used, the Kalman filter would have to estimate many variables at once, resulting in lower performance. By simplifying the model and reducing the number of variables, the Kalman filter can more accurately estimate the remaining variables, leading to better performance.

The NNMPC was carried out in the biochemical engineering field to perform the yeast fermentation temperature control by manipulating the coolant flow rate, the controller can manipulate the coolant flow rate to control the temperature inside the reactor to the desired varying setpoint under external disturbances [32]. The weighting factor in the objective function of MPC influences the dynamic response, the low weight shows aggressive control action corresponding to the oscillatory control variable (Temperature) but reaches setpoint in a short time while high weighting factor shows conservative control action with smooth output [32]. The advantage of NNMPC is simplicity of tuning based on the model training on Tensorflow (a machine learning library on Python) to be covered the process operating condition to obtain the model and it supports the high dimensional models [32].

Designing an efficient MPC controller needs to specify appropriate prediction and control horizons, there are no exact criteria for the determining optimal number of horizons. In polystyrene synthesis operation in a batch reactor using MPC control to manipulate a 500 W heater, thereby ensuring precise tracking of the optimal temperature profile as a result of horizon length. Through trial and error method, it was found that the efficient temperature could be achieved by a prediction horizon of 27 sample intervals. However, employing shorter intervals led to unstable responses. While the control

doi:10.6342/NTU202302309

horizon was varied between 2, 4, and 8 revealed no significant differences in temperature tracking performance. Therefore, 2 or 4 sample intervals of control horizon is sufficient to provide good performance [33].

Kittisupakorn et al [34] reported the neural network-based model predictive control implemented in the steel pickling process in order to control the concentration of highly concentrated acid substances employed in the process baths along with 5%, 10%, and 15% of HCl concentration bath. The model could simulate and predict the process's state variables of the nonlinear and multivariable interaction chemical process under disturbance, model mismatch, and process noise. The control performance of acid baths using NNMPC and PI control were compared under disturbance case using IAE criteria, for 5% HCl bath with NNMPC had a smaller IAE error value of 0.223 while PI control yielded the IAE 0.355. The control under the model mismatch case of 5% HCl using NNMPC showed 0.218 IAE error and PI control accounted for 0.356 which is higher for around 50 %. It is evidence that NNMPC can provide an excellent control performance beyond the PI controller without oscillation in all cases.

1.3 Objectives

The objective of this study is to simulate the dynamic of PBS esterification and polycondensation process and develop advanced control strategies for reactor temperature control. Specifically, the study aims to develop both the NNMPC and Multi-NNMPC strategies and compare their control performance. The controlled variable, which is the reactor temperature, must reach the setpoint rapidly and without overshoot or offset to achieve high control performance. The proposed control techniques are also expected to maintain temperature control effectively, even under the interference of white noise and model mismatch.

doi:10.6342/NTU202302309

1.4 Scope of the research

The scope of this research is to study the synthesis of polybutylene succinate (PBS) using a simulation approach that focuses on the esterification and polycondensation processes. Python programming is utilized for the simulation. The esterification reaction is carried out in a 1 m^3 semi-batch reactor equipped with a 0.2 m^3 recirculating jacket and oil is used as the heating and cooling fluid. The process is conducted at different temperature ranges: 25 to 135^{o}C from 0 to 50 minutes, 225^{o}C from 50 to 400 minutes, and 150^{o}C from 400 to 450 minutes. The polycondensation reaction is performed in a 1 m^3 vacuumed semi-batch reactor with a 0.2 m3 recirculating jacket, starting at 150^{o}C and maintained at 245^{o}C for 200 minutes, followed by cooling to 100 ^{o}C. Various control strategies, including split range PID, MPC, NNMPC, and Multi-NNMPC, are implemented to regulate the temperature inside the reactor by adjusting the oil flow rate. The proposed control techniques are tested for robustness against uncertainty events, such as white noise case and model mismatch case. The control performance of each process is compared based on IAE in different scenarios. This research is expected to contribute to the advancement of the PBS synthesis process.

1.5 Benefit of this research

The research offers significant benefits to the production of polybutylene succinate (PBS). One major benefit is the developed neural network model, which can replace the mathematical model in the MPC optimizer. This reflects the strength of data-driven technology, enabling a more efficient and higher robustness of the proposed control strategy. The NNMPC and Multi-NNMPC control strategy also delivers superior control performance and energy usage efficiency, outperforming both conventional MPC and split range PID control strategies. Additionally, the neural network model approaches

doi:10.6342/NTU202302309

offer a fast optimization procedure that overcomes the disadvantage of mathematical-based MPC, which typically takes longer to optimize the oil flow rate. These benefits have significant implications for the industry, as they offer a superior temperature control approach for PBS production that is more efficient, cost-effective, and reliable.

doi:10.6342/NTU202302309

Chapter 2 Methods

2.1 The synthesis of polybutylene succinate

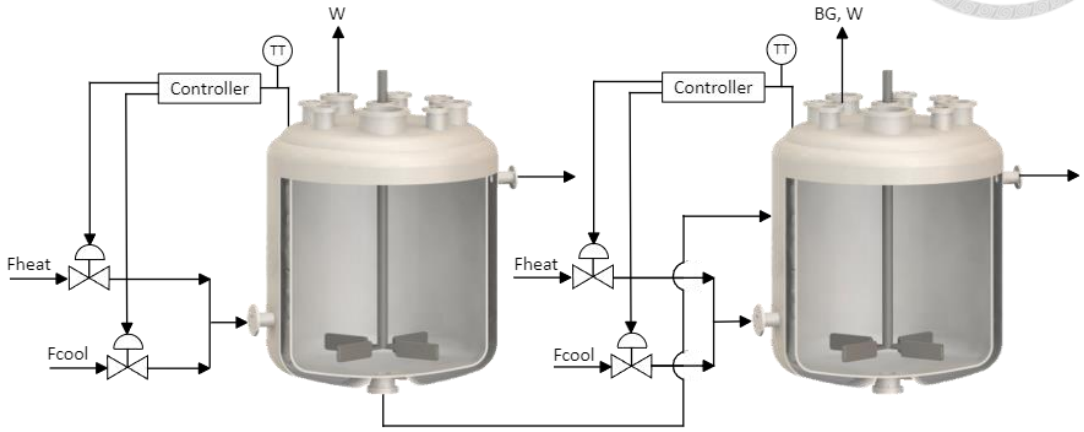

Figure 2-1 The relationship of the five elements in RL

The synthesis of polybutylene succinate (PBS) is carried out through a two-stage melt polycondensation process in which two semi-batch reactors are employed in a series configuration with distinct operating conditions as shown in Figure 2-1. The primary reactor, designed for esterification of 5500 mol of succinic acid and butylene glycol in a molar ratio of 1.1, operates in three steps at atmospheric pressure. Each step has an important role in ensuring the final product quality. In the preheating phase the reactor contents are gradually heated from 25°C to 135°C over 50 minutes, followed by isothermal reaction step which proceeds until almost no additional water is liberated [35]. This step requires 350 minutes. The reaction is then finalized during a cooling step in which the temperature is reduced to 150°C [35]. The water produced from the reactions is assumed to be removed instantaneously that directly affecting the concentration of the mixture due to the significantly reduced volume.

In the second reactor, a polycondensation proceeds in a vacuum environment. Butylene glycol is liberated in polycondensation reaction and is removed in vapor phase.

doi:10.6342/NTU202302309

The temperature is controlled for 200 minutes after reaching a setpoint in the range of 245°C [35], to simulate the effect of the temperature on the dynamic change of number average molecular weight of PBS.

Reactor temperature control is assumed to be achieved using a jacket with two feeds (hot and cold oil). Either a split-range PID controller or a multivariable MPC controller are used to manipulate the final control elements (the heating and cooling oil control valves). Heating oil is assumed to be available with a maximum opening of 10 L/s and constant inlet temperature of 250°C for the esterification batch and 280°C for the polycondensation batch. It is circulated in the jacket to heat the reactor contents to the setpoint and compensate for heat loss due to removal of substances through evaporation. The efficient control of fluid flow rate enables precise temperature control and stability during chemical reactions, particularly those involving exothermic reactions. Cooling oil at 25°C is used for cooling with a maximum flow rate of 10 L/s.

2.1.1 Esterification

Esterification reaction is the reaction between an organic acid (RCOOH) and alcohol (ROH) to form an ester (RCOOR) and water. In the synthesis of polybutylene succinate (PBS), the esterification occurs in the first step that generates various types of oligomers that collide to the formed molecules to react and proceed the esterification reaction again and other oligomers are formed as shown the reaction r1 to r4. Bikiaris et al [3] reported the reaction schemes and mathematical reaction models of the esterification reaction of the three of poly (alkylene succinate) including polyethylene succinate (PES), polypropylene succinate (PPS), and polybutylene succinate (PBS) for determining the best process conditions to maximize esterification reaction rate and conversion. Succinic acid was reacted with a variety of glycols (ethylene, propylene, and butylene glycol) to

doi:10.6342/NTU202302309

obtain the corresponding poly (alkylene succinate) using Tetrabutoxy-titanium (TBT) as the catalyst. After the reaction proceeds, succinic acid and glycol will react to form oligomers (tSA, tG, bSA, bG, and bDG) and water [3]. Those oligomers influence the subsequent polymerization. All the species involved in the esterification reactions are indicated in Table 2-1.

The kinetic of esterification process is derived by rate law and mass balance equations are shown in eq. 2-7 to 2-21. These equations are related to volume that described by the remaining substance volume subtract evaporated volume of water at each time step as shown in eq. 2-22.

Table 2-1 The molecular structure of monomer, oligomers and product in esterification reactions of polybutylene succinate (PBS)

Material	Symbol and description	Molecular structure
Monomers	SA Succinic acid	HOOC- CH_2CH_2 -COOH
	BG Butylene glycol	HO- $CH_2CH_2CH_2CH_2$ -OH
Oligomer	tSA SA end group	HOOC- CH_2CH_2 –CO-
	tBG Butylene glycol end group	HO- $CH_2CH_2CH_2CH_2$ -O-
	bSA SA repeating unit	-OC- CH_2CH_2 -CO-
	bBG Butylene glycol repeating unit	-O- $CH_2CH_2CH_2CH_2$ -O-
	bDBG Dibutylene glycol repeating unit	- O- $CH_2CH_2CH_2CH_2$ -O- $CH_2CH_2CH_2CH_2$ -O-
Product	W Water	H_2O

doi:10.6342/NTU202302309

Reaction Schemes:

r_1 $$SA + BG \underset{k_1'}{\overset{k_1}{\rightleftharpoons}} tSA + tBG + W \quad (2\text{-}1)$$

r_2 $$tSA + BG \underset{k_2'}{\overset{k_2}{\rightleftharpoons}} bSA + tBG + W \quad (2\text{-}2)$$

r_3 $$SA + tBG \underset{k_3'}{\overset{k_3}{\rightleftharpoons}} tSA + bBG + W \quad (2\text{-}3)$$

r_4 $$tSA + tBG \underset{k_4'}{\overset{k_4}{\rightleftharpoons}} bSA + bBG + W \quad (2\text{-}4)$$

r_5 $$tBG + tBG \underset{k_5'}{\overset{k_5}{\rightleftharpoons}} bBG + BG \quad (2\text{-}5)$$

r_6 $$tBG + tBG \overset{k_6}{\rightarrow} bDBG + W \quad (2\text{-}6)$$

Rate law equations:

$$r_1 = \left\{4k_1(SA)(BG) - \left(\frac{k_1}{K_1}\right)(tSA)(W)\right\}/V^2 \quad (2\text{-}7)$$

$$r_2 = \left\{2k_2(tSA)(BG) - 2\left(\frac{k_2}{K_2}\right)(bSA)(W)\right\}/V^2 \quad (2\text{-}8)$$

$$r_3 = \left\{2k_3(SA)(tBG) - \left(\frac{k_3}{K_3}\right)(tSA)(W)\right\}/V^2 \quad (2\text{-}9)$$

$$r_4 = \left\{k_4(tSA)(tBG) - 2\left(\frac{k_4}{K_4}\right)(bSA)(W)\right\}/V^2 \quad (2\text{-}10)$$

$$r_5 = \left\{k_5(tBG)(tBG) - 4\left(\frac{k_5}{K_5}\right)(bBG)(BG)\right\}/V^2 \quad (2\text{-}11)$$

$$r_6 = \{k_6(tBG)(tBG)\}/V^2 \quad (2\text{-}12)$$

$$k_i = A_i e^{-\frac{Ea}{RT_R}} \quad (2\text{-}13)$$

Mass balance equations:

$$\frac{1}{V}\frac{d(SA)}{dt} = -r_1 - r_3 \quad (2\text{-}14)$$

$$\frac{1}{V}\frac{d(BG)}{dt} = -r_1 - r_2 + r_5 \quad (2\text{-}15)$$

$$\frac{d(W)}{dt} = V(r_1 + r_2 + r_3 + r_4 + r_6) - F_W = 0 \quad (2\text{-}16)$$

$$\frac{1}{V}\frac{d(tSA)}{dt} = r_1 - r_2 + r_3 - r_4 \quad (2\text{-}17)$$

doi:10.6342/NTU202302309

$$\frac{1}{V}\frac{d(tBG)}{dt} = r_1 + r_2 - r_3 - r_4 - 2r_5 - 2r_6 \quad (2\text{-}18)$$

$$\frac{1}{V}\frac{d(bSA)}{dt} = r_2 + r_4 \quad (2\text{-}19)$$

$$\frac{1}{V}\frac{d(bBG)}{dt} = r_3 + r_4 + r_5 \quad (2\text{-}20)$$

$$\frac{1}{V}\frac{d(bDBG)}{dt} = r_6 \quad (2\text{-}21)$$

$$V = \frac{(SA)MW_{SA}}{\rho_{SA}} + \frac{(G)MW_G}{\rho_G} + \frac{W_{Olig}}{\rho_{Olig}} - \frac{(W)MW_W}{\rho_W} \quad (2\text{-}22)$$

Energy balance equations:

At the reactor:

$$\frac{dH_R}{dt} = H_{R,in} - H_{R,out} + Q_R \quad (2\text{-}23)$$

$$\rho_{mix}VC_{p,mix}\frac{dT_R}{dt} = -\rho_w F_w\left(C_{p,w}T_R(t) + \Delta H_{W,vap}\right) - (r_1 + r_2 + r_3 + r_4)V\Delta H_{ester} \quad (2\text{-}24)$$
$$-r_6 V\Delta H_{byprod} - U_{est}A(T_R(t) \text{ - } T_J(t))$$

$$\frac{dT_R}{dt} = -\frac{m_w(C_{p,w}T_R(t) + \Delta H_{W,vap})}{\rho_{mix}VC_{p,ix}} - \frac{(r_1 + r_2 + r_3 + r_4)V\Delta H_{ester}}{\rho_{mix}VC_{p,mix}} \quad (2\text{-}25)$$
$$-\frac{r_6 V\Delta H_{byprod}}{\rho_{mix}VC_{p,mix}} - U_{est}A(T_R(t) - T_J(t))$$

At the jacket:

$$\frac{dH_J}{dt} = H_{J,in} - H_{J,out} + Q_J \quad (2\text{-}26)$$

$$\rho_{oil}V_J C_{p,cool}\frac{dT_J}{dt} = \rho_{oil}F_{heat}C_{p,oil}T_{Jheat,in} + \rho_{oil}F_{cool}C_{p,oil}T_{J,in} - \rho_{oil}F_{heat}C_{p,oil}T_J(t) \quad (2\text{-}27)$$
$$-\rho_{oil}F_{cool}C_{p,oil}T_J(t) + U_{est}A(T_R(t) - T_J(t))$$

$$\frac{dT_J}{dt} = \frac{\rho_{oil}F_{heat}\ C_{p,oil}T_{J,heatin}}{\rho_{oil}V_J C_{p,oil}} + \frac{\rho_{oil}F_{cool}\ C_{p,oil}T_{J,coolin}}{\rho_{oil}V_J C_{p,oil}} \quad (2\text{-}28)$$
$$-\frac{\rho_{oil}F_{heat}C_{p,oil}T_J(t)}{\rho_{oil}V_J C_{p,oil}} - \frac{\rho_{oil}F_{cool}C_p T_J(t)}{\rho_{oil}V_J C_{p,oil}} + \frac{U_{est}A(T_R(t) - T_J(t))}{\rho_{oil}V_J C_{p,oil}}$$

$$\frac{dT_J}{dt} = \frac{F_{heat}(T_{J,heatin} - T_J(t))}{V_J} + \frac{F_{cool}(T_{J,coolin} - T_J(t))}{V_J} \quad (2\text{-}29)$$
$$+\frac{U_{est}A(T_R(t) - T_J(t))}{\rho_{oil}V_J C_{p,oil}}$$

doi:10.6342/NTU202302309

Table 2-2 The molecular structure of monomer, oligomers and product in esterification reactions of polybutylene succinate (PBS)

Symbol	Description	Unit
H_R	Enthalpy at reactor	J
H_J	Enthalpy at jacket	J
$H_{R,in}$	Enthalpy at inlet	J/s
$H_{R,out}$	Enthalpy at outlet	J/s
Q_R	Heat from/to reactor	J/s
Q_J	Heat from/to jacket	J/s
T_R	Temperature of reactor	°C
T_J	Temperature of jacket	°C
$T_{J,heatin}$	Temperature at jacket inlet	°C
$T_{J,coolin}$	Temperature at jacket inlet	°C
$\Delta H_{W,vap}$	Heat of vaporization	J/mol
ΔH_{ester}	Heat of esterification reactions	J/mol
ΔH_{byprod}	Heat of by-product reactions	J/mol
$C_{p,mix}$	Heat capacity of mixture	J/g*K
$C_{p,oil}$	Heat capacity of coolant	J/g*K
$C_{p,w}$	Heat capacity of water	J/g*K
ρ_{mix}	Density of the mixture	g/L
ρ_{cool}	Density of the coolant	g/cm3
ρ_w	Density of water	g/cm3
U_{est}	Overall heat transfer coefficient of esterification unit	W/m^2°C
A	Heat transfer area	m^2
F_{heat}	Heating oil flow rate	L/s
F_{cool}	Cooling oil flow rate	L/s
m_w	Mass flow rate of water	g/s
V	Volume of reactor	L
V_J	Volume of jacket	L

doi:10.6342/NTU202302309

When the process is carried out, there is enormous heat generated and consumed simultaneously as exothermic reactions proceed with evaporation of water. The esterification reactions (r1 to r4) and di-glycol reaction (r6) are strong exothermic reactions that produce a mole of water after reacted. The energy involved in the reactor is derived in eq.2-23 to 2-25. In order to maintain the temperature isothermally, thermal fluid (oil) is supplied into the jacket to transfer heat into the jacket or absorb heat from the reactor depend on temperature different in each side as derived in eq.2-26 to 2-29 as energy balance at the jacket. All the parameters related to energy balance equations for both sides are indicated in Table 2-2. The transfer of energy between two volumes can be described by the overall heat transfer coefficient (U). In a stainless-steel jacketed vessel containing an organic mixture, the facilitation of heat transfer by utilization of heat transfer oil. The overall heat transfer coefficient in this system typically ranges from 170 to 680 J/m²sK [36].

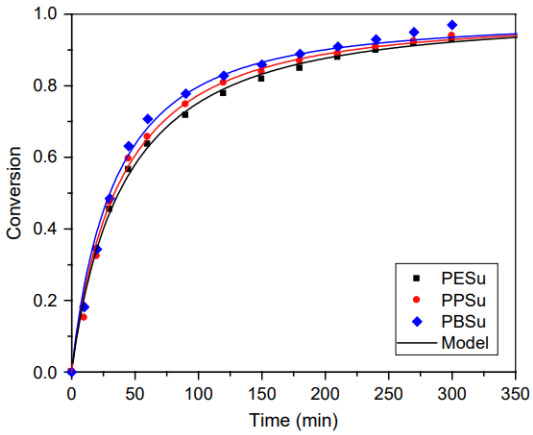

Figure 2-2 The synthesis of PESu, PPSu and PBSu conversion at 190°C and 3.0×10-4 mol TBT/mol SA. Kinetics model (lines) and experimental data (points) [3]

The authors developed a kinetic model for the reaction at 190°C in the presence of 3.0×10-4 mol TBT/mol SA by fitting reaction rate constants (k) to the experimental data of different poly (alkylene succinate) as shown in Figure 2-2. Temporal difference (TD)

doi:10.6342/NTU202302309

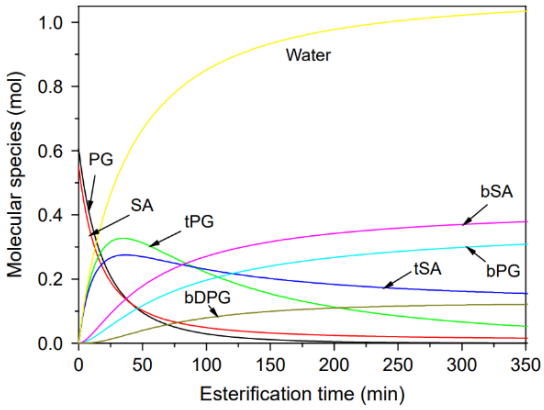

Figure 2-3 The mole of each particular species as a function of time during the esterification reaction of polypropylene succinate at 190 °C [3]

When the esterification reactions of polypropylene succinate proceed as shown in Figure 2-3, oligomers of tSA and tPG and water are formed because SA and PG reactant rapidly. Subsequently, the oligomers continue to react. As a consequence, the tSA and tPG concentration gradually decrease after the reactions have been carried out for a period of time [3]. High conversion was obtained for all glycols [37].

The type and amount of catalyst present in the reactor has a strong influence on the kinetics of the reaction substantially the K value in the rate law equations, therefore, obtaining the desired properties of the polymer, the selection of catalyst types and amount of usage are significant [37]. The synthesis of polypropylene terephthalate (PPT) with a variety of different catalyst types to find the catalyst that yields the highest conversion. It was found that Tetrabutoxy-titanium (TBT) contributes well to the reaction of both esterification and polycondensation beyond other catalysts. The PPT reaction schemes has reaction schemes similar to PBS therefore TBT catalyst is reasonable to provide the esterified succinic acid in the synthesis of PBS.

The esterification of PBS is commonly known as an acid-catalyzed reaction means succinic acid as a monomer acts as a catalyst in the reaction. The esterification of PBS with the presence of a TBT catalyst, both acid and the metal catalyst generally influence

doi:10.6342/NTU202302309

the k values and also the rate of reaction in consequence. However, when the metal catalyst utilized in the reaction could lower the acid-catalyzed activity [38].

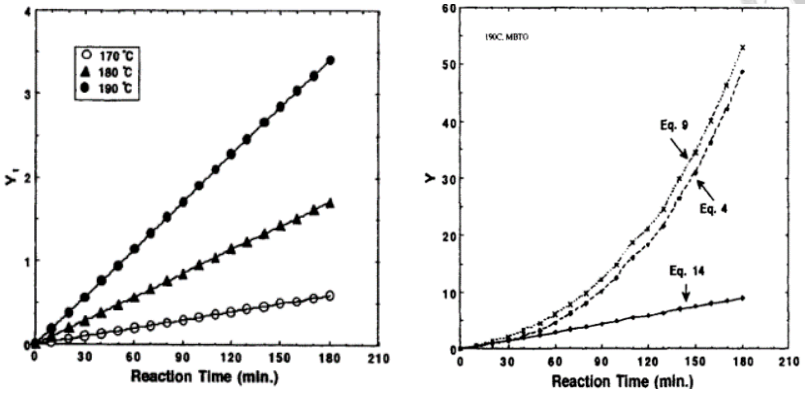

(a) (b)

Figure 2-4 (a) Kinetic value with reaction time with the absence of metal catalyst and (b) Kinetic value with reaction time with metal catalyst [38]

The mathematic model and using the extent of reaction values from the experiment with the absence of the monobutyl tinoxide (MBTO) catalyst to illustrate the kinetic of polyesterification in figure 2-4a, the kinetic values of 3 different temperatures ranging from 170, 180, and 190 C shows linear behavior with time. However, when the model was implemented in the presence of an MBTO catalyst environment, the nonlinearity behavior curves occurred which deviated a lot as shown in the figure 2-4b therefore, the developed model was assumed that the rapid increase of the rate of reaction is only from the effect of metal catalyst usage due to low activity of self-catalyzed acid shows linear behavior with reaction time as an uncatalyzed reaction [38].

2.1.2 Polycondensation

The esterified acid product is fed into another reactor which is operated at a high vacuum environment with the presence of a catalyst where the polycondensation or transesterification reaction is carried out in the vacuum environment and high temperature in order to reduce pressure and assist the devolatilization leading to remove the by-

doi:10.6342/NTU202302309

product of 1,4-butanediol or butylene glycol [39] as to increase the molecular weight and viscosity of the product. During the process, the oligomers are stirred by mechanical agitation to transfer the by-product to the vaporization surface to increase the rate of removal.

In polycondensation reaction, there are 2 reactions where acid and glycol are reacted that occur simultaneously including 1. transesterification or polycondensation where glycols are generated, and 2. esterification where water is produced as a by-product as shown in figure 2-5 and 2-6.

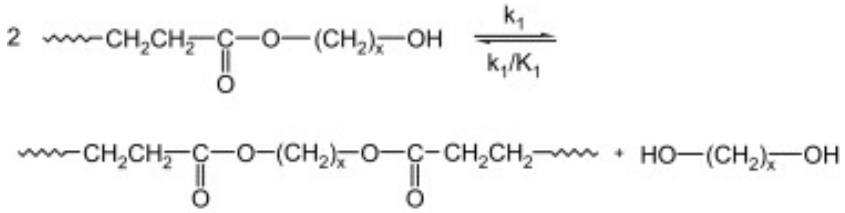

Figure 2-5 Transesterification/polycondensation reaction [4]

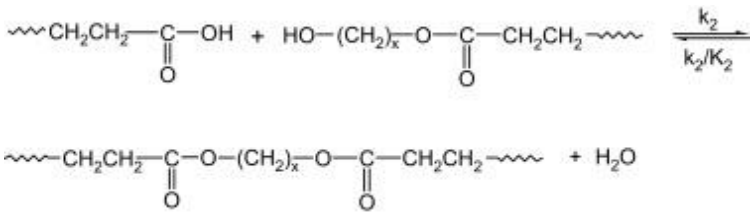

Figure 2-6 Esterification reaction [4]

doi:10.6342/NTU202302309

Mass balance equations:

r_7 $$\frac{d[OH]_t}{dt} = -2k_1[OH]_t^2 - k_2[COOH]_t[OH]_t \quad (2\text{-}30)$$

r_8 $$\frac{d[COOH]_t}{dt} = -k_2[COOH]_t[OH]_t \quad (2\text{-}31)$$

$$[OH]_t = [OH] - [OH]_i \quad (2\text{-}32)$$

$$[COOH]_t = [COOH] - [COOH]_i \quad (2\text{-}33)$$

$$[OH]_i = -773 + \frac{443648}{T} \quad (2\text{-}34)$$

$$[COOH]_i = -47 + \frac{28507}{T} \quad (2\text{-}35)$$

Energy balance equations:

At the reactor

$$\frac{dH_R}{dt} = H_{R,in} - H_{R,out} + Q_R \quad (2\text{-}36)$$

$$M_{mix}C_{p,mix}\frac{dT_R}{dt} = -\dot{M}_{BG}\left(C_{p,BG}T_R(t) + \Delta H_{vap,BG}\right) - \dot{M}_W\left(C_{p,W}T_R(t) + \Delta H_{vap,W}\right) - r_7 M_{mix}\Delta H_{polycon} - r_8 M_{mix}\Delta H_{ester} - U_{polyc}A(T_R(t) - T_J(t)) \quad (2\text{-}37)$$

$$\frac{dT_R}{dt} = -\frac{\dot{M}_{BG}\left(C_{p,BG}T_R(t) + \Delta H_{vap,BG}\right)}{M_{mix}C_{p,mix}} - \frac{\dot{M}_W\left(C_{p,w}T_R(t) + \Delta H_{vap,W}\right)}{M_{mix}C_{p,mix}} - \frac{r_7\Delta H_{polyc}}{C_{p,mix}} - \frac{r_8\Delta H_{ester}}{C_{p,mix}} - \frac{U_{polyc}A(T_R(t) - T_J(t))}{M_{mix}C_{p,mix}} \quad (2\text{-}38)$$

At the jacket:

$$\frac{dT_J}{dt} = \frac{F_{heat}(T_{J,heatin} - T_J(t))}{V_J} + \frac{F_{cool}(T_{J,coolin} - T_J(t))}{V_J} + \frac{U_{polyc}A(T_R(t) - T_J(t))}{\rho_{oil}V_J C_{p,oil}} \quad (2\text{-}39)$$

Bikiaris et al proposed k1 and k2 of both reactions provided by fitting the values to the dynamic models of the variation of carboxyl and hydroxyl content with time to the experimental results using 4 different temperatures (210, 220, 230, 245 °C) and they also measured the intrinsic viscosity using an Ubbelohde viscometer at 25°C after the reaction carried out to calculate the average molecular weight. The rate of change of true hydroxyl

doi:10.6342/NTU202302309

$[OH]_t$ and true carboxyl end group $[COOH]_t$ are described by the expression of eq. 2-30 and 2-31.

To achieve higher accuracy in the synthesis of the polymer simulation, the consideration of defective chemicals must be involved because the defect of degraded chemicals leads to inactive chain end groups that are unable to proceed with polycondensation and are ineffective to incorporate in crystalline parts as a result of chain mobility restriction [40]. However, it was found that the higher temperature could enhance chain end group ability as the inactive end group concentrations decrease when the synthesis temperature reached the higher point. The true concentration expressions are modified by deducting the inactive chain end group concentrations $[OH]_i$ and $[COOH]_i$ from the total chain end group concentrations $[OH]$ and $[COOH]$ [4]. The mathematical relationships are shown in eq. 2-32 to 2-35.

Energy balance in the polycondensation unit is derived in eq. 2-36 to 2-38, show the influence of exothermic reaction for both of the main and minor reactions and evaporation of 2 components including butylene glycol and water simultaneously. The rate of jacket temperature change is shown in eq. 2-39.

The hydroxyl content while accounting for inactive end group substantially decreased with increasing temperature as shown in Figure 2-7a. At 245°C the hydroxyl content was only 143 meq/kg after 3 hrs while the synthesis temperature of 210°C (35°C lower) and there were triple times hydroxyl content left over from the reactions (418 meq/kg). COOH contents showed minor differences at varying temperatures at around 14 meq/kg after 3 hrs of reaction [4] as illustrated in Figure 2-7b.

The chemical reactions involved in this process can be described as follows: reactions labeled as r_1 to r_4 and r_8 represent the interaction between esterified acid and glycol, while r_5 and r_7 denote the polycondensation reaction primarily taking

doi:10.6342/NTU202302309

place in the second batch. Furthermore, r_6 is the di-glycol reaction that produces dibutylene glycol repeating units after the reaction of two units of butylene glycol end groups. All of these reactions are inherently exothermic processes, entailing the release of heat as the reactions progress. The corresponding heat of reaction values at a temperature of 200°C are shown in Table 2-3.

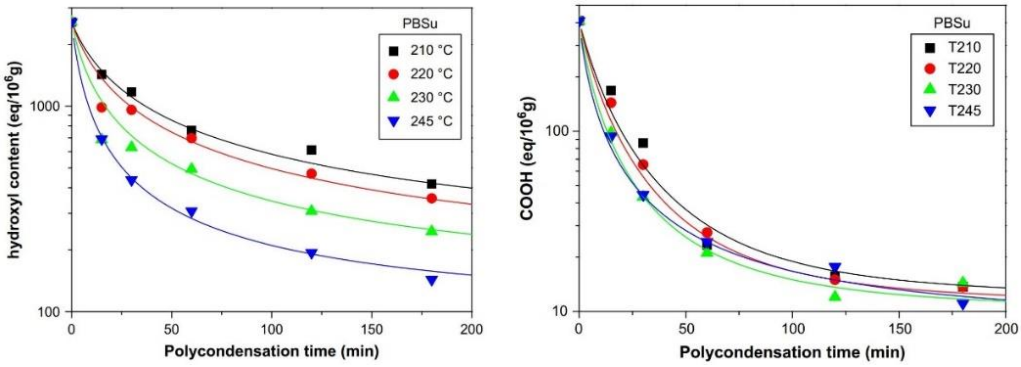

(a) (b)

Figure 2-7 (a) The true [OH] concentration and (b) the true [COOH] concentration as a function of time during PBS polycondensation process [4]

Table 2-3 Heat of reactions

Reactions	Heat of reaction (J/mol)
Esterification	-18576
Polycondensation	-29906
di-glycol	-18576

In both reactors, a mass removal process is employed to evaporate water and butylene glycol as by-products, thereby increasing the concentration of the mixture. This procedure necessitates the absorption of heat by the molecules to facilitate a phase change. The specific quantity of heat required for vaporization, known as the heat of vaporization, is indicated in Table 2-4.

doi:10.6342/NTU202302309

Table 2-4 Heat of vaporization

Molecules	Heat of vaporization (J/g)
Water (W)	1941.2
Butylene glycol (BG)	798.92

The mechanical properties of the polymer are directly influenced by molecular weight. A very low molecular weight polymer is in viscous liquid form if the Tg (glass transition temperature) is lower than ambient temperature, the material is brittle when Tg is higher than room temperature. For longer polymer chains usually called elastomer which has low strength but high elongation. Rubber characteristics of polymer could be found at MW around 105 exhibits a higher elongation [41]. Therefore, molecular weight measurement is a crucial procedure to verify the desired mechanical properties and the polymer viscosity. The number average molecular weight ($\bar{M}_n$) of PBS is described by acid end group content [COOH] and hydroxyl end group content [OH] in the milli-equivalent per kilogram (meq/kg) as depicted in the following.

$$\bar{M}_n = \frac{\sum_{i=1}^{N} n_i Mw_i}{\sum_{i=1}^{N} n_i} = \frac{\sum_{i=1}^{N} m_i}{\sum_{i=1}^{N} n_i} = \frac{1}{\sum_{i=1}^{N} n_i/m_i} = \frac{1}{\frac{[COOH]+[OH]}{2}} \tag{2-40}$$

$$\bar{M}_n = \frac{2}{[COOH]+[OH]} \tag{2-41}$$

Mark-Houwink equation (MHE) [42] is proposed in this work to simulate the viscosity of the synthesized PBS as a function of time without using viscometer to measure the collected samples. The equation presents the nonlinear relationship of the polymer's intrinsic viscosity (η) and the number average molecular weight ($\bar{M}_n$).

$$[\eta] = K\bar{M}_n^a \tag{2-42}$$

$$ln[\eta] = lnK + a ln\bar{M}_n \tag{2-43}$$

From eq. 2-43, multiply the natural log on both sides of eq. 2-42 in order to transform the non-linear to a linear relationship. Therefore, ln K and a value are the y-

doi:10.6342/NTU202302309

axis intercept and slope of the plotted experimental result, respectively. The MHE parameters of K and a are affected by the selected solvent in the experiment [43].

Bikaris et al [4] presented the K and a values of the Mark-Houwink equation in eq. 2-44 and Solomon-Ciuta equation (conventional viscosity evaluation method) as shown in the eq. 2-45 where C is the concentration of the solution, t is the flow time of the solution, and t_0 is the flow time of the pure solvent.

$$\bar{M}_n = 3.29 \times 10^4 [\eta]^{1.54} \tag{2-44}$$

$$[\eta] = 7.44 \times 10^{-4} \bar{M}_n^{0.648} \tag{2-45}$$

$$[\eta] = \frac{\left[2\left\{\frac{t}{t_0} - \ln\left(\frac{t}{t_0}\right) - 1\right\}\right]^{\frac{1}{2}}}{C} \tag{2-46}$$

The PBS polycondensation at the different temperatures ranging from 210, 220, 230, and 245°C showed the diverse of intrinsic viscosity as shown in Figure 2-7. The intrinsic viscosity increased with higher temperature as well as higher reaction rates. The result showed the model (lines) corresponding to experiment (dots) results in the similar trends. The maximum viscosity was observed at 245°C at 0.55 dL/g.

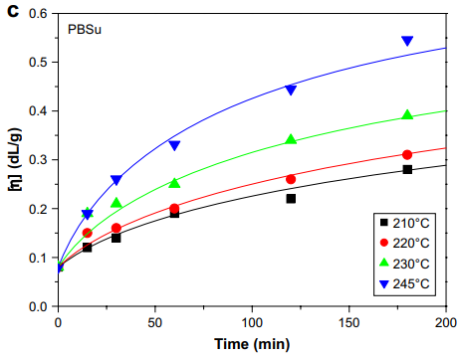

Figure 2-8 Intrinsic viscosity [n] as a function of time during polycondensation [4]

doi:10.6342/NTU202302309

2.2 Split range PID control

Q-learning in the previous section tries to compute Q^* to determine the policy π. Policy gradient method, instead, tries to calculate the optimal policy π^* directly [30]. The objective of policy gradient method is to maximize the expected return $J(\pi_\theta)$ of a parameterized policy π_θ. Optimization can be realized by gradient ascent [31],

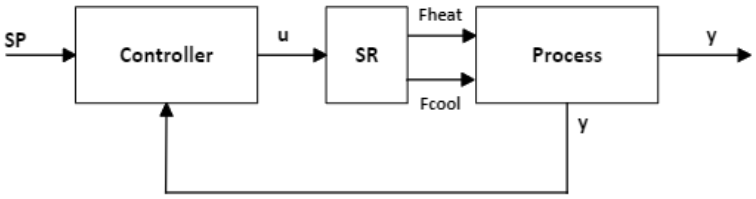

Figure 2-9 Split range PID control structure

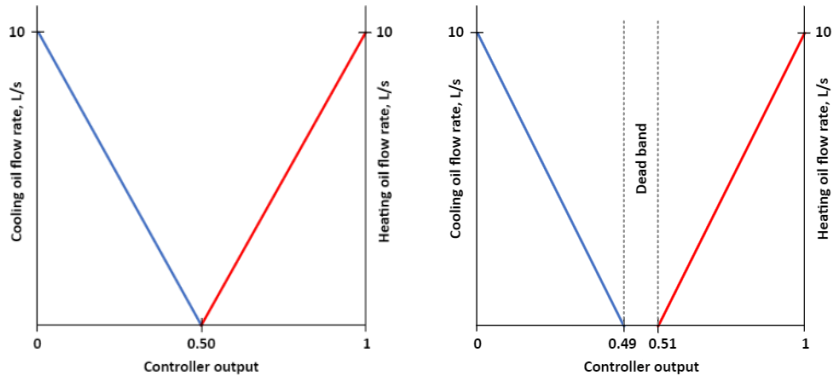

(a) **(b)**

Figure 2-10 (a) Split range control signal range, (b) Split range control signal range with dead band.

PID control is widely employed in many industries due to its simplicity feedback control structure and practical ease of use. In this study, split range PID control was simulated for both reactors to regulate the heating and cooling oil valves (The control structure is depicted in Figure 2-9). The controller output is split into two ranges 0 to 0.5 for cooling valve opening and 0.5 to 1 for heating valve opening. At each time step, only one valve is opened while another one is fully closed to restrict wasting energy and also achieve full performance [44]. However, this resulted in oscillation around the setpoint,

doi:10.6342/NTU202302309

which was mitigated by introducing a dead band at the controller output from 0.49 to 0.51 to prevent valve movement when the temperature reached the setpoint. The proposed control signal ranges are depicted in Figure 2-10.

PID were tuned by minimizing an ITAE objective function as depicted in eq. 2-47. The proposed tuning method can provide excellence performance in terms of reactor temperature control, it may also result in highly aggressive control action. To address this is-sue, the weighting matrix are included in both valves to adjust the optimal tuning parameters for more efficient control action of each valve, a balance between aggressive control action and efficient control performance can be achieved.

$$ITAE = \int t\left|T_{sp} - T_R(t)\right| dt + w_{Fheat}(\Delta u_{Fheat})^2 + w_{Fcool}(\Delta u_{Fcool})^2 \qquad (2\text{-}47)$$

2.3 Model predictive control (MPC)

Model predictive control (MPC) or receding horizon control (RHC) is one of the feedback control techniques that utilizes a mathematic model in order to calculate the manipulated variable (u(t)) as shown in Figure 2-11. The manipulated variable in every time step is obtained from the measured process variable to solve the optimal manipulated variable via online dynamic optimization in the closed loop therefore it will drive the process in the direction that has minimum objective function or performance index under the assigned dynamic process model, the constraints on state, and control variables.

In traditional control techniques, when the process has more than one control variable and also more than one manipulated variable thus this case requires multiple control loops to control the process to the desired set point, which is a very complex control structure. However, MPC could completely perform the control of the Multiple Input Multiple Output (MIMO) process by using one controller in one control loop which would reduce the huge complexity of the traditional control structure. In addition, the

doi:10.6342/NTU202302309

distinctive point of the optimal control strategy is constraints of the manipulated variable could be formulated thereby the dynamic of the process will be more efficient under the manipulated variable changes related to the constraints.

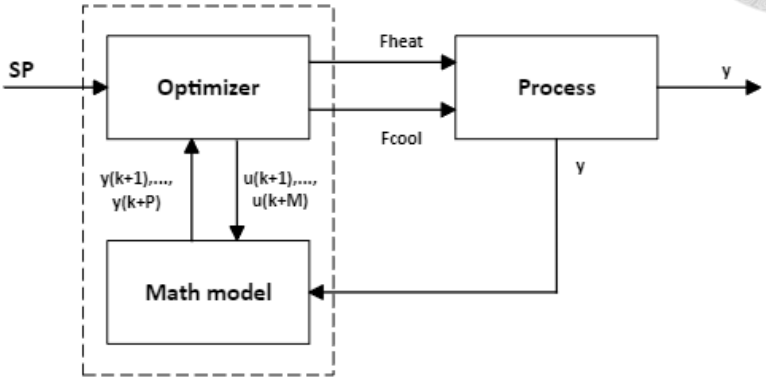

Figure 2-11 MPC control structure

2.3.1 MPC control principle

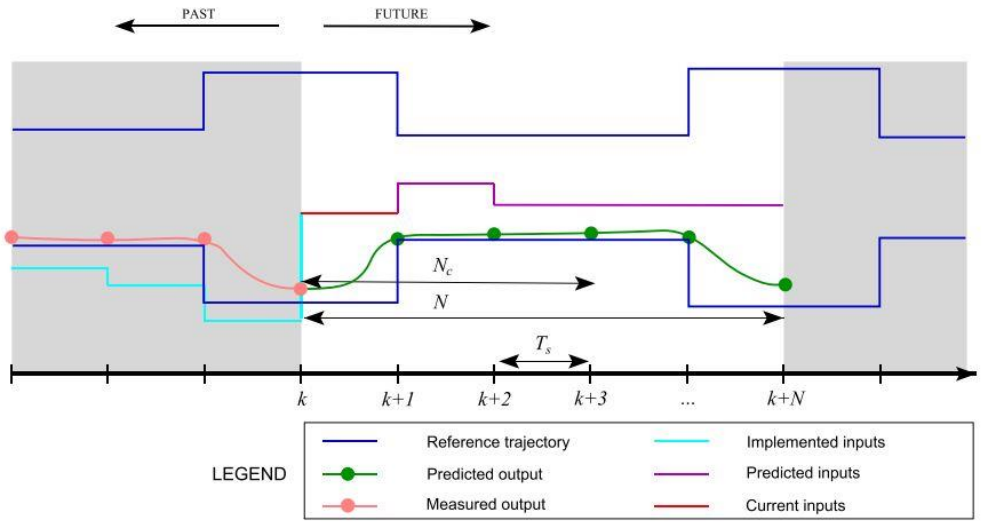

Figure 2-12 MPC for temperature control [45]

At the k time step, the controller will calculate the set of manipulated variables including at the present time and the next M time step which is u(k), u(k+1),…,u(k+M) by predicting the future output of the process in P time step from y(k+1),y(k+2),…,y(k+P) to obtain the output values that related to the desired target by optimizing the objective function as shown below.

doi:10.6342/NTU202302309

Find the control u(t) minimizing or maximizing:

Objective function:

$$J = \int_0^{t_f} \{(x(t) - x^{sp})^2 + W(\Delta u)^2\} dt \quad (2\text{-}48)$$

$$\frac{dx}{dt} = f(x, u) \quad (2\text{-}49)$$

$$x(t_0) = x_0 \quad (2\text{-}50)$$

Constraints on controls and states:

$$u_{min} \leq u \leq u_{max}$$

$$x_{min} \leq x \leq x_{max}$$

$$x(t + t_f) = x_{sp}$$

When

W Weight matrix in order to tune the process response

t_f Final time step

u_{max} Maximum value of manipulated variable

u_{min} Minimum value of manipulated variable

x_{max} Maximum value of controlled variable

x_{min} Minimum value of controlled variable

doi:10.6342/NTU202302309

2.4 Artificial neural network

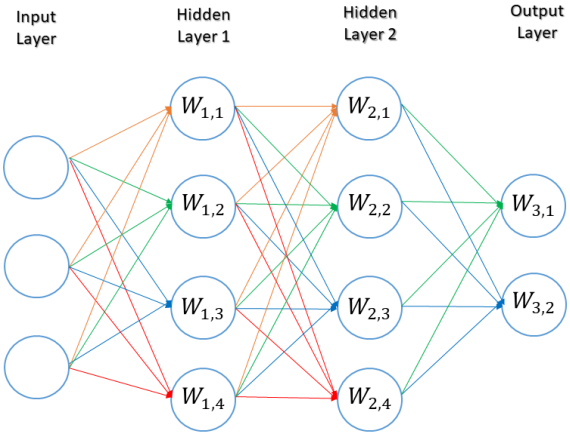

Figure 2-13 A Deep learning neural network [46]

The neural network is a multi-layered network of perceptron or neurons linking together as illustrated in figure 2-13, which is composed of 3 input nodes, 2 hidden layers which contain 4 nodes in each layer, and 2 nodes at the output layer. In each connection, there are the crucial relevant neural network elements that attempt to replicate the organization of neurons in the human brain.

2.4.1 Artificial neural network component

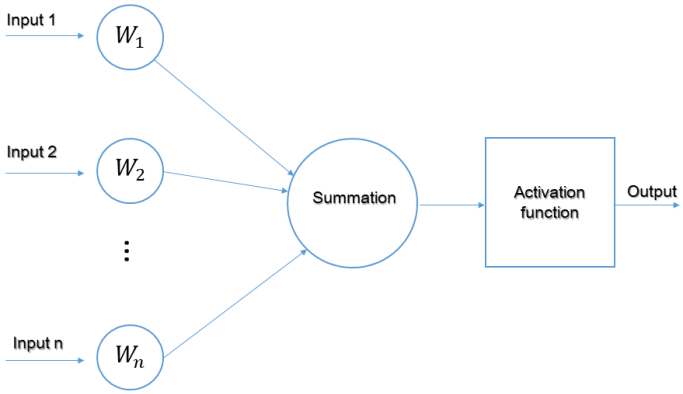

Figure 2-14 An illustration of artificial neuron [46]

doi:10.6342/NTU202302309

Input layer is the data inputted to the neural network in each node at this layer. In case the data is qualitative data such as nationality, sex, marriage, blood type, etc. must be changed to quantitative data or numerical data before input into the neural network.

Weight represents the knowledge that the neural network learned the relation of data in order to predict the probability therefore weight values could be tuned by training the large amount of data.

Summation function is the layer that sums up the inputted data (x_i) or the data from the preceding layer multiplied by corresponding weights (w_i) and pass to the activation function as depicted in the equation below.

$$S = \sum_{i=1}^{n} x_i w_i \tag{2-51}$$

Activation function is a nonlinear function that transforms the output data from the summation function to the form of output in the assigned form depend on the relation of the inputted data and the model applications to assist in preventing problems such as exploding and vanishing gradient.

Output layer is the terminal layer of the network where the result of prediction or data output from the neural network will be released at this layer.

2.4.2 Artificial neural network architecture

The architecture could be classified on the basis of data flow direction that consists of feedforward and feedback neural networks.

Feedforward neural network

A feed-forward neural network or other word is called a non-recurrent network is a neural network structure where the data is inputted into the linked multi-layer network and only flows in the forward direction and processed via mathematical calculation

doi:10.6342/NTU202302309

through the particular neural network components then send to the next hidden layers in consequent and terminates at the output layer as shown in Figure 21.

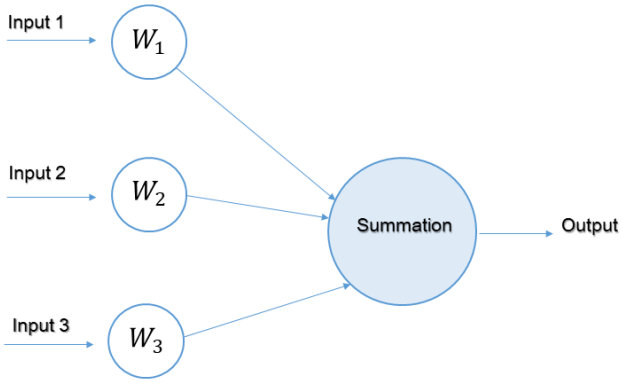

Figure 2-15 Feed forward neural network [46]

Feedback neural network

In the feedback neural network, such as recurrent neural network (RNN), the processed signal is allowed to flow forward and backward in the loop. The backward direction from the output to the prior neurons leads to the recognition of data's sequential characteristics and then the learned scenarios are used to forecast the next likely outcomes. The recurrence connection is possible to connect in any way as shown in the example of the connection in the figure above and it could be the path from output linked to the input node as the external feedback loop and internal feedback loops connected inside as minor feedback loops as shown in Figure 2-16.

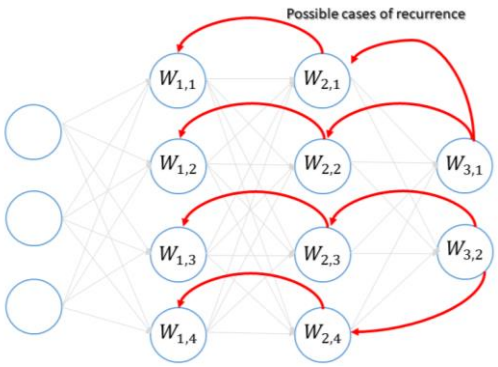

Figure 2-16 Feedback neural network [46]

doi:10.6342/NTU202302309

2.4.3 Neural network training

Forward propagation

In this procedure, the neural network is trained by the data flow direction from left to right. Initially, the inputted data is multiplied by the weights in each layer to calculate the loss or the difference of the actual and predicted output in order to prepare for the backpropagation in the following step.

Backpropagation

the training direction from right to left utilizes the supervised learning principle, the algorithm adjusts the weights of the neural network in each layer until the loss of NN is in the acceptable range.

2.4.4 Activation function

1. Binary step function

Binary step function is a function that give the output equal to 1 when the input is equal or more than 0 and when input is lower or equal to 0, the output will be 0.

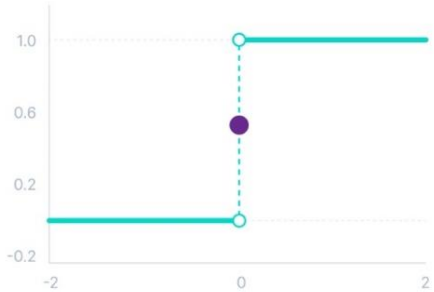

Figure 2-17 Binary step function [47]

$$f(x) = \begin{cases} 1 \text{ if } x \geq 0 \\ 0 \text{ if } x < 0 \end{cases} \quad (2\text{-}52)$$

2. Linear activation function

This activation function type will return the output value equal to any inputted data into the function.

doi:10.6342/NTU202302309

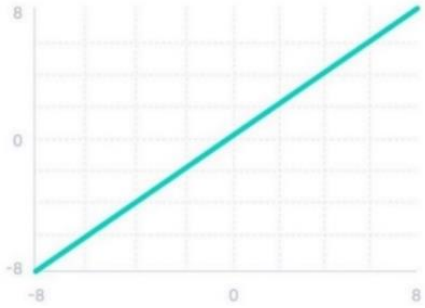

Figure 2-18 Linear activation function [47]

$$f(x) = \mathrm{x} \tag{2-53}$$

3. Sigmoid Function

Sigmoid function or logistic function is the S-shaped curve function that is frequently used as activation function in neural network applications. The output value of the function is in the range of 0 to 1.

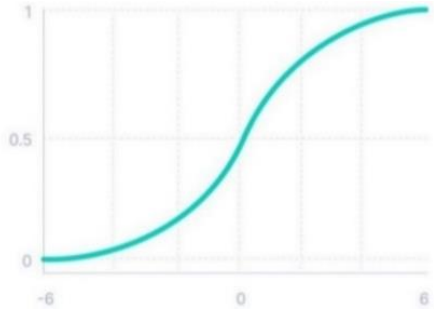

Figure 2-19 Sigmoid/logistic function [47]

$$f(x) = \frac{1}{1 + \exp(-x)} \tag{2-54}$$

4. Rectified linear unit (ReLU)

ReLU is a linear activation-based function that has the output value of the function from 0 to infinity as clearly shown in the graph below. When the input value is less than or equal to 0 then the output will be 0. Otherwise, the output will be equal to the input which is in the positive range.

doi:10.6342/NTU202302309

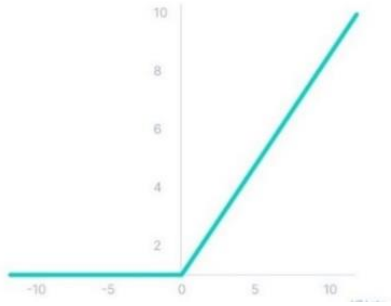

Figure 2-20 ReLU activation function [47]

$$f(x) = \max(0, x) \tag{2-55}$$

2.5 Artificial neural network

The control simulations were executing on Python for entire work, which was divided into 2 parts including esterification and polycondensation. Both parts are connected together to study the dynamics of the process after various controllers are implemented to perform the control actions. Starting from the model development, the controller design, neural network training, NNMPC deployment, and the control performance under IAE criteria were analyzed and discussed.

2.5.1 Model development

At first, the processes were simulated under isothermal conditions to study the dynamic of the developed model at different temperatures. The dynamics model is related to numerous differential equations therefore Scipy library is installed to perform solving differential equation tasks including the mass and energy balances, rate laws equation and etc. to verify that the dynamics and the final conversion that corresponds to the reported experiment to implement controllers in the further action.

2.5.2 The controller design

When the developed dynamic model is satisfied, the open loop control was performed at the initial state because it was uncomplicated to analyze the dynamic

doi:10.6342/NTU202302309

response after inputting one step change action to the model and the relevant parameters could be adjusted conveniently at this stage.

Split range PID control strategy is carried out in the next step which is a classic controller that is widely used in industries, this control strategy requires tuning therefore optimal tuning by minimizes the Integral of Time multiplied by Absolute Error criteria (ITAE) as objective function is introduced in this work to achieve the K_c, τ_I and τ_D that provide minimum ITAE for highly efficient control performance.

$$ITAE = \int t\left|T_{sp} - T_R(t)\right| dt \tag{2-56}$$

$$ITAE = \int t\left|T_p - T_R(t)\right| dt + w_{Fheat}(\Delta u_{Fheat})^2 + w_{Fcool}(\Delta u_{Fcool})^2 \tag{2-57}$$

The proposed tuning method can provide excellence performance in terms of reactor temperature control, it may also result in highly aggressive control action. To address this issue, the weighting matrix are included in both terms to adjust the optimal tuning parameters for more efficient control action of each valve, we can achieve a more optimal balance between aggressive control action and efficient control performance.

In the section on model predictive control (MPC), the prediction horizon (P) is assigned to be 10 units of time and the manipulating horizon (M) is 3 units of time. The optimization runs by Scipy optimize library using the SLSQP method to obtain the set of optimal manipulated variables in the control horizon. In this work, the industrial process data is unavailable therefore the developed mathematic models represent the actual process.

2.5.3 Neural network model training

The data from the simulation of both of the reactor with mathematic-based model predictive control are collected to train the neural networks compose of 4 layers in total. For esterification process, starting with the 11 nodes of input layer followed by 2 hidden

doi:10.6342/NTU202302309

layers that contain varying nodes each, and the final layer is the output layer shows each of particular predicted results of the model in the next time step. The rectified linear unit (ReLU) activation function is implemented in both hidden layers and output as illustrated in Figure 2-21. Polycondensation NN model, 8 inputs involve all species, temperature at both sides, and process inputs followed by 2 hidden layers with varying number of nodes at each layer with ReLU activation function. The neural network model structure of the process is shown in Figure 2-22.

In the neural network training, the number of neurons in the hidden layer will be varied from 20, 50, 100, and 200 neurons to monitor the change in the accuracy of prediction and computational time after implementing the neural models to MPC then the appropriate conditions for the NN model training are discussed.

One of the crucial procedures in training artificial neural network models, it is the preprocess of input data before feeding them into the model. One of the most common preprocessing techniques is data normalization, which adjusts the database to be in the range of 0 to 1. This technique is crucial as it helps to improve the performance and convergence speed of the neural network model. By rescaling the input data, we can avoid the dominance of certain variables and ensure that all the variables contribute equally to the model. To achieve this, the following equations are used to normalize the variable dataset [48].

doi:10.6342/NTU202302309

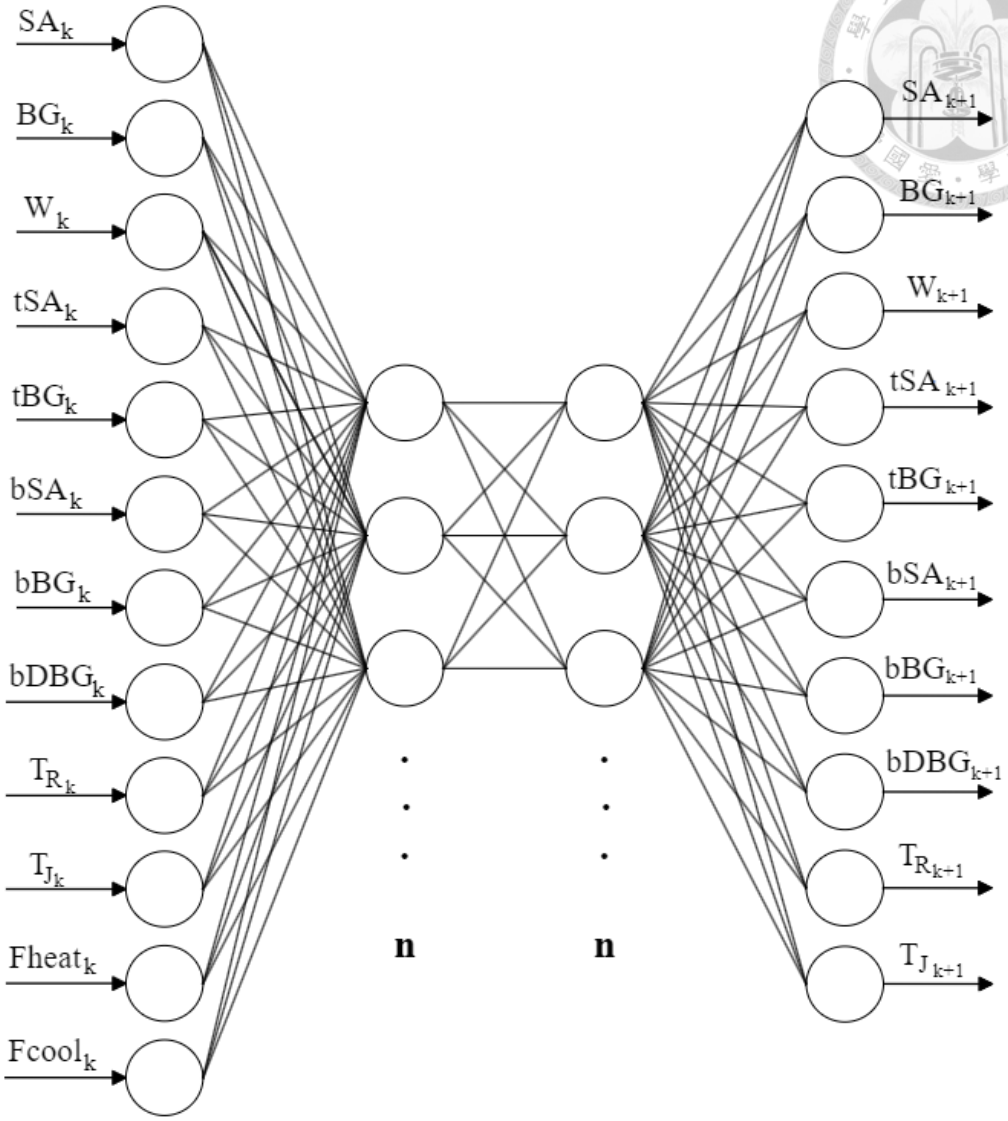

Figure 2-21 The neural network model schematic diagram of polybutylene succinate (PBS) esterification process.

doi:10.6342/NTU202302309

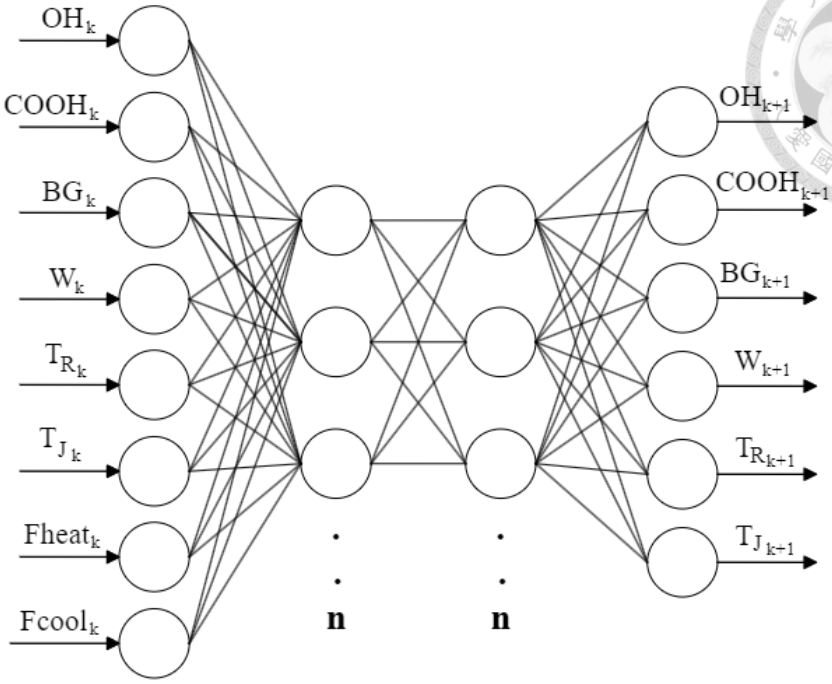

Figure 2-22 The neural network model schematic diagram of polybutylene succinate (PBS) polycondensation process.

$$X' = \left[\frac{X - Min(X)}{Max(X) - Min(X)}\right] \tag{2-58}$$

X Raw value

X' Normalized data

$Max(X)$ The maximum of raw value

$Min(X)$ The minimum of raw value

doi:10.6342/NTU202302309

2.5.4 NNMPC deployment

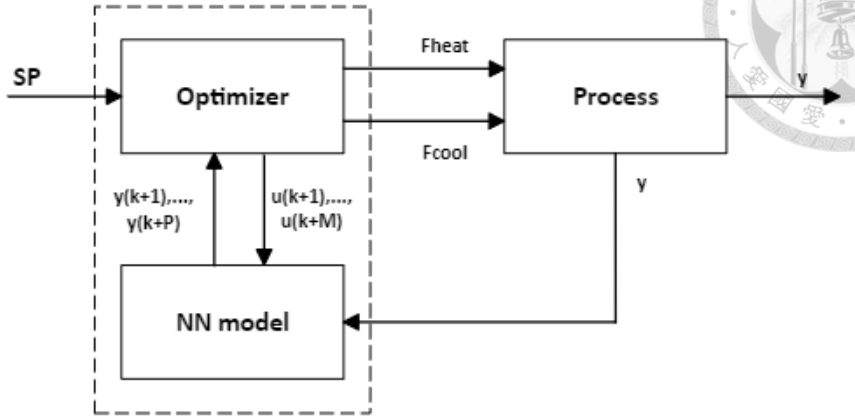

Figure 2-23 The neural network model schematic diagram of polybutylene succinate (PBS) polycondensation process

The neural network model was deployed in the optimizing process substituting the mathematic model in conventional MPC as illustrated in Figure 2-23. All input state values from the process and the optimizer are normalized in the range of 0 – 1 at every time step before inputting to the neural network model as training procedure thus the output or prediction result are denormalized before sending to the optimizer.

2.5.5 Multi-NNMPC deployment

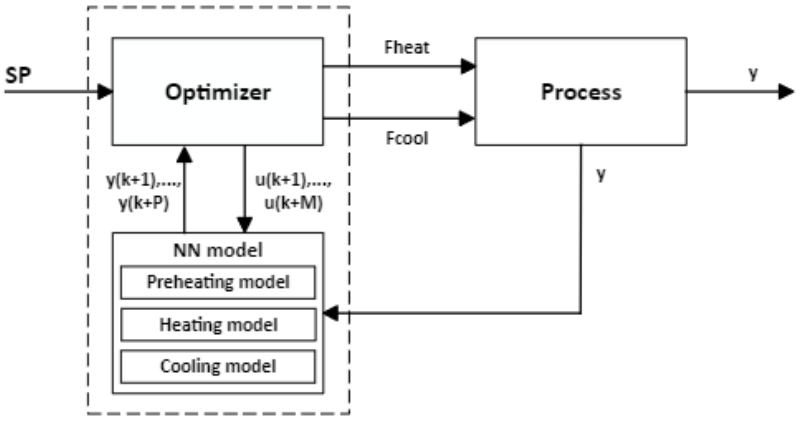

Figure 2-24 Multi-NNMPC control structure

Multiple neural network models were designed for use in preheating, heating, and cooling steps of esterification process, the proposed control structure is depicted in Figure

doi:10.6342/NTU202302309

2-24. The polycondensation process is divided the single neural network model into 3 models including heating, isothermal control, and cooling. This approach is intended to improve performance and accelerate the optimization process by reducing the complexity of a single neural network model through its division into multiple neural network models [49]. The neural network models were deployed in a sequential manner, with the preheating model utilized from 0 to 50 minutes, the heating model utilized from 50 to 400 minutes, and the cooling model from 400 to 450 minutes.

2.5.6 Control performance comparison

The developed NNMPC is compared to split range PID and MPC control on the basis of the IAE criteria under various scenarios such as nominal case, the presence of white noise, model mismatch case.

$$IAE = \int \left| T_{sp} - T(t) \right| dt \tag{2-59}$$

doi:10.6342/NTU202302309

Chapter 3 Results and discussion

3.1 Model development

Bikaris et al [3] reported the k of individual reaction at 190°C to estimate the rate of related reactions between 0.55 mol of succinic acid and 0.605 mol of butylene glycol of r1 to r4, while r5 was considered a polycondensation reaction that had a relatively low rate of reaction and therefore, its effect was neglected. r6, which is a diglycol reaction, was observed to occur minimally. The reactions proceed simultaneously create various types of oligomers with water until 400 minutes then obviously low rate of water generated is observed as shown in Figure 3-1.

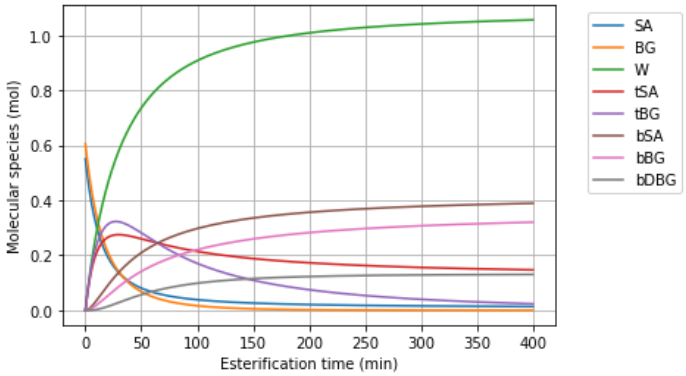

Figure 3-1 The molecular species profile in esterification process at 190 °C

The rate constant (k) of chemical reactions is highly sensitive to temperature. The Arrhenius equation (Eq. 3-1) is commonly used to describe the temperature dependence of k values, and it includes variables such as the universal gas constant (R), activation energy (Ea), and pre-exponent factor (A). The value of A could be determined by calculating the y-intersection of the linearized Arrhenius equation as shown in Eq. 3-2 in order to simulate the molecular specie profile at any temperature for isothermal conditions. The result of Ea and A of each individual reaction are indicated in Table 3-1 and 3-2.

doi:10.6342/NTU202302309

$$k = Ae^{-\frac{Ea}{RT}} \quad (3\text{-}1)$$

$$lnk = -\frac{Ea}{R}\left(\frac{1}{T}\right) + lnA \quad (3\text{-}2)$$

Table 3-1 Esterification reaction schemes with rate constants, activation energy (Ea), and pre-exponential factor (A)

	Reactions	k_i @ 190°C (L/mol×min)	Ea (J/mol)	A_i
r_1	$SA + BG \underset{k_1'}{\overset{k_1}{\leftrightharpoons}} tSA + tBG + W$	0.0027	47400	601.340
r_2	$tSA + BG \underset{k_2'}{\overset{k_2}{\leftrightharpoons}} bSA + tBG + W$	0.0027	47400	601.340
r_3	$SA + tBG \underset{k_3'}{\overset{k_3}{\leftrightharpoons}} tSA + bBG + W$	0.00135	47400	300.670
r_4	$tSA + tBG \underset{k_4'}{\overset{k_4}{\leftrightharpoons}} bSA + bBG + W$	0.00135	47400	300.670
r_5	$tBG + tBG \underset{k_5'}{\overset{k_5}{\leftrightharpoons}} bBG + BG$	0	0	0
r_6	$tBG + tBG \overset{k_6}{\rightarrow} bDBG + W$	0.0011	78473	784988.7

Table 3-2 Polycondensation reaction schemes with rate constants, activation energy (Ea), and pre-exponential factor (A)

	Reactions	k_i @ 245°C (kg/meq) h^{-1}	Ea (J/mol)	A_i
r_7	$2ROH \underset{k_7'}{\overset{k_7}{\leftrightharpoons}} PBS + BG$	0.0020	85700	839,028.53
r_8	$RCOOH + OH \underset{k_8'}{\overset{k_8}{\leftrightharpoons}} PBS + W$	0.0060	47400	363.07

The esterification process at isothermal simulation results, the process operated at 50°C shows the extremely low rate of reaction as shown in Figure 3-2. Thus, it is evident that the synthesis temperature has to be over than 150°C to yield a high conversion after 400 minutes of operation. From Figure 3-3, shows the different factors in polycondensation process including the rate of change in polymer end groups, and properties at different temperature ranging from 210, 220, 230, 245°C.

doi:10.6342/NTU202302309

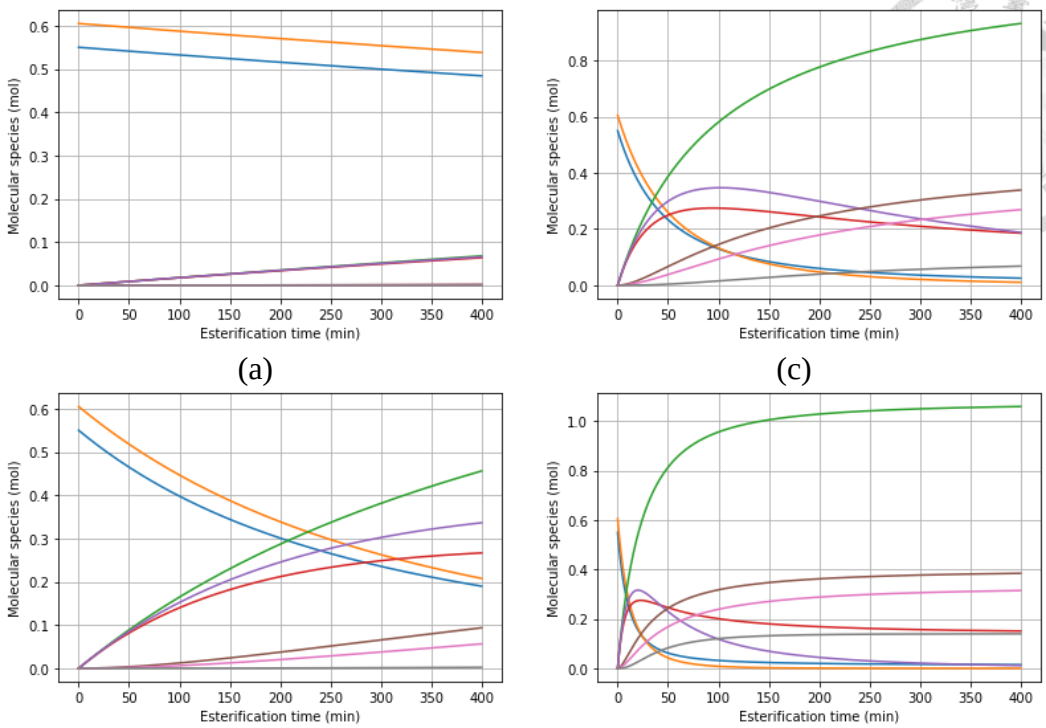

Figure 3-2 The molecular species profile in esterification process for 400 minutes at various temperature a) 50°C, b) 100°C, c) 150°C, and d) 200°C

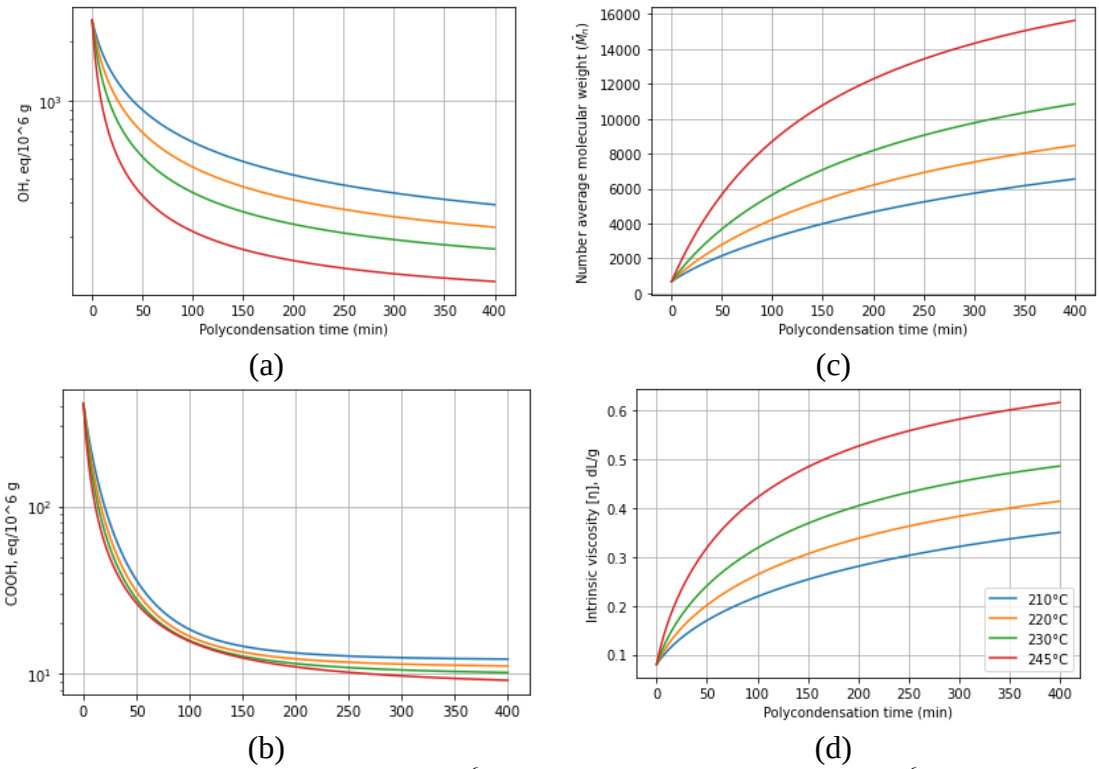

Figure 3-3 (a) OH end group (eq/10^6g), (b) COOH end group (eq/10^6g), (c) Number average molecular weight ($\bar{M}_n$), (d) Intrinsic viscosity (dL/g) during polycondensation process for 400 minutes under isothermal operation at various temperatures

doi:10.6342/NTU202302309

3.2 Split range PID control

In this section, the split range PID control is applied in the synthesis of polybutylene succinate (PBS), under varying split range arrangements to analyze the dynamic behavior and control performance of the process under nominal condition and in the presence of white noise case.

The split range PID control with different split range arrangements are varied by shifting the controller output of the heating and cooling oil valve intersection with introducing a dead band size of 0.02 to stop valve movement after reaching the setpoint. These arrangements are illustrated in Figure 3-4 and are denoted as split rage A (0.24 – 0.26), split rage B (0.49 – 0.51), and split rage C (0.74 - 0.76). The main reason for the shifting of the controller output's intersection point impacts the slope of each controller output and the sensitivity of the control response. The split range PID control is effectively tuned by minimizing ITAE tuning method.

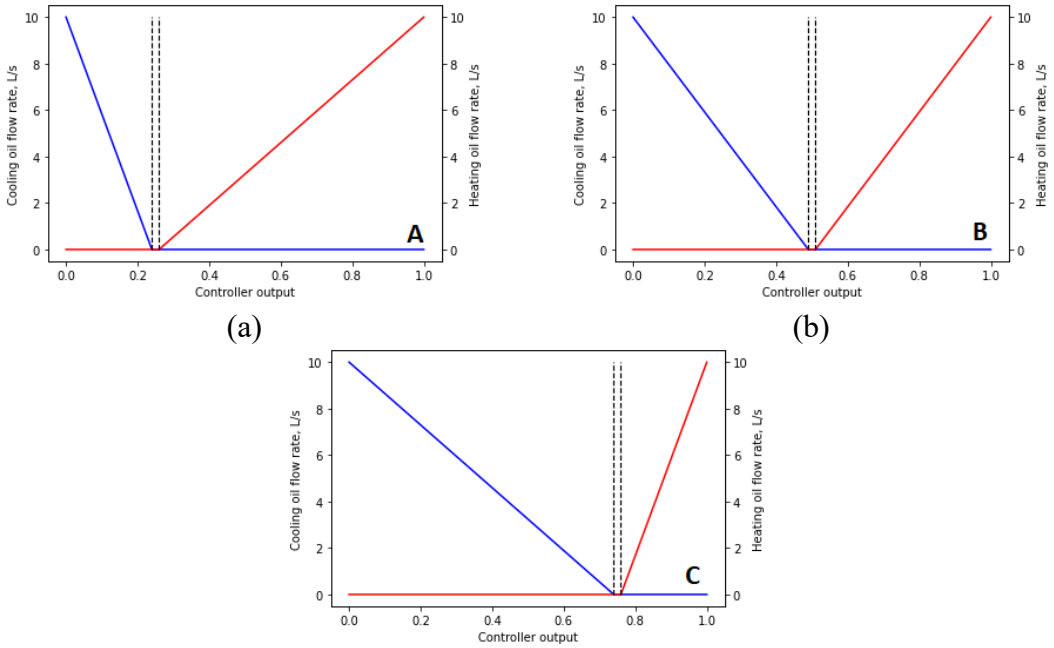

(a) (b) (c)

Figure 3-4 Split range arrangement (blue line: cooling valve, red line: heating valve)

doi:10.6342/NTU202302309

3.2.1 Nominal case

Table 3-3 IAE performance criteria comparison of esterification and polycondensation process under split range PID control with various arrangements.

Process	IAE		
	A	B	C
Esterification	3719.88	3271.83	2276.00
Polycondensation	6724.87	6663.46	6596.73

The tuning parameters of each of the proposed split range PID control arrangements for both esterification and polycondensation processes were found to have approximately similar values. Specifically, the esterification process, the tuning parameters were found to be K_c = 0.02, τ_I = 64.03, and τ_D= 0.63. For the polycondensation process, were K_c = 0.01, τ_I = 7.90, and τ_D= 1.78.

At the end of the process, the final number of moles of each species under split range PID control (B arrangement) were determined as shown in Figure 3-5, SA = 178.381 mol, BG = 0.002 mol, W = 10,551.340 mol, tSA = 1,624.245 mol, tBG = 16.304 mol, bSA = 3,697.372, bBG = 2,968.993 mol, and bDBG = 1,532.350 mol.

Upon performing temperature control in the esterification process, it is clear that the temperature during the preheating phase could not be effectively controlled at 135°C due to the high rate of reaction and heat release rates at the initial state. This resulted in a large overshoot, indicating that all split range PID control with varied arrangements were unable to maintain the temperature within the desired range as shown in Figure 3-6a. Additionally, a slight overshoot was observed during the heating phase of 225°C, which had a noticeable impact on the slow response of setpoint tracking. However, the C arrangement performed the least overshoot at controlled temperature and the fastest setpoint tracking throughout all the arrangements due to the highest slope of the heating

doi:10.6342/NTU202302309

oil valve controller output, reflecting the higher speed in the valve manipulation. Split range PID control with C arrangement received the best control performance with the lowest IAE value of 2276.00.

In the temperature control of polycondensation process, split range PID control with C arrangement provided the lowest IAE value across all arrangements of 6596.73 with the smallest overshoot in the heating phase as shown in Figure 3-8a. The final number average molecular weight and viscosity under split range PID control (C arrangement) were 13265.80 and 0.5544 dL/g, respectively. The split range control with the A arrangement showed better control performance in the cooling phase as the temperature slightly declined lower than the setpoint of 100°C compared to other split range arrangements. As the result of the higher slope of the cooling oil valve controller output. However, the overshoot in cooling procedure is not significantly affecting the chemical properties because of the low operating temperature.

The temperature profile is highly influencing the physical and chemical properties of the final product. Thus, tight temperature control during the synthesis is crucial in the operation. The split range PID control, which employs an A and B arrangement was observed to gradually decrease the heating oil flow rate, thereby leading to unable to control the temperature and the polymer molecular weight rapidly shooting at around 120 minutes as shown in Figure 3-7c.

doi:10.6342/NTU202302309

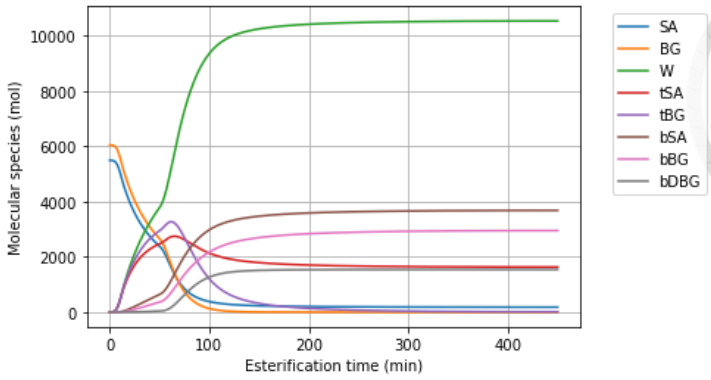

Figure 3-5 Molecular species profile in esterification process under split range PID control (B arrangement)

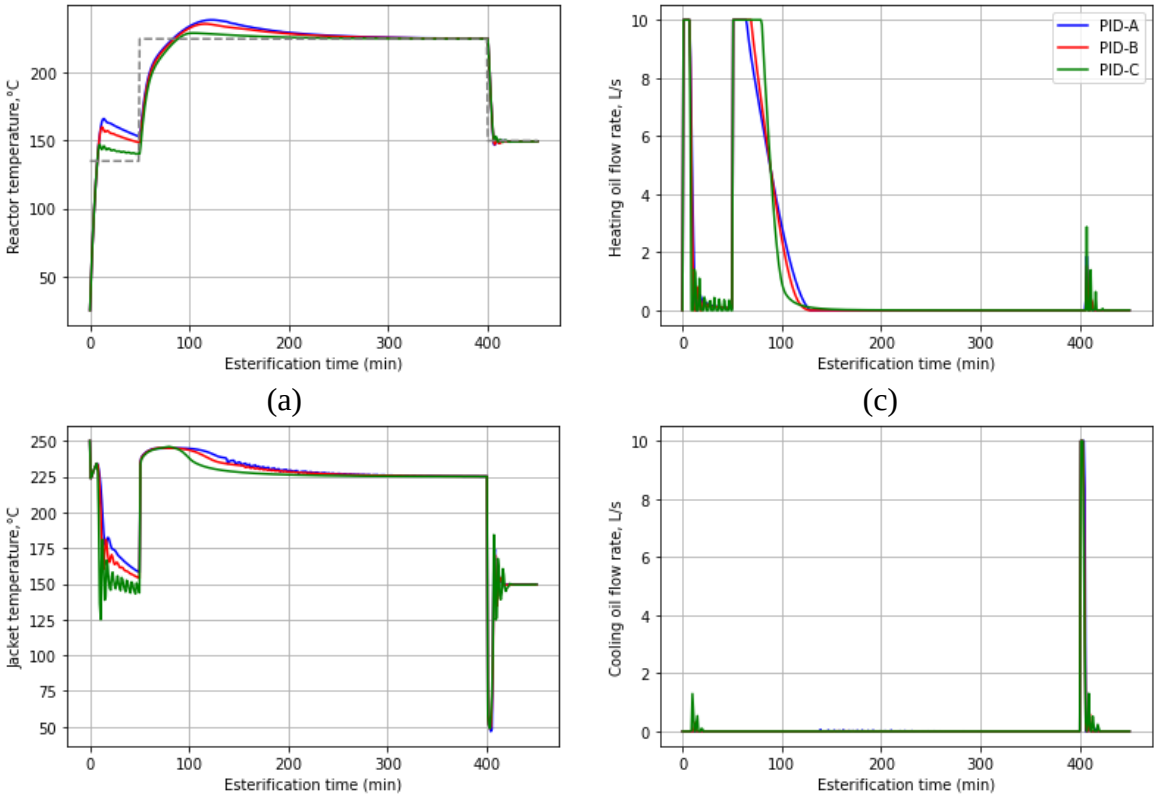

Figure 3-6 (a) Reactor temperature (°C), (b) Jacket temperature (°C), (c) Flow rate of heating oil (L/s), (d) Flow rate of cooling oil (L/s) in esterification process under split range PID control (A, B, and C arrangement)

doi:10.6342/NTU202302309

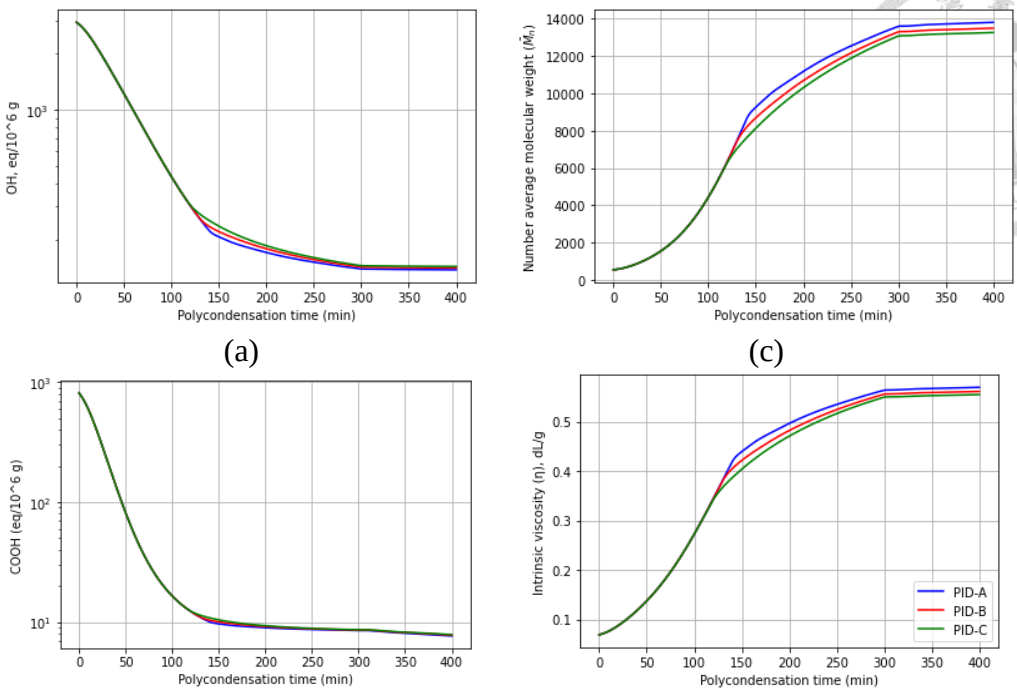

Figure 3-7 (a) OH end group (eq/10^6g), (b) COOH end group (eq/10^6g), (c) Number average molecular weight ($\bar{M}_n$), (d) Intrinsic viscosity (dL/g) during polycondensation process under split range PID control

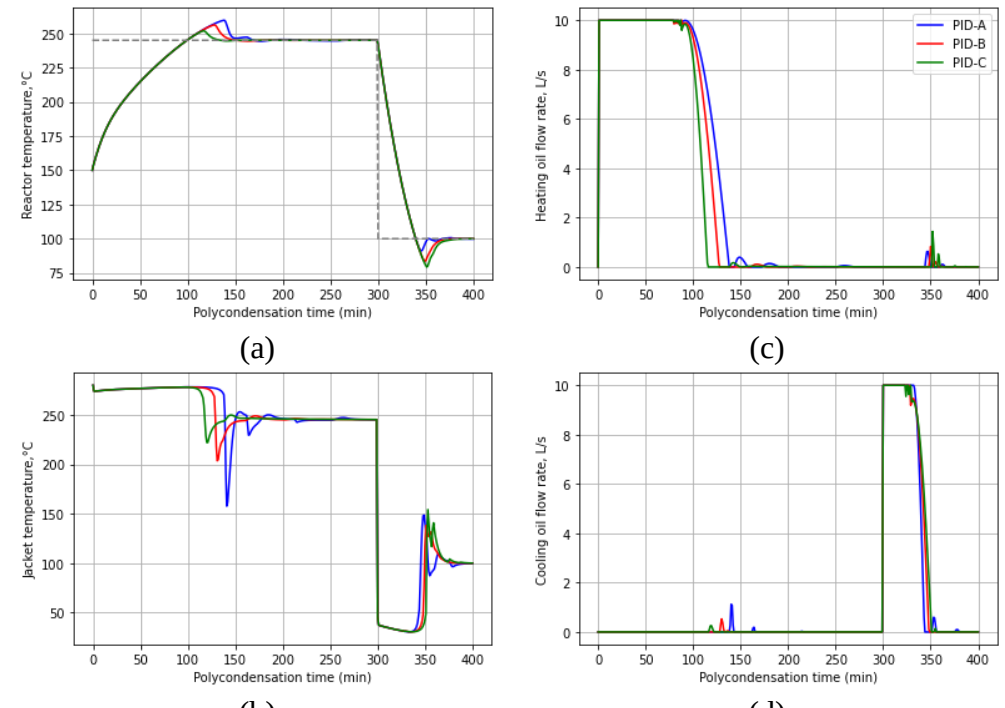

Figure 3-8 (a) Reactor temperature (°C), (b) Jacket temperature (°C), (c) Flow rate of heating oil (L/s), (d) Flow rate of cooling oil (L/s) in polycondensation process under split range PID control

doi:10.6342/NTU202302309

3.2.2 White noise case

Table 3-4 performance criteria comparison of esterification and polycondensation process under split range PID control with various arrangements for noise case.

Process	IAE		
	A	B	C
Esterification	4308.96	3868.96	3001.82
Polycondensation	6769.90	6717.38	6613.99

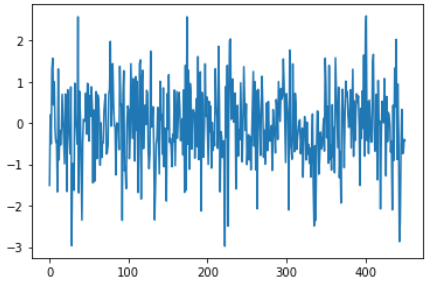

Figure 3-9 The set of white noise interferes with the reactor temperature

The efficacy of split range PID control in the presence of white noise was tested. This is a significant aspect of the controller's operation since real processes are often subject to white noise interference. In the simulation with noise interference, a set of white noise was randomly generated at all time steps (450 minutes) with zero mean and a standard deviation of 1 as shown in Figure 3-9, resulting in a maximum deviation of roughly ±3°C from the actual value in order to corrupt the measurement of the reactor temperature. All split range PID arrangements exhibited an oscillatory response but the controller demonstrated the ability to drive the temperature to the setpoint and maintain the reactor temperature during the isothermal stage.

The split range PID (C arrangement) showed the lowest IAE value in both processes of 3001.82 and 6613.99, respectively. However, the control action of both valves was highly aggressive. Over-utility consumption was observed in Figure 3-11 and 3-13. This reflects the tradeoff between tight temperature control and robustness.

doi:10.6342/NTU202302309

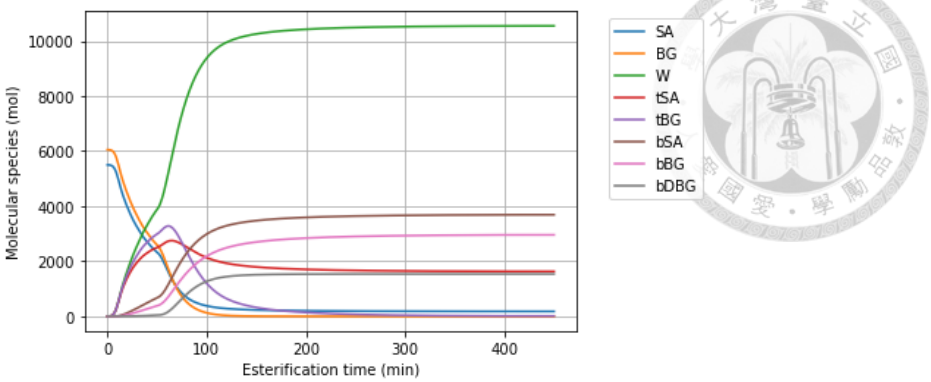

Figure 3-10 Molecular species profile in esterification process under split range PID control with white noise

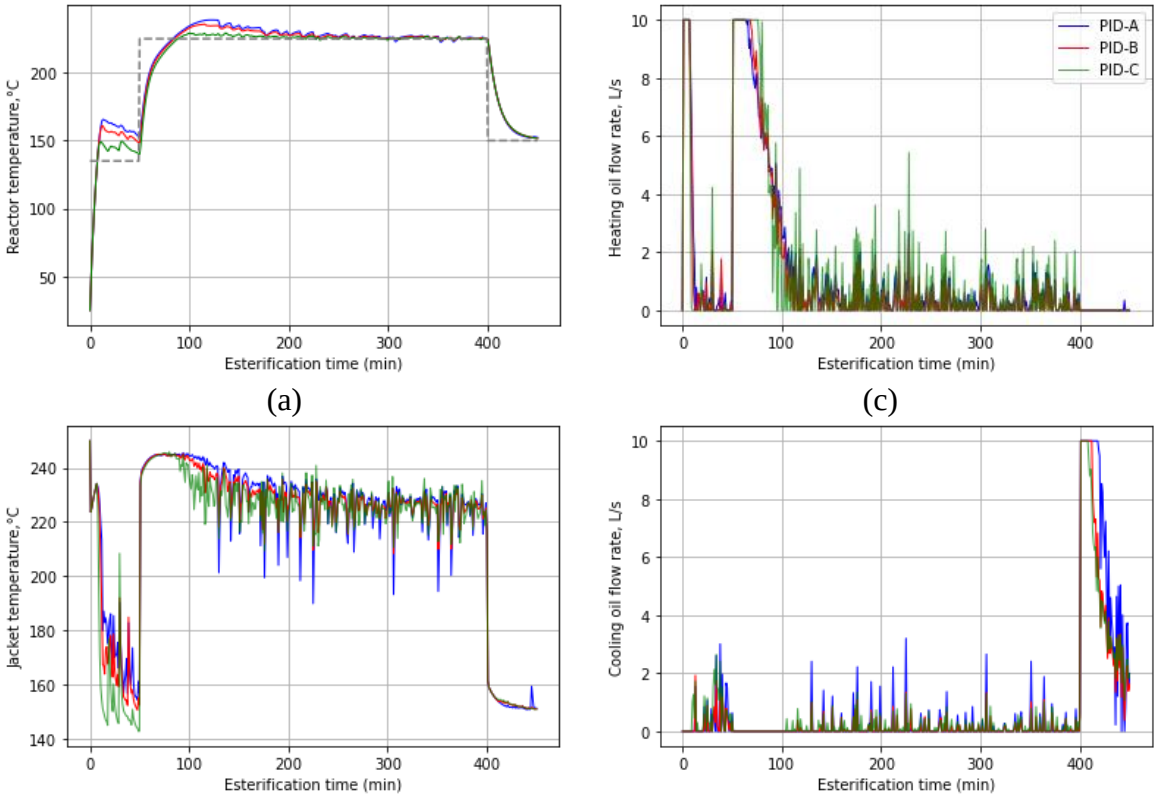

Figure 3-11 (a) Reactor temperature (°C), (b) Jacket temperature (°C), (c) Flow rate of heating oil (L/s), (d) Flow rate of cooling oil (L/s) in esterification process under split range PID control with white noise

doi:10.6342/NTU202302309

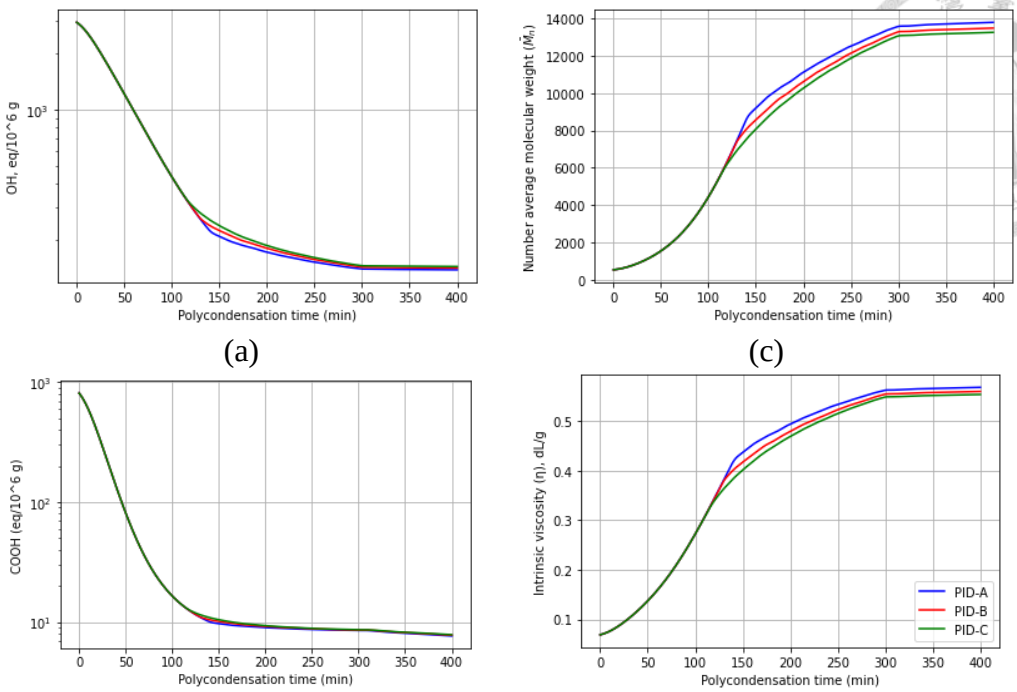

Figure 3-12 (a) OH end group (eq/10^6g), (b) COOH end group (eq/10^6g), (c) Number average molecular weight ($\bar{M}_n$), (d) Intrinsic viscosity (dL/g) during polycondensation process under split range PID control with white noise

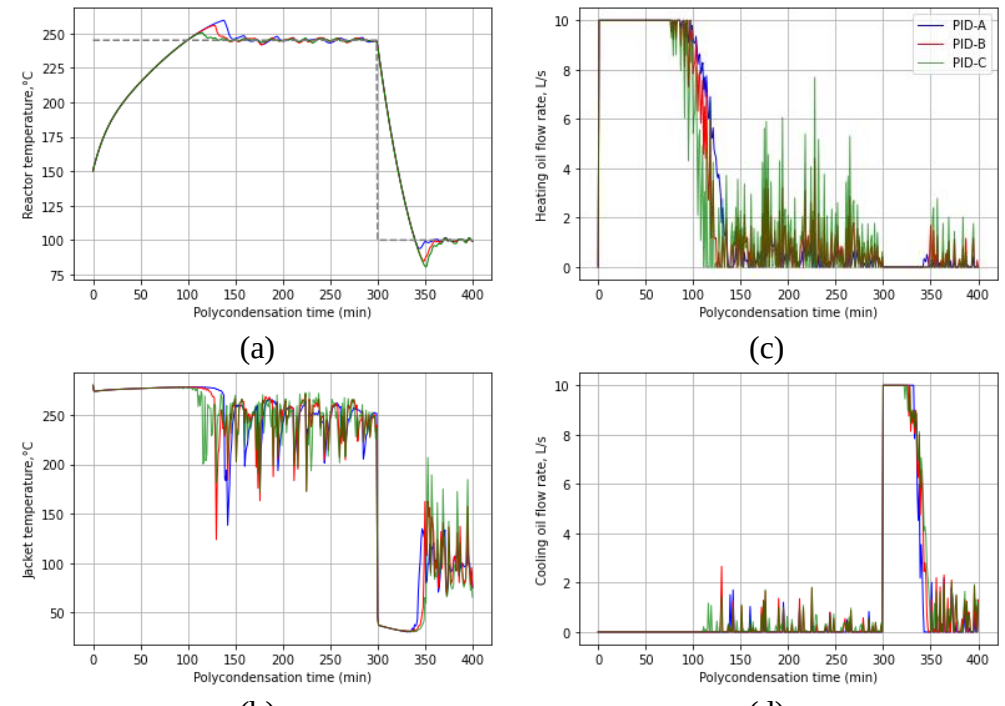

Figure 3-13 (a) Reactor temperature (°C), (b) Jacket temperature (°C), (c) Flow rate of heating oil (L/s), (d) Flow rate of cooling oil (L/s) in polycondensation process under split range PID control with white noise

doi:10.6342/NTU202302309

3.3 MPC control

Model predictive control (MPC) is an advanced control technique that was employed in this research. a multivariable model predictive control technique is carried out to manipulate the heating and cooling oil valve simultaneously with the optimal trajectories under given constraints.

The mathematical process model, as derived in Chapter 2 of this research, is implemented to predict the future state outputs over the prediction horizon (P). The set of manipulated variables in the manipulated horizon (M) is determined by solving a minimization problem based on a given objective function, which is including three terms. The first term represents the deviation of the temperature from the desired setpoint, while the second and third terms correspond to the change of manipulation of the heating oil valve and the cooling oil valve, respectively.

The control action can be effectively tuned by specifying the value of the prediction horizon (P), manipulated horizon (M), and weight matrices in each term of the objective function. A long time in the prediction and manipulated horizon can result in better control performance but requires more time to solve for the optimal set of manipulated variables. In this research, the prediction horizon is proposed to be 10 time steps and the manipulated horizon is 3 time steps were found to be appropriate for both processes. However, determining the exact weight matrices that are optimal for a specific control task cannot be achieved through a systematic method. Generally, a lower value of weight tends to result in a more aggressive control action, which may trigger oscillatory responses in the system. Conversely, a higher weight value leads to a more conservative control action, which may prevent overshooting and guarantee greater stability. Thus, the value of weight matrices should be guided by the control objectives and the characteristics

doi:10.6342/NTU202302309

of the system being controlled.

The weight matrices were chosen based on careful consideration of process characteristics to achieve stable and effective control. The weight matrices for the esterification process are setpoint deviation term (1), heating oil valve term (20), and cooling oil valve term (20). For the polycondensation process are setpoint deviation term (1), heating oil valve term (50), and cooling oil valve term (50).

Objective function:

$$\min_{u(k)\ \ldots\ u(k+M-1)} \sum_{i=k+1}^{k+P} w_{sp}(T_{sp} - T_r(t))^2 + w_{Fheat}(\Delta u_{Fheat})^2 + w_{Fcool}(\Delta u_{Fcool})^2 \tag{3-3}$$

While $u = \begin{bmatrix} u_{Fheat} \\ u_{Fcool} \end{bmatrix}$ and $0 \leq u_{Fheat} \leq 10,\ 0 \leq u_{Fcool} \leq 10$

w_{sp}	Weight matrix of deviation of setpoint term
w_{Fheat} and w_{Fcool}	Weight matrix of heating oil valve and cooling oil valve
P and M	Prediction and Manipulated horizon
T_{sp}	Temperature setpoint
T_r	Reactor temperature
u	Manipulated variables
k	Present time

doi:10.6342/NTU202302309

3.3.1 Nominal case

Table 3-5 IAE performance criteria comparison of esterification and polycondensation process under MPC control

Process	IAE	Time (s)
Esterification	1880.69	122.22
Polycondensation	6425.58	45.44

Efficient temperature setpoint tracking throughout the esterification process for preheating, heating, and cooling phases is achieved through multivariable model predictive control, enabling the reactor temperature of the process to reach setpoints without overshoot and offset, as depicted in Figure 3-15a. The IAE performance criteria was 1880.69, and the simulation took 122.22 seconds to generate the entire result.

This control strategy has also demonstrated a good performance in the polycondensation process with an IAE of 6425.58, as shown in Figure 3-17a. The temperature reached the setpoint of 245°C at 105 minutes without overshoot and offset, and was then isothermally controlled for 200 minutes, followed by a cooling procedure at 305 minutes to reduce the temperature down to 100°C. The final molecular weight was recorded after the operation to be 13,257.23 and viscosity was 0.55 dL/g. The results were taken 45.44 seconds to generate the entire simulation.

Model predictive control approach shows a relatively higher control performance compared to the split range PID control technique for all split range arrangements as lower IAE values. This control technique has been successful in addressing control issues that occurred in the processes under feed-back control such as a large overshoot and slow setpoint tracking, which can affect final product quality. Moreover, the utility consumptions were lesser than split range PID control.

doi:10.6342/NTU202302309

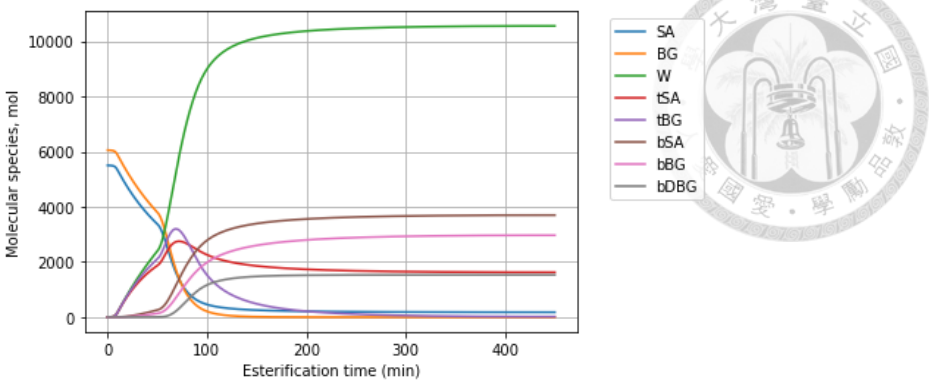

Figure 3-14 Molecular species profile in esterification process under MPC control

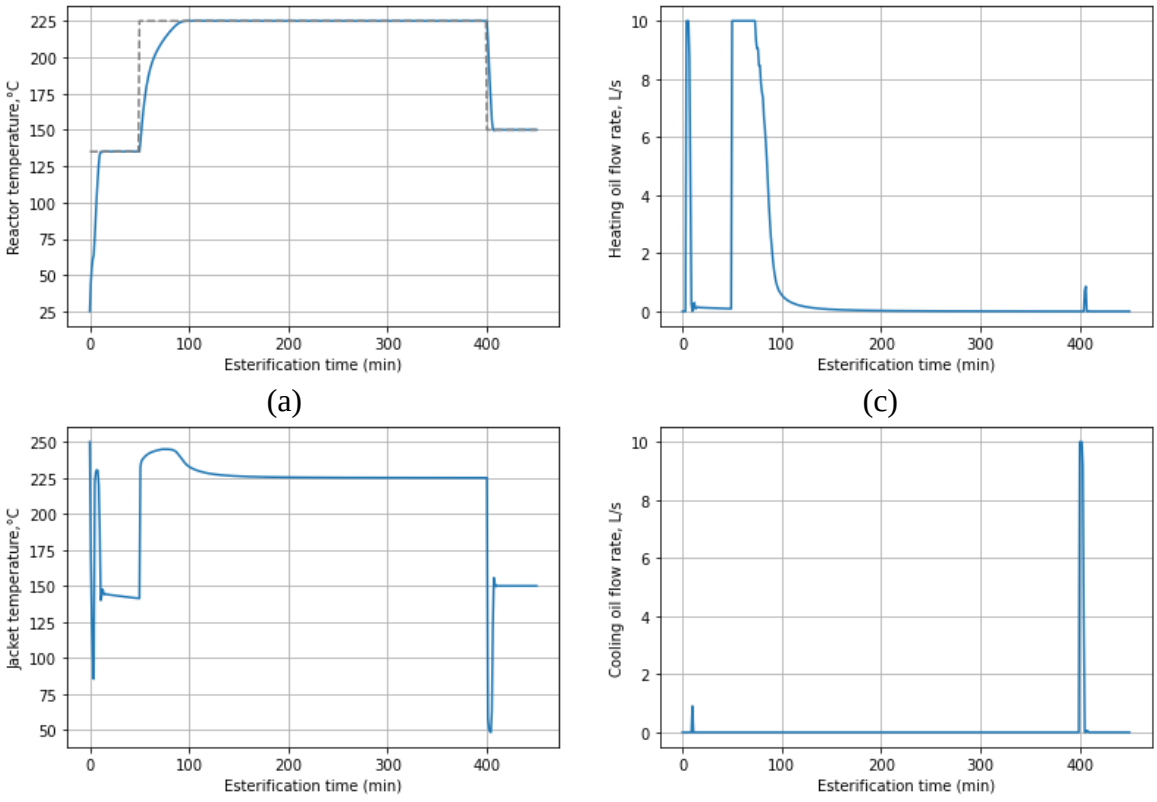

Figure 3-15 (a) Reactor temperature (°C), (b) Jacket temperature (°C), (c) Flow rate of heating oil (L/s), (d) Flow rate of cooling oil (L/s) in esterification process under MPC control

doi:10.6342/NTU202302309

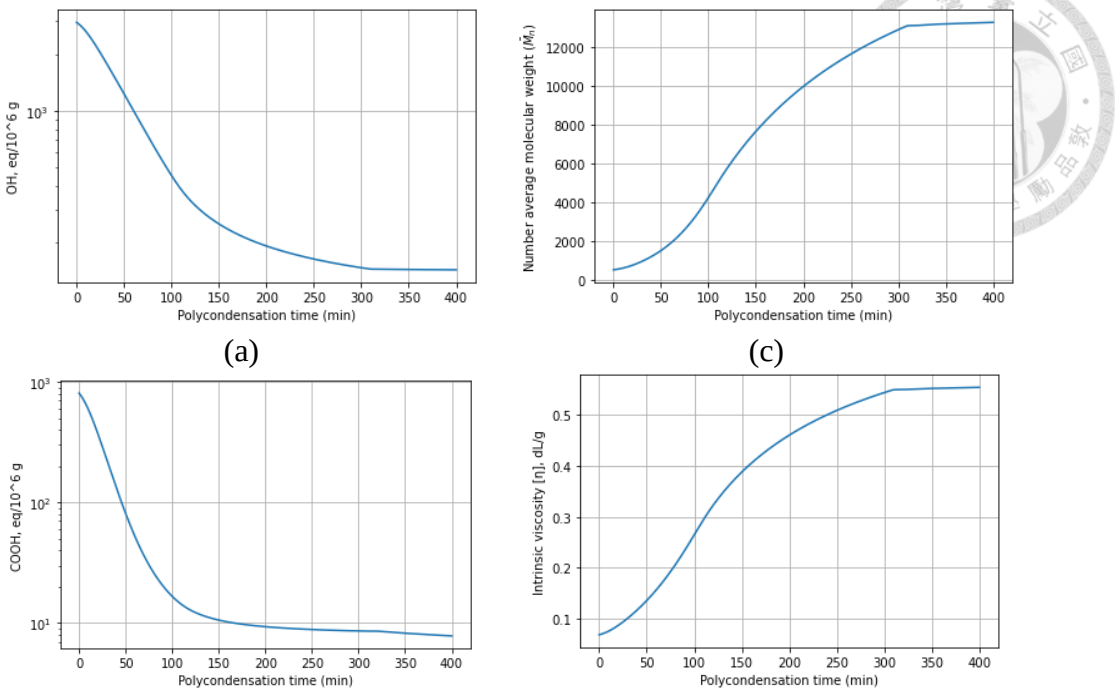

Figure 3-16 (a) OH end group (eq/10^6g), (b) COOH end group (eq/10^6g), (c) Number average molecular weight ($\bar{M}_n$), (d) Intrinsic viscosity (dL/g) during polycondensation process under MPC control

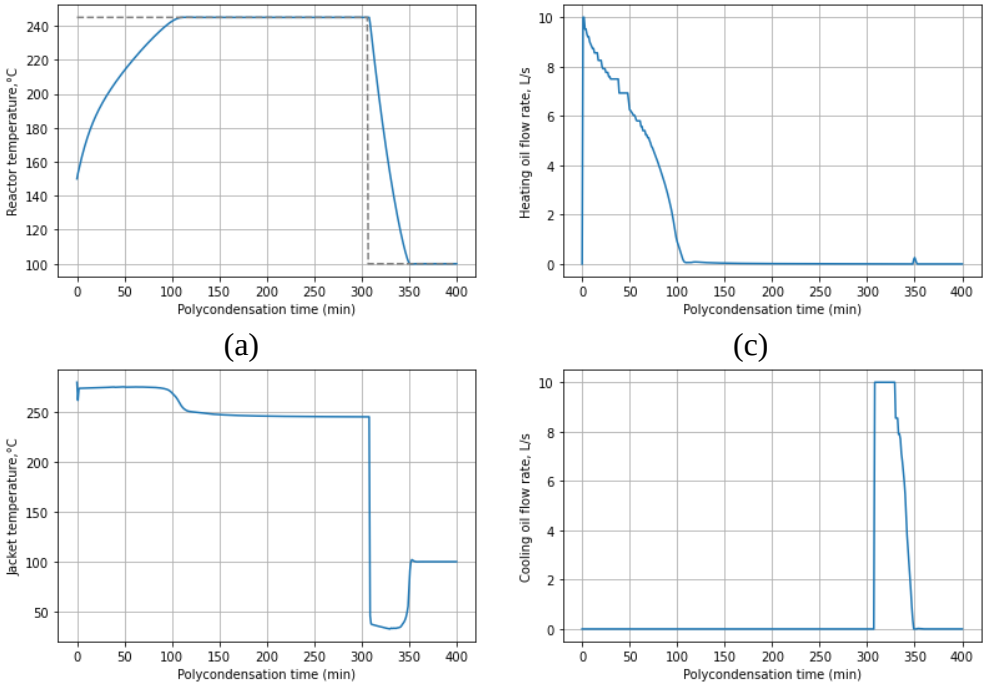

Figure 3-17 (a) Reactor temperature (°C), (b) Jacket temperature (°C), (c) Flow rate of heating oil (L/s), (d) Flow rate of cooling oil (L/s) in polycondensation process under MPC control

doi:10.6342/NTU202302309

3.3.2 White noise case

Table 3-6 IAE performance criteria comparison of esterification and polycondensation process under MPC control

Process	IAE	Time (s)
Esterification	2472.37	364.61
Polycondensation	6806.14	121.62

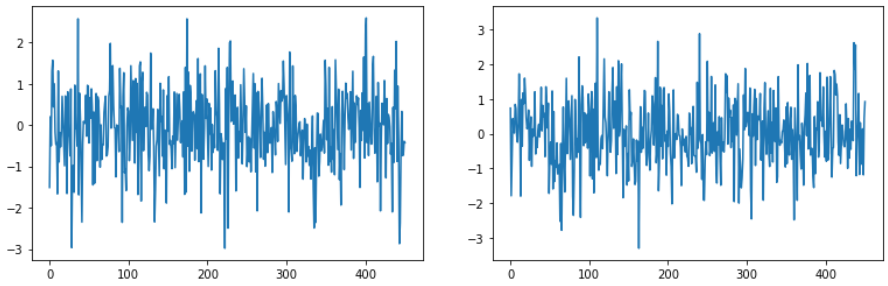

(a) (b)

Figure 3-18 The set of white noise interferes with the reactor temperature, (b)The set of white noise interferes with the jacket temperature

In the simulation with noise interference, two sets of white noise were randomly generated at all time steps (450 minutes) with zero mean and a standard deviation of 1, resulting in a maximum deviation of roughly ±3°C from the actual value in order to corrupt the measurement of the reactor and jacket temperature before sending to the optimizer to perform computation as shown in Figure 3-18a and 3-18b.

The results of the study demonstrate the MPC strategy was able to efficiently track the reactor temperature setpoint and maintain isothermal control for all stages even when the process encountered white noise. This highlights the robustness and effectiveness of the MPC approach in regulating complex polymerization processes subject to noise and disturbance. However, the simulation time increased significantly for almost three times longer than the nominal case for both esterification and polycondensation processes. This was attributed to the fluctuation of temperature after the measurement, which complicated the task of the optimizer.

doi:10.6342/NTU202302309

In esterification process (the IAE value was 2472.37), the temperature was controlled to reach the setpoint of 225°C in the heating phase at 90 minutes as shown in Figure 3-20. For polycondensation process, the temperature reached the setpoint of 245°C at 105 minutes (Figure 3-22). The reactor temperature of both processes reached the setpoint at the similar time as nominal case even white noise corrupted the control operation. The number average molecular weight and intrinsic viscosity were observed after the operation to be 13259.41 and 0.55 dL/g, respectively as shown in Figures 3-22c and 3-22d. These values are similar to the nominal case, this reflects the effectiveness and robustness of MPC control in chemical processes.

The result of the simulations indicates that during the isothermal control with white noise interference for both processes, the control action of the heating and cooling oil valve showed a lesser aggressive action than split range PID control (C arrangement) as depicted in Figures 3-11c and 3-11d for esterification process, and 3-13c and 3-13d for polycondensation process. While the MPC's optimizer was able to effectively reduce the aggressiveness of the control action, it was found that increasing the weighting matrices of the valves led to a more conservative approach. however, resulted in slower attainment of the setpoint of the controlled variable.

doi:10.6342/NTU202302309

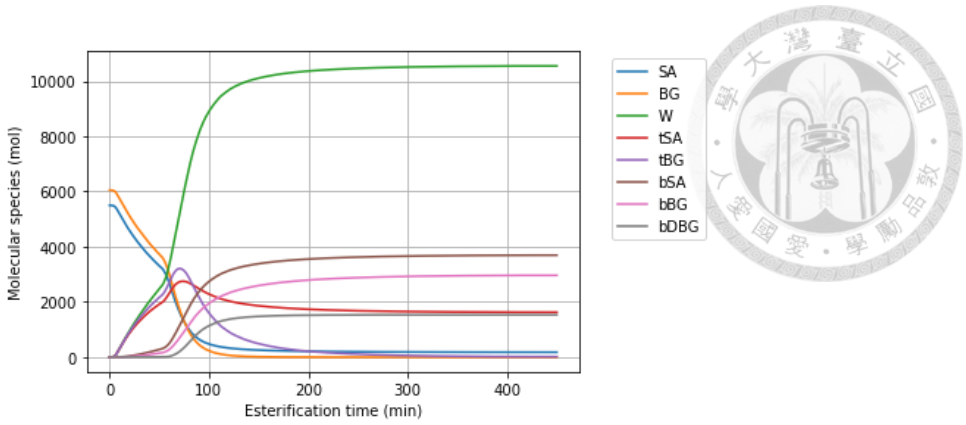

Figure 3-19 Molecular species profile in esterification process under MPC control with white noise

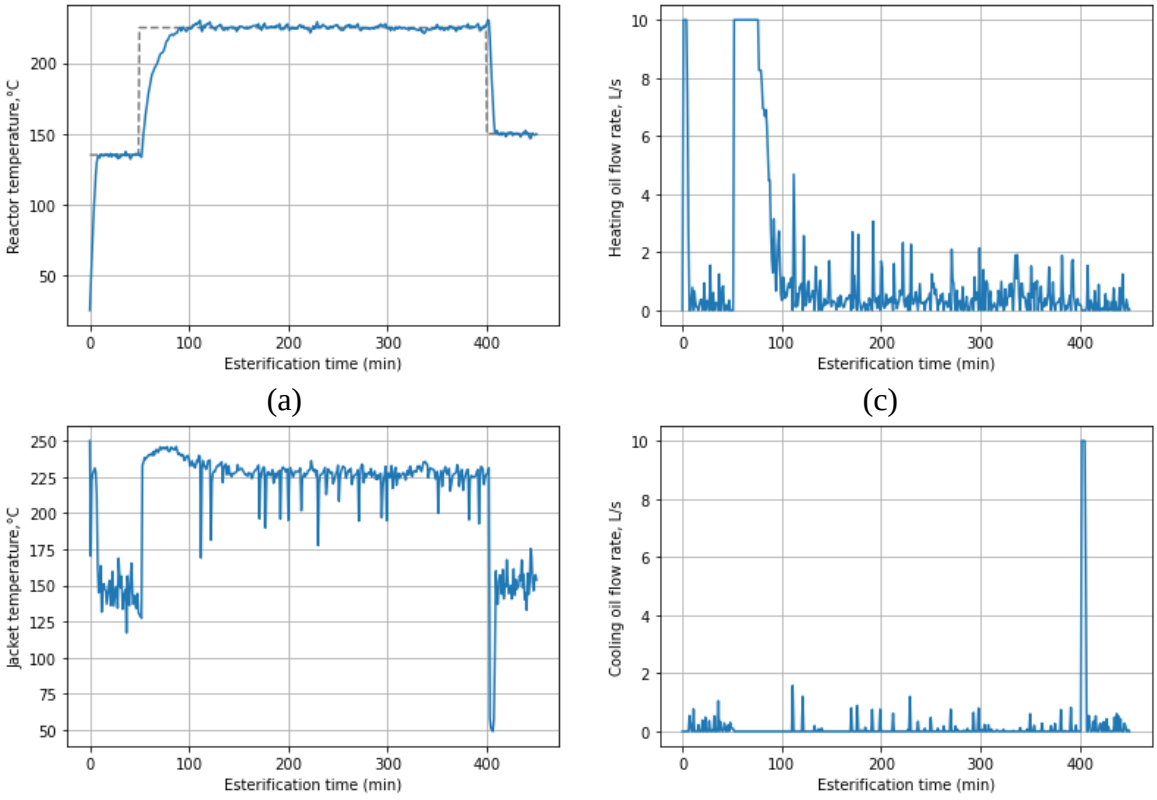

Figure 3-20 (a) Reactor temperature (°C), (b) Jacket temperature (°C), (c) Flow rate of heating oil (L/s), (d) Flow rate of cooling oil (L/s) in esterification process under MPC control with white noise

doi:10.6342/NTU202302309

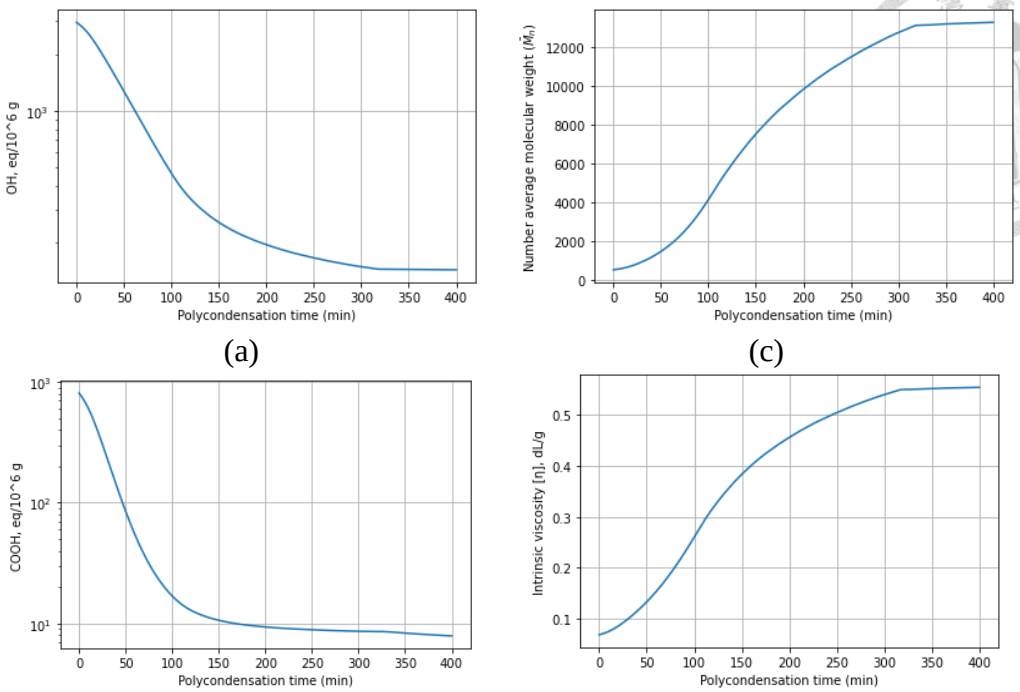

Figure 3-21 (a) OH end group (eq/10^6g), (b) COOH end group (eq/10^6g), (c) Number average molecular weight ($\bar{M}_n$), (d) Intrinsic viscosity (dL/g) during polycondensation process under MPC control with white noise

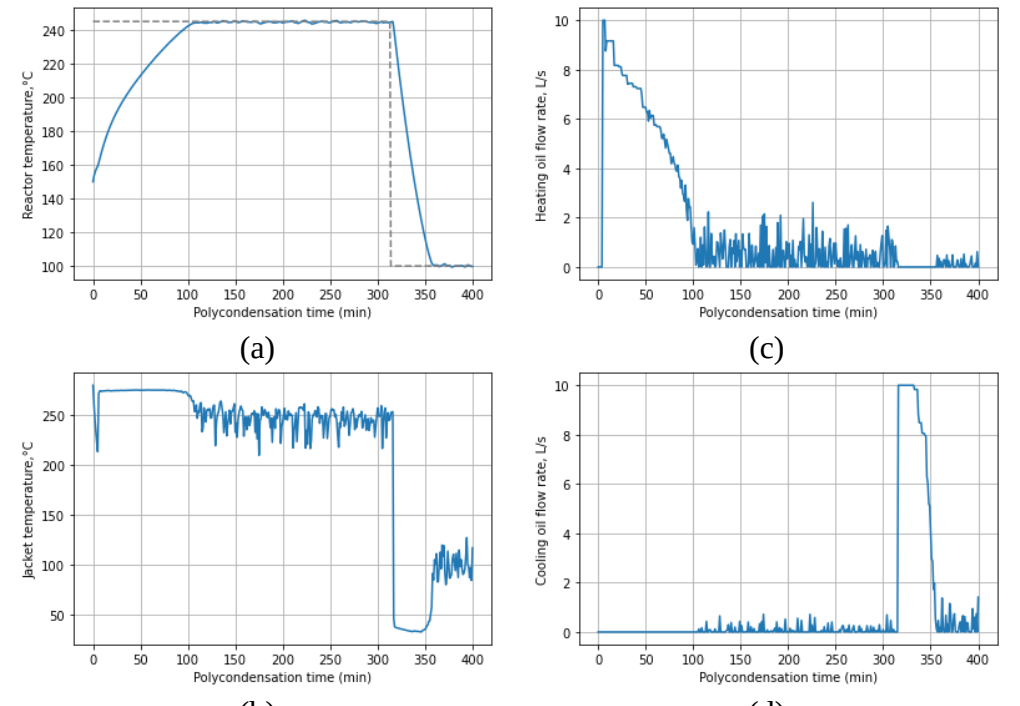

Figure 3-22 (a) Reactor temperature (°C), (b) Jacket temperature (°C), (c) Flow rate of heating oil (L/s), (d) Flow rate of cooling oil (L/s) in polycondensation process under MPC control with white noise

doi:10.6342/NTU202302309

3.3.3 Model mismatch case

Table 3-7 IAE performance criteria comparison of esterification and polycondensation process under MPC control with model mismatch

Process	IAE	Time (s)
Esterification	3009.59	128.74
Polycondensation	10160.21	53.88

In the actual process, a well-formulated mathematical model may deviate from the process after a period of operation, Therefore, in this research uncertainty events involving model mismatch are considered. The overall heat transfer coefficient of esterification unit of 545 W/m^2°C and polycondensation unit of 200 W/m^2°C were reduced by 30% to simulate fouling in both reactors after a long period of processing to study the robustness of the control.

The esterification process, the dynamic response of the reactor temperature control for the model mismatch case under MPC takes a longer time to reach the setpoint of 225°C (approximately 15 minutes) as shown in Figure 3-24a resulting in a higher IAE of 3009.59 compared to the nominal case because of the lower heat transfer capability of the process. Despite a large difference between the process and the model, the controllers still show efficient control performance.

In polycondensation process, the reactor temperature was able to reach the setpoint of 245°C at 144 minutes which was 33 minutes slower than the nominal case as shown in Figure 3-26a. The cooling down procedure to 100°C was also impacted due to model mismatch. Specifically, the nominal case took 49 minutes to complete the cooling process, while the model mismatch caused a delay of 18 minutes, resulting in a total time of 67 minutes to reach the setpoint. The final molecular weight and viscosity were 13669.66 and 0.56 dL/g.

doi:10.6342/NTU202302309

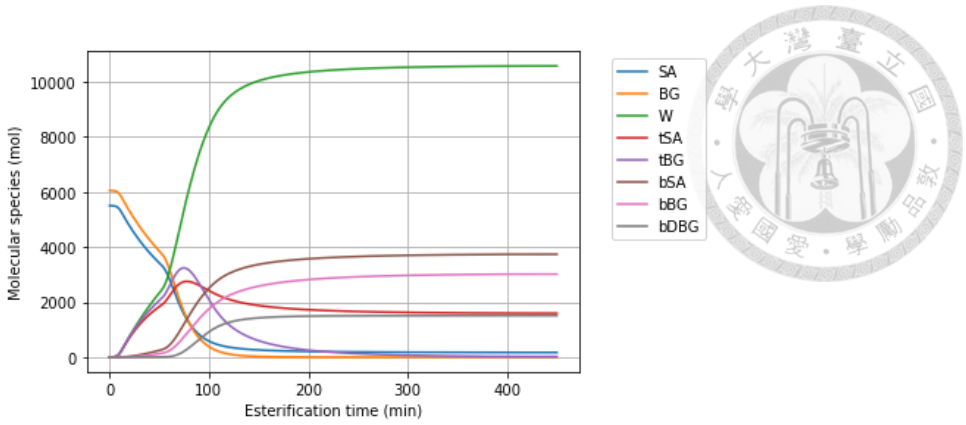

Figure 3-23 Molecular species profile in esterification process under MPC control with model mismatch

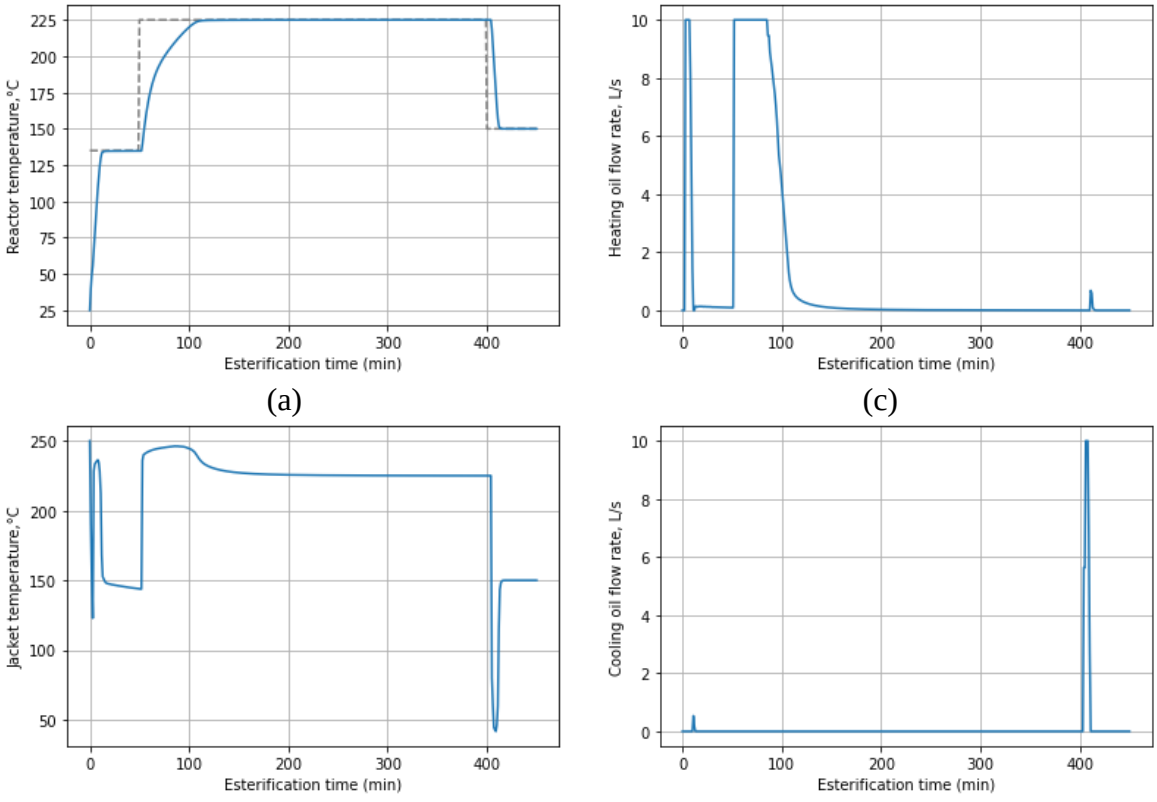

Figure 3-24 (a) Reactor temperature (°C), (b) Jacket temperature (°C), (c) Flow rate of heating oil (L/s), (d) Flow rate of cooling oil (L/s) in esterification process under MPC control with model mismatch

doi:10.6342/NTU202302309

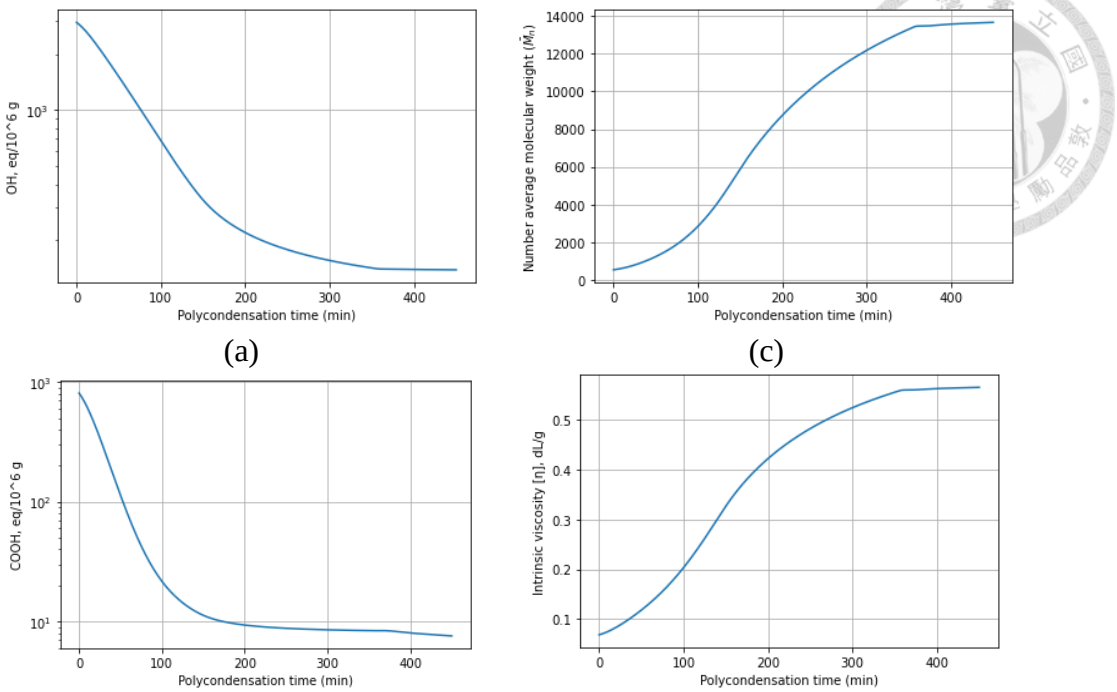

Figure 3-25 (a) OH end group (eq/10^6g), (b) COOH end group (eq/10^6g), (c) Number average molecular weight ($\bar{M}_n$), (d) Intrinsic viscosity (dL/g) during polycondensation process under MPC control with model mismatch

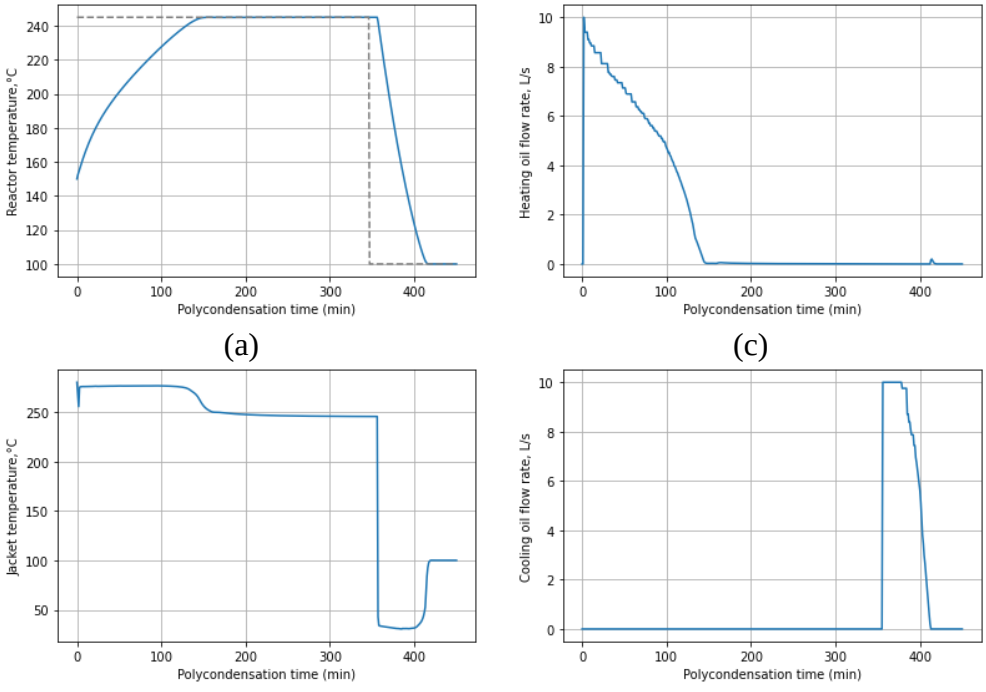

Figure 3-26 (a) Reactor temperature (°C), (b) Jacket temperature (°C), (c) Flow rate of heating oil (L/s), (d) Flow rate of cooling oil (L/s) in polycondensation process under MPC control with model mismatch

doi:10.6342/NTU202302309

3.4 NNMPC control

A neural network model was deployed in model predictive control (MPC) and used a similar objective function as used in the first principle model predictive control for the optimization procedure. The NN model complexity is the crucial factor that affects prediction accuracy. Therefore, the neural network models with 2 hidden layers and a range of neurons in each hidden layer from 20, 50, 100, and 200 neurons were trained and deployed to simulate the process in several scenarios such as nominal case, the presence of white noise case, and model mismatch case in order to investigate the most appropriate complexity that provides a high control performance with good robustness.

To ensure that the control actions remained comparable, the MPC tuning parameters, such as the horizons and the weight matrices, were to be similar to those used in MPC. This allowed us to study the process dynamics under equivalent control actions. Specifically, the prediction horizon and manipulated horizon were set at 10 and 3 time steps, respectively. For the weight matrices of the esterification process, the setpoint deviation term was set at 1, while the heating oil valve and cooling oil valve terms were set to 20. Meanwhile, in the polycondensation process, the setpoint deviation term was set at 1, while the heating oil valve and cooling oil valve terms were set to 50.

3.4.1 Neural network model training and validation

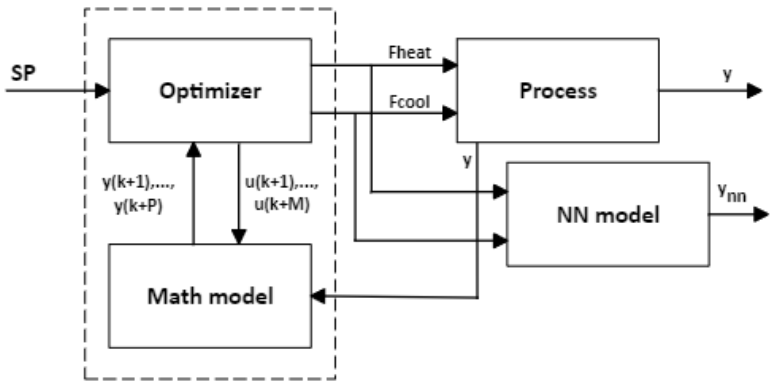

Figure 3-27 MPC structure for NN model validation

doi:10.6342/NTU202302309

50 sets of simulation data in each process were generated from a mathematic model based predictive controller to random set points. 80% of the data were randomly selected by the train-test split function, therefore, 40 sets were training data sets, 8 sets were prepared for validation, and the last 2 sets were testing data set.

After neural network models of each process are successfully trained, it is essential to validate their accuracy by testing models outside of the training data set to investigate the controllability while driving the controlled variable to the setpoints outside training data. This is accomplished by process dynamic testing (the validation structure is illustrated in Figure 3-27), the process model is represented by ordinary differential equations, whereby both optimal inputs (heating and cooling oil flow rate) are sent from mathematic model based predictive control to the process model and neural network model. During validation proceeded the actual values of the process were sent to update to the neural network model in every 10 time steps following the prediction horizon length.

The trained neural network model was validated across three different setpoints following the unique of the setpoints in the testing set. In esterification process, the process was heated up to 189°C, then isothermally controlled at 162°C, then cooled down to 59°C. While polycondensation model was validated by cooling down and controlling the temperature at 117°C for the first stage and then heating up to 235°C in the consequence step. Then, both results from process and neural network model were compared with the neural network model by using mean square error (MSE) as shown in Eq.3-4.

$$MSE = \frac{1}{n}\sum_{k=1}^{n}(y_k - y_{nn_k})^2 \tag{3-4}$$

y_k State variables from mathematical process model

y_{nn_k} State variables from NN model

doi:10.6342/NTU202302309

Table 3-8 Mean square error of different NN structure

Neural network structures	Mean square error (MSE)	
	Esterification	Polycondensation
20 neurons	18.896	1.298
50 neurons	4.958	0.904
100 neurons	13.250	57.890
200 neurons	21.366	20.518

The validation results of the esterification neural network model are indicated in Table 3-8, it reveals that 50 neuron NN structure had a good performance with low MSE value of 4.958, the neural network model with 100 neurons also performed well, with an MSE of 13.250. The result from both NN models could track the process result efficiently, however, the are slightly accumulated error at particular durations as shown in Figure 3-29 and 3-30. On the other hand, the NN structure with 20 and 200 neurons showed a lower performance in reaching the test setpoint as shown in Figure 28 and 31, with the MSE of 18.896 and 21.366, respectively.

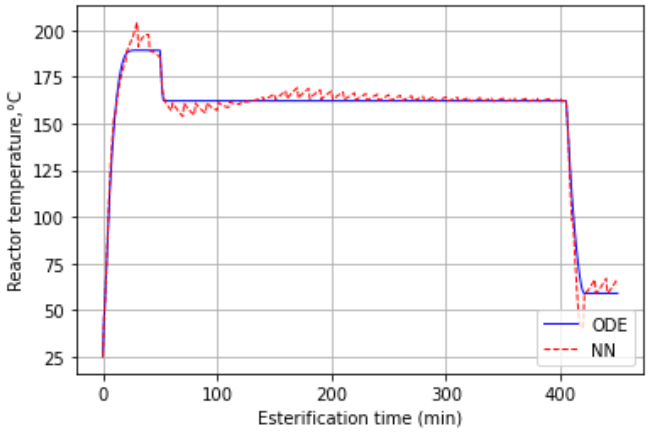

Figure 3-28 Esterification NN model validation result (12 – 20 – 20 – 10)

doi:10.6342/NTU202302309

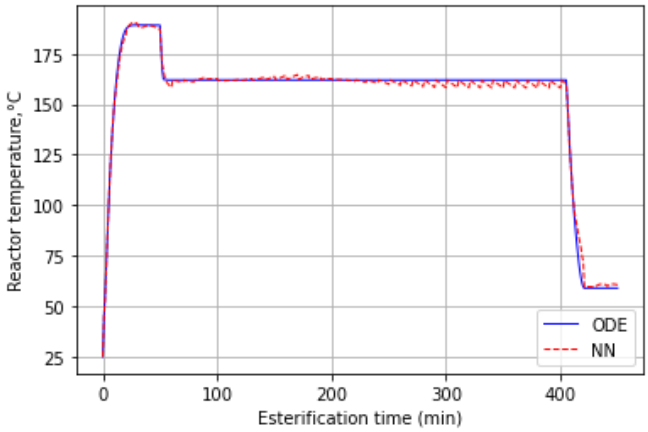

Figure 3-29 Esterification NN model validation result (12 – 50 – 50 – 10)

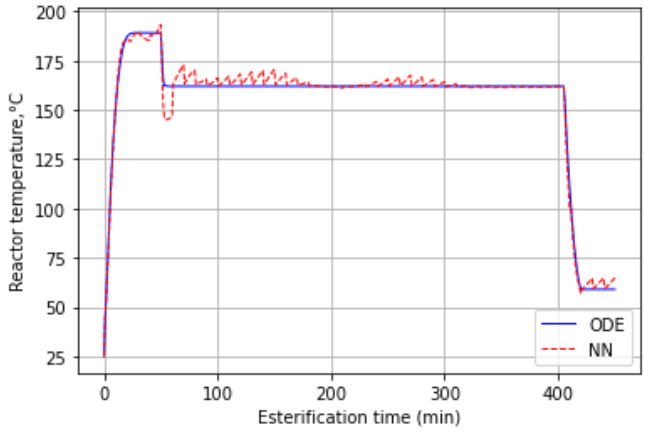

Figure 3-30 Esterification NN model validation result (12 – 100 – 100 – 10)

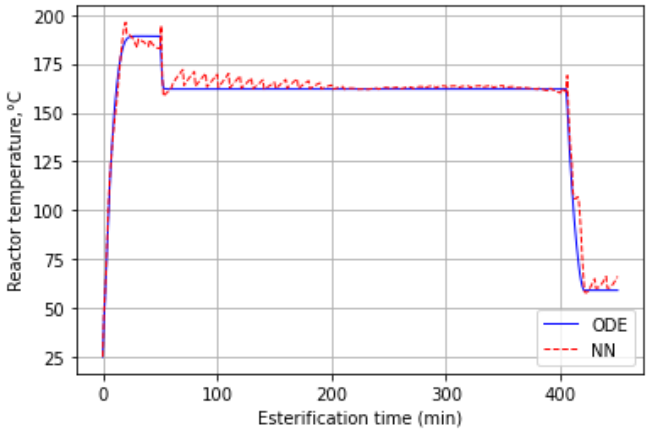

Figure 3-31 Esterification NN model validation result (12 – 200 – 200 – 10)

doi:10.6342/NTU202302309

In the section of polycondensation process, 20 and 50 neuron NN structure were deployed in validation procedure, it was found that the smaller size of NN structure is trend to be efficient due to the lower number of inputs as the MSE value of 1.298 and 0.904, respectively. The 100 and 200 neuron NN structure, the exceeded complexity of NN structure led to the declined of the control performance. the NN output for reactor temperature was unable to track the result from the ODE in the isothermal temperature control in some particular periods. Therefore, the MSE values are remarkably higher than the smaller structures.

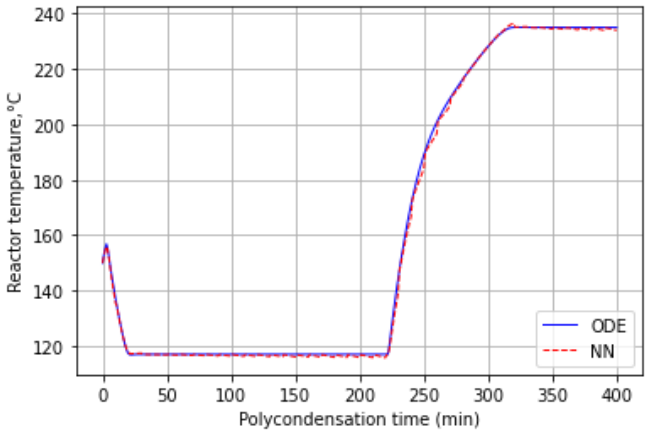

Figure 3-32 Polycondensation NN model validation result (12 – 20 – 20 – 10)

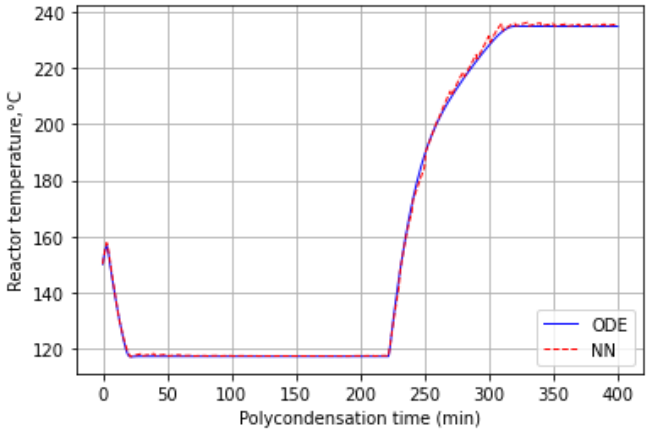

Figure 3-33 Polycondensation NN model validation result (12 – 50 – 50 – 10)

doi:10.6342/NTU202302309

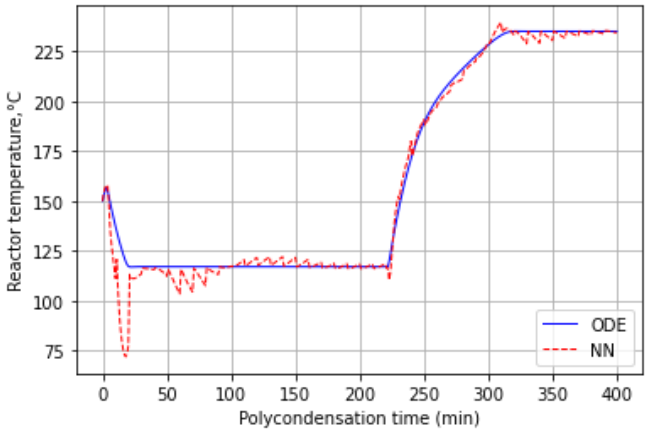

Figure 3-34 Polycondensation NN model validation result (12 – 100 – 100 – 10)

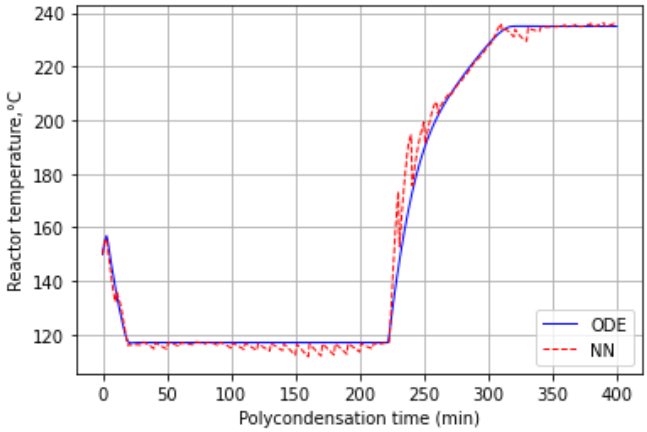

Figure 3-35 Polycondensation NN model validation result (12 – 200 – 200 – 10)

doi:10.6342/NTU202302309

3.4.2 Nominal case

Table 3-9 IAE performance criteria and simulation time under various NNMPC controller in esterification and polycondensation processes

	NNMPC				MPC
	20	**50**	**100**	**200**	
Esterification process					
IAE	2418.45	2104.77	2208.10	2734.14	1880.69
Time (s)	13.45	16.61	16.67	29.56	122.22
Polycondensation process					
IAE	8535.75	7239.28	7904.65	9107.39	6425.58
Time (s)	16.62	19.05	21.80	53.68	45.44

In both processes, all NN architectures in NNMPC performed a lower performance than mathematic model based MPC because the process is assumed to be represented by ordinary differential equations as the model in MPC optimizer. Therefore, the model is 100% matching the process leading to the highest control performance throughout all controllers.

The least complex 20 neuron NN structure showed a low performance as a result of insufficient complexity of the NN structure leading to a lower prediction accuracy of the model. The esterification process is shown in Figure 3-37, the temperature was regulated to the setpoint of 135°C in preheating phase with an offset of around 2°C. Afterward, the temperature was gradually increased to the synthesis temperature setpoint of 225°C at 154 minutes. In polycondensation process under 20 neuron NNMPC is shown in Figure 3-39, the temperature was controlled to reach the setpoint of 245°C with highly conservative action resulting in a high IAE of 8535.75.

The 50 neuron and 100 neuron NNMPC controllers demonstrated exceptional temperature control capabilities in the esterification process provided a low IAE value of

doi:10.6342/NTU202302309

2104.77 and 2208.10, respectively. The setpoints were reached in all stages without any offset as shown in Figures 3-41a and 3-45a. The isothermal control of 225°C during the heating phase was achieved in a remarkably short time of around 115 minutes, which is faster than 20 neuron NNMPC by up to 39 minutes. Additionally, the heating and cooling oil utilities were more sufficiently consumed compared to the process under MPC control. A similar trend is also found in the polycondensation process that showed an IAE value of 7239.28 when the process under 50 neuron NNMPC, the reactor temperature was regulated to the synthesis setpoint of 245°C, which reached the setpoint at 120 minutes. The heating oil valve regulated by 100 neuron NNMPC performed an aggressive action at the beginning, leading to reaching the target setpoint slightly slower as shown in Figure 3-47c.

When using the highest neural network model complexity, with 200 neurons in both the esterification and polycondensation processes, the highest IAE value was observed among the varied models tested, at 2734.14 and 9107.39, respectively. The high complexity caused overfitting, resulting in lower control performance.

The simulation time of the NNMPCs is significantly lower than the first principle MPC. The length of simulation time is highly influenced by the complexity of the NN model as indicated in Table 3-9, which in turn affects the optimization process that is carried out at each time step. In particular, the first principle MPC took 122.22 seconds, while the 20 neuron NNMPC required only 13.45 seconds to complete the simulation. The NNMPCs are a highly efficient and promising approach for carrying out complex simulations, with considerably reduced computational time.

doi:10.6342/NTU202302309

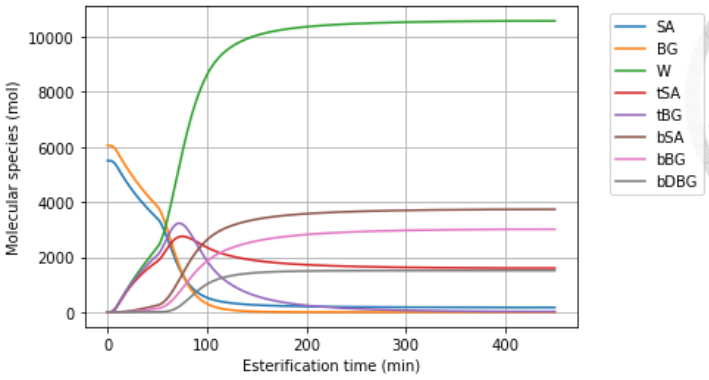

Figure 3-36 Molecular species profile in esterification process under 20 neuron NNMPC control

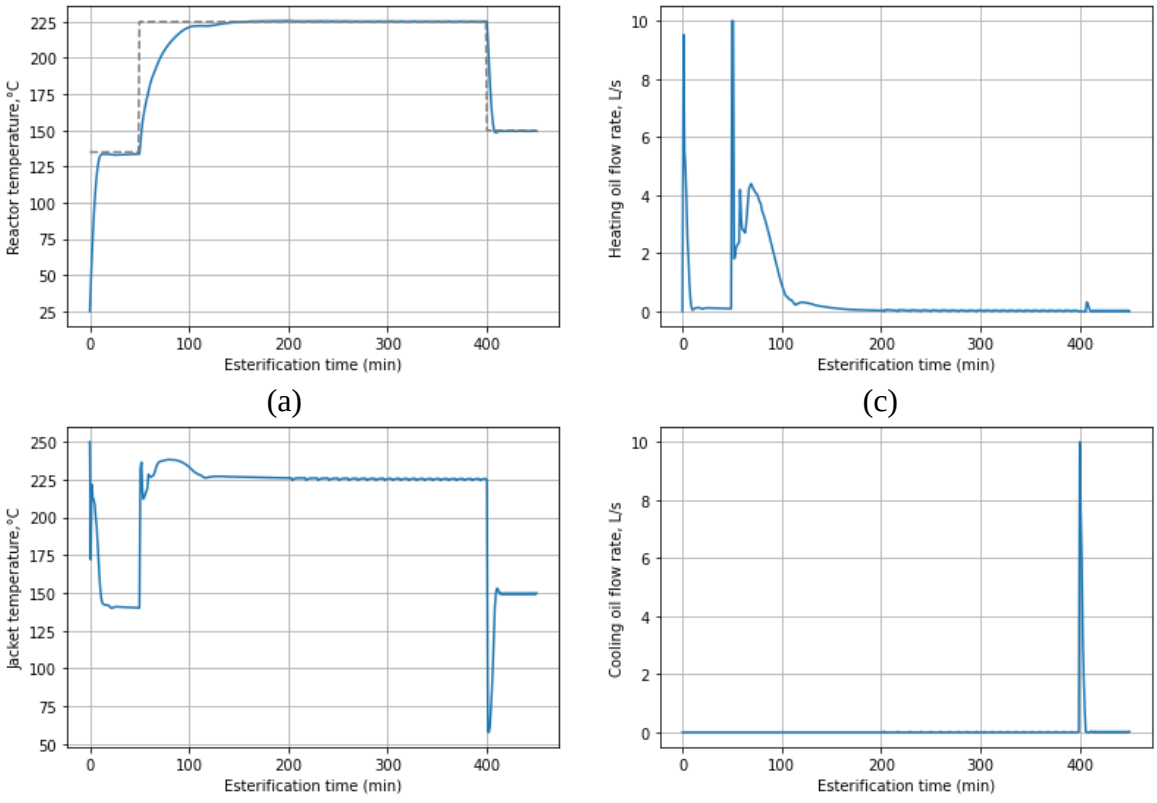

Figure 3-37 (a) Reactor temperature (°C), (b) Jacket temperature (°C), (c) Flow rate of heating oil (L/s), (d) Flow rate of cooling oil (L/s) in esterification process under 20 neuron NNMPC control

doi:10.6342/NTU202302309

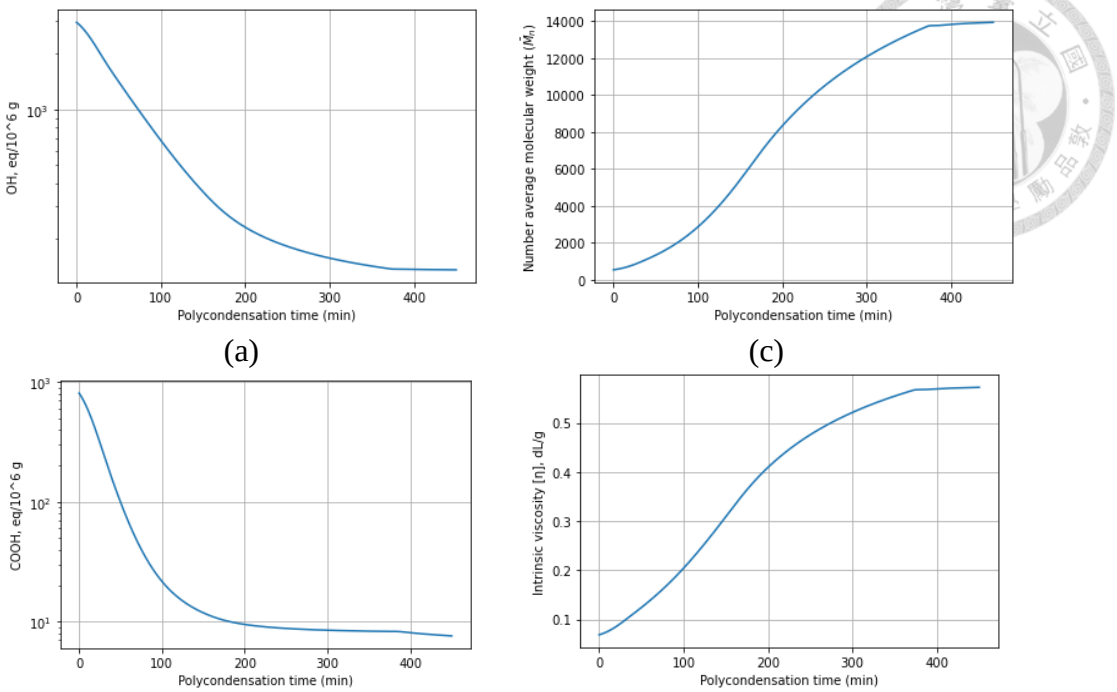

Figure 3-38 (a) OH end group (eq/10^6g), (b) COOH end group (eq/10^6g), (c) Number average molecular weight ($\bar{M}_n$), (d) Intrinsic viscosity (dL/g) during polycondensation process under 20 neuron NNMPC control

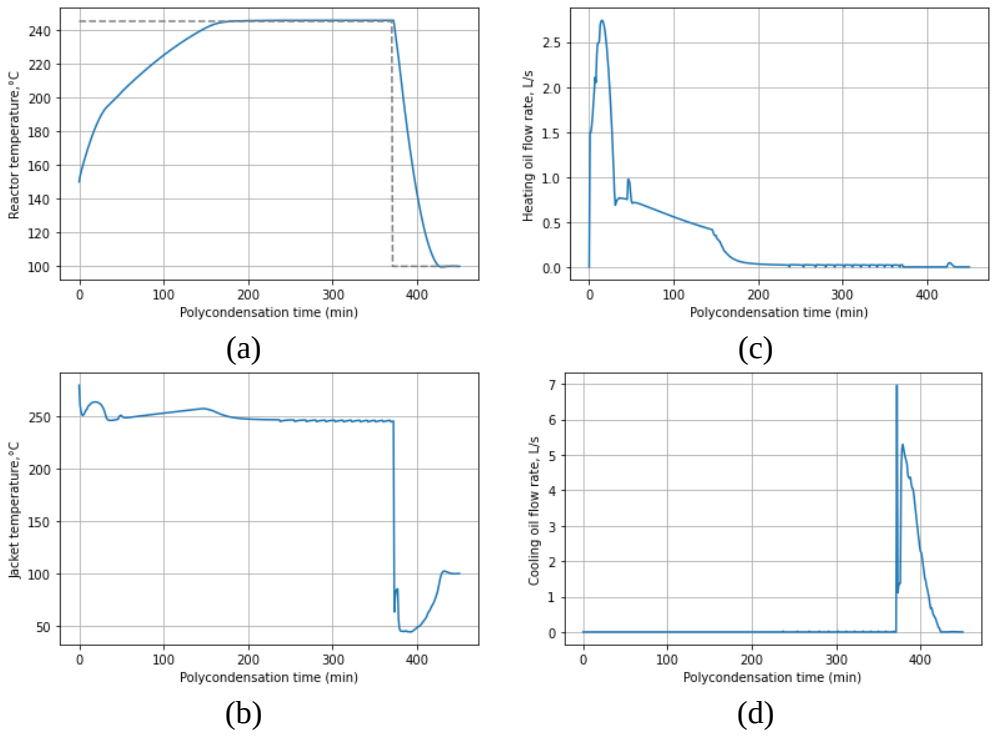

Figure 3-39 (a) Reactor temperature (°C), (b) Jacket temperature (°C), (c) Flow rate of heating oil (L/s), (d) Flow rate of cooling oil (L/s) in polycondensation process under 20 neuron NNMPC control

doi:10.6342/NTU202302309

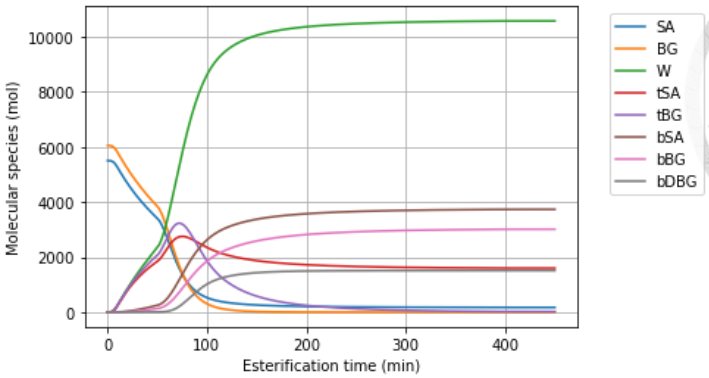

Figure 3-40 Molecular species profile in esterification process under 50 neuron NNMPC control

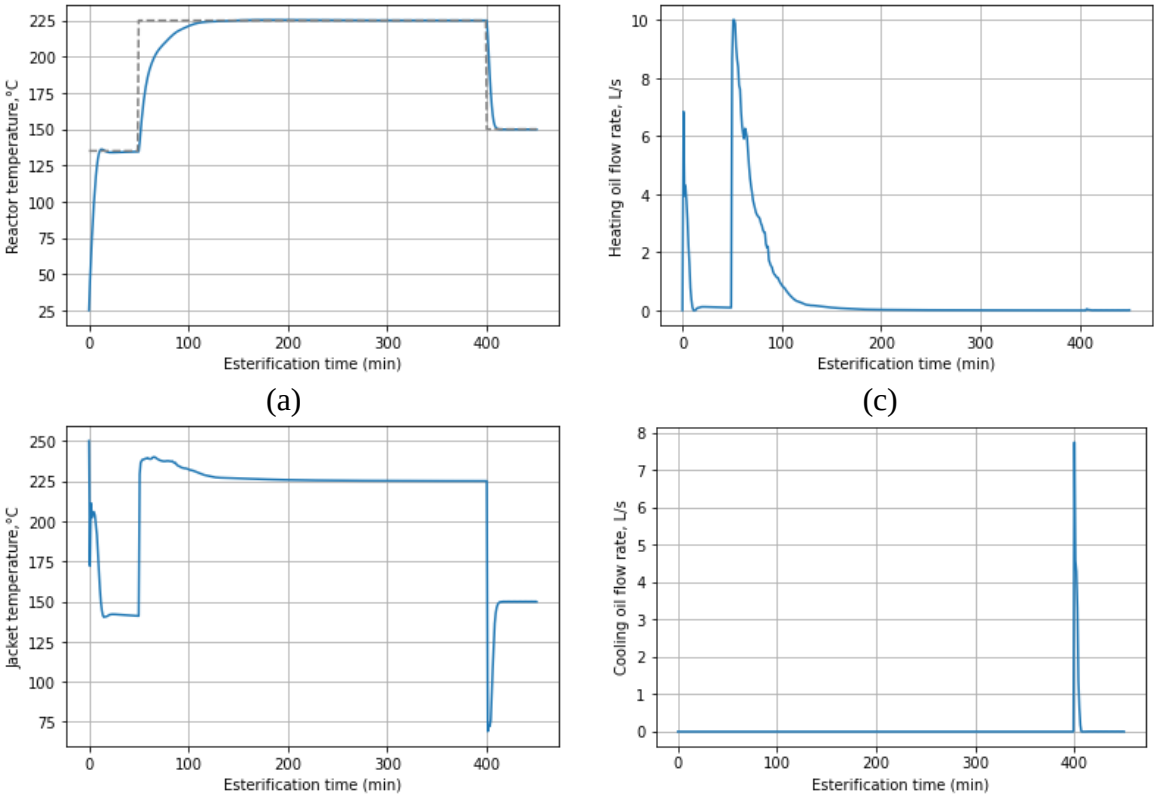

Figure 3-41 (a) Reactor temperature (°C), (b) Jacket temperature (°C), (c) Flow rate of heating oil (L/s), (d) Flow rate of cooling oil (L/s) in esterification process under 50 neuron NNMPC control

doi:10.6342/NTU202302309

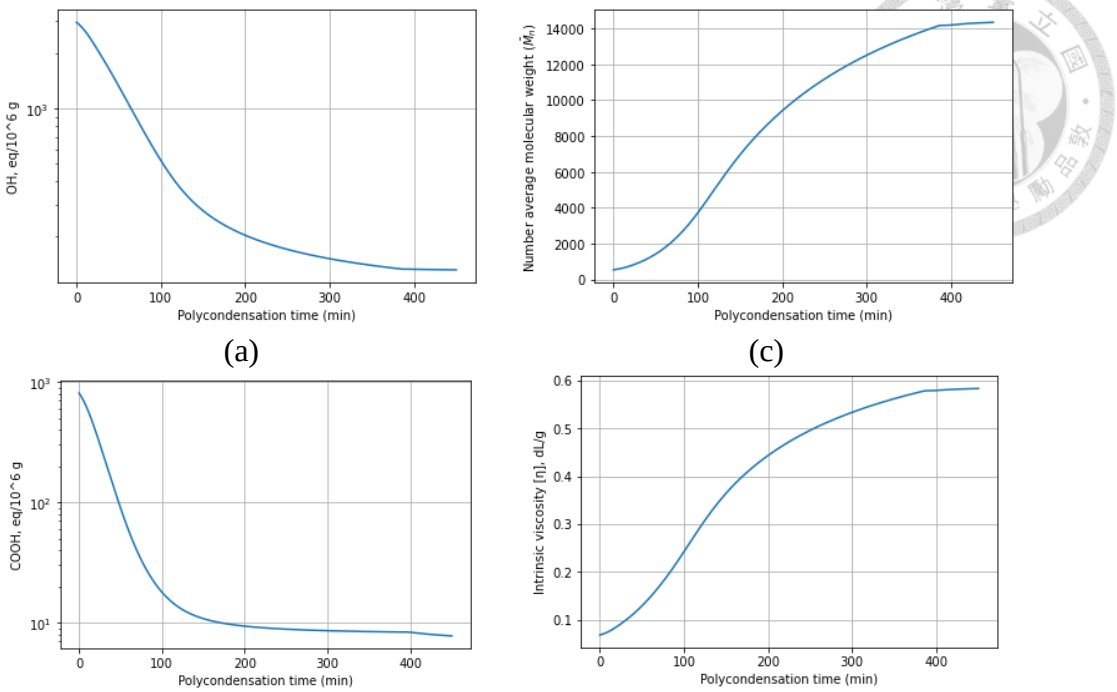

Figure 3-42 (a) OH end group (eq/10^6g), (b) COOH end group (eq/10^6g), (c) Number average molecular weight ($\bar{M}_n$), (d) Intrinsic viscosity (dL/g) during polycondensation process under 50 neuron NNMPC control

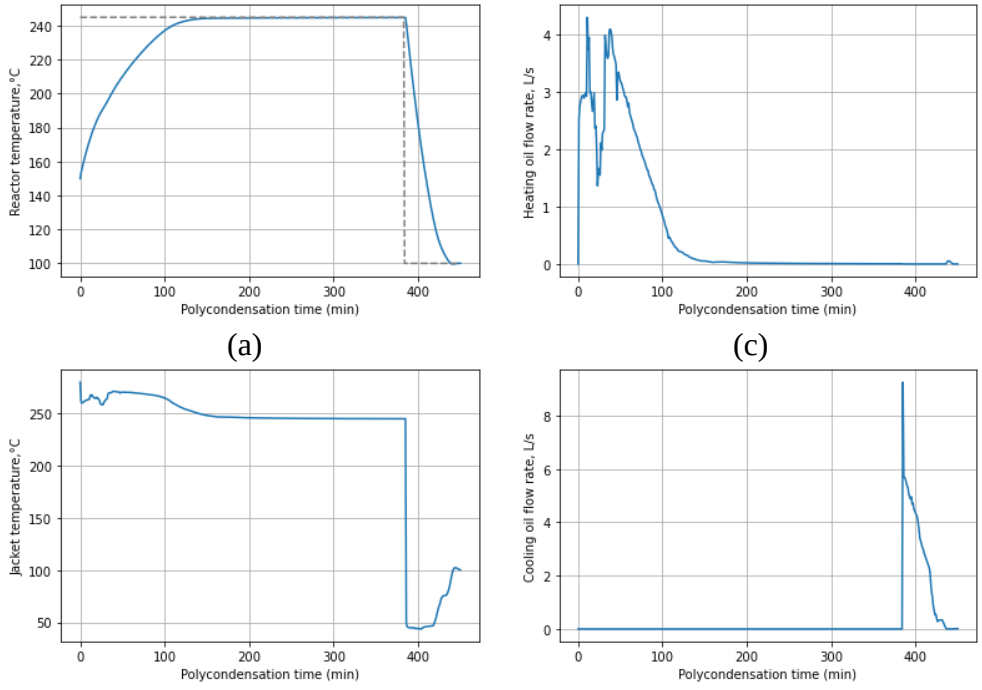

Figure 3-43 (a) Reactor temperature (°C), (b) Jacket temperature (°C), (c) Flow rate of heating oil (L/s), (d) Flow rate of cooling oil (L/s) in polycondensation process under 50 neuron NNMPC control

doi:10.6342/NTU202302309

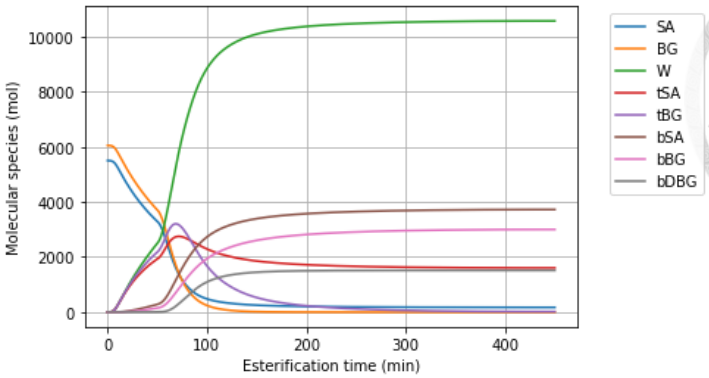

Figure 3-44 Molecular species profile in esterification process under 100 neuron NNMPC control

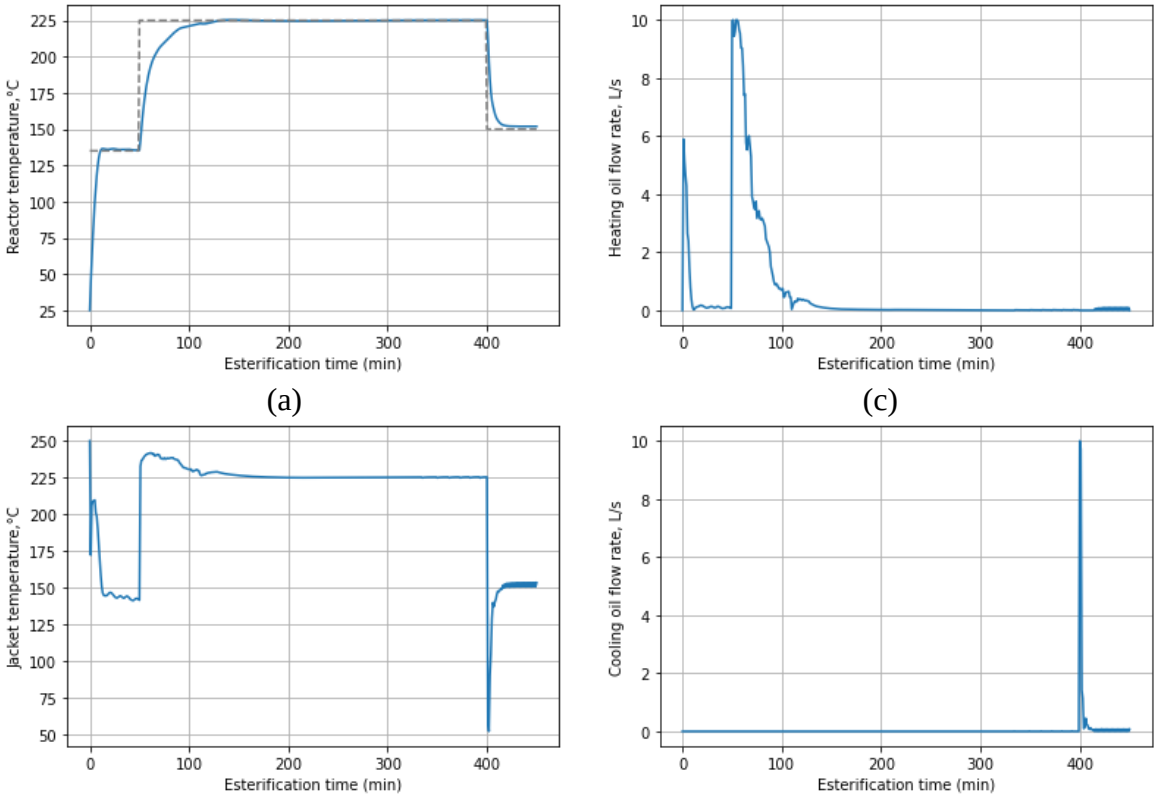

Figure 3-45 (a) Reactor temperature (°C), (b) Jacket temperature (°C), (c) Flow rate of heating oil (L/s), (d) Flow rate of cooling oil (L/s) in esterification process under 100 neuron NNMPC control

doi:10.6342/NTU202302309

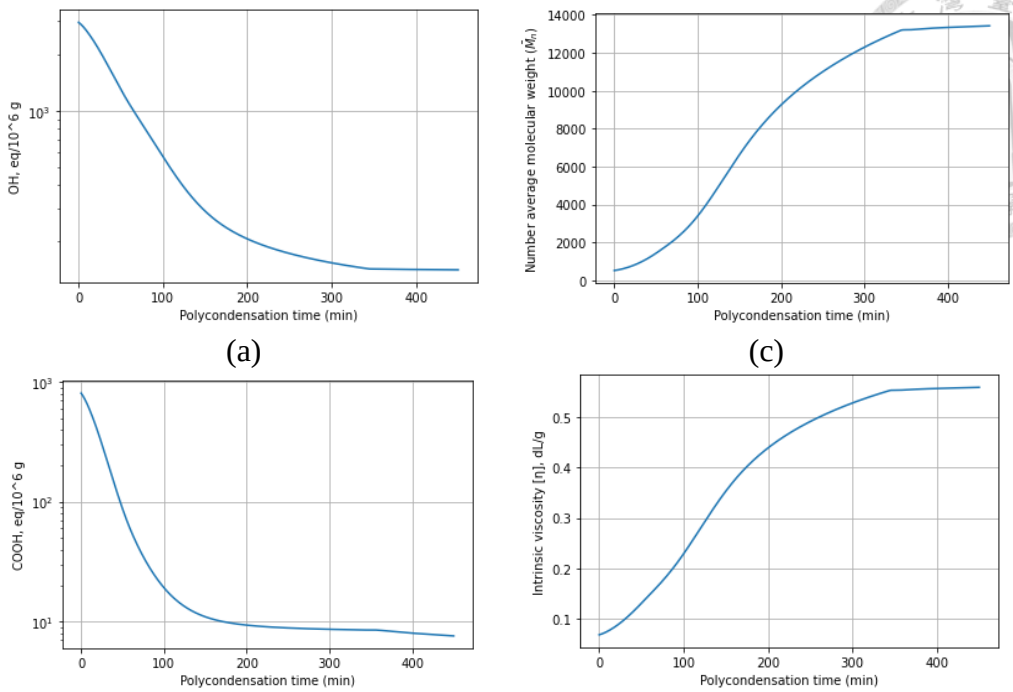

Figure 3-46 (a) OH end group (eq/10^6g), (b) COOH end group (eq/10^6g), (c) Number average molecular weight ($\bar{M}_n$), (d) Intrinsic viscosity (dL/g) during polycondensation process under 100 neuron NNMPC control

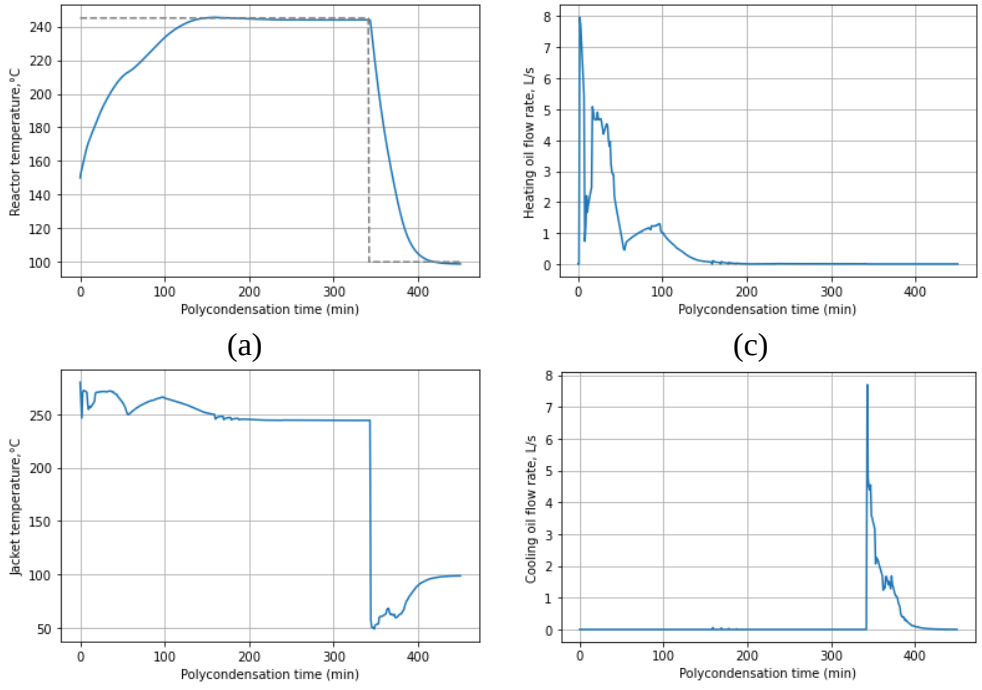

Figure 3-47 (a) Reactor temperature (°C), (b) Jacket temperature (°C), (c) Flow rate of heating oil (L/s), (d) Flow rate of cooling oil (L/s) in polycondensation process under 100 neuron NNMPC control

doi:10.6342/NTU202302309

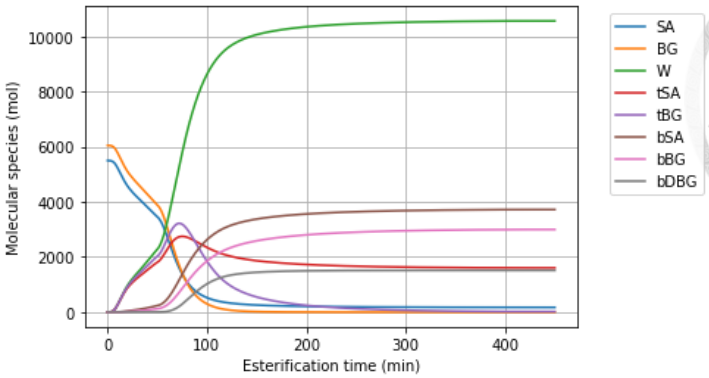

Figure 3-48 Molecular species profile in esterification process under 200 neuron NNMPC control

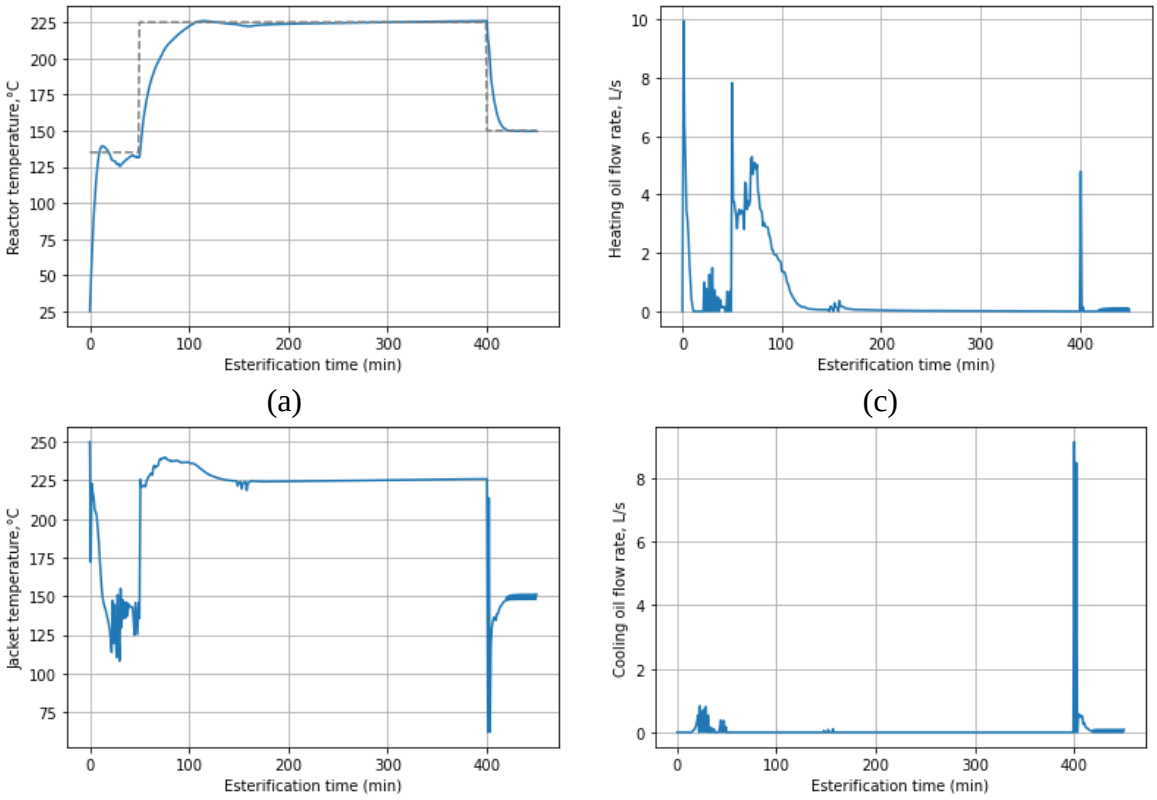

Figure 3-49 (a) Reactor temperature (°C), (b) Jacket temperature (°C), (c) Flow rate of heating oil (L/s), (d) Flow rate of cooling oil (L/s) in esterification process under 200 neuron NNMPC control

doi:10.6342/NTU202302309

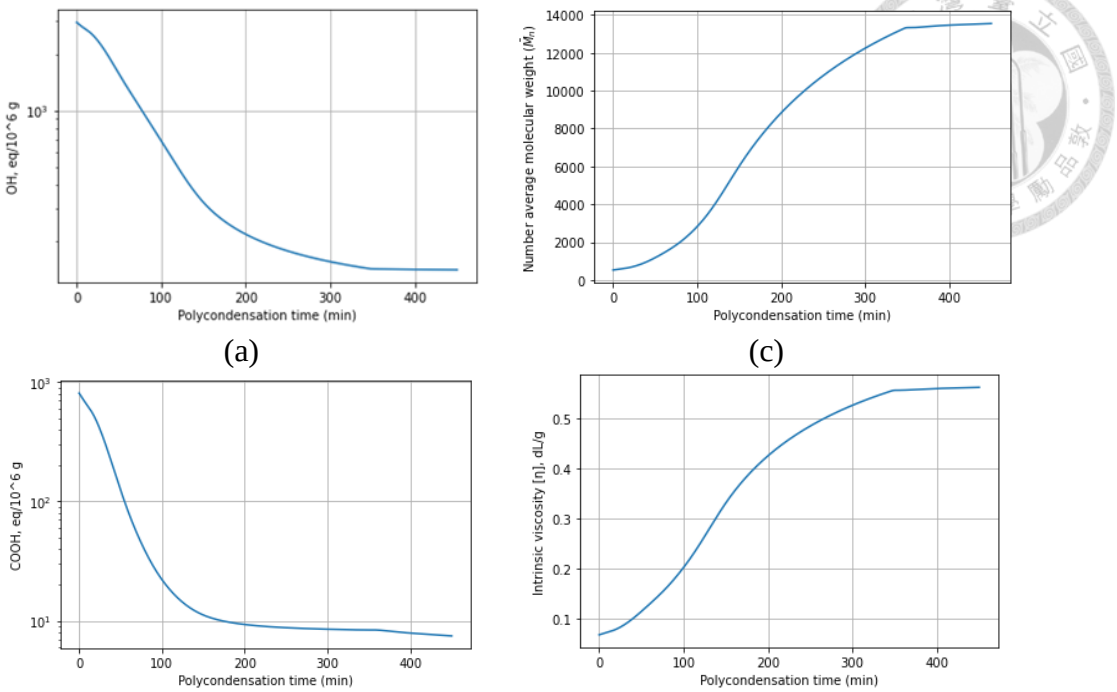

Figure 3-50 (a) OH end group (eq/10^6g), (b) COOH end group (eq/10^6g), (c) Number average molecular weight ($\bar{M}_n$), (d) Intrinsic viscosity (dL/g) during polycondensation process under 200 neuron NNMPC control

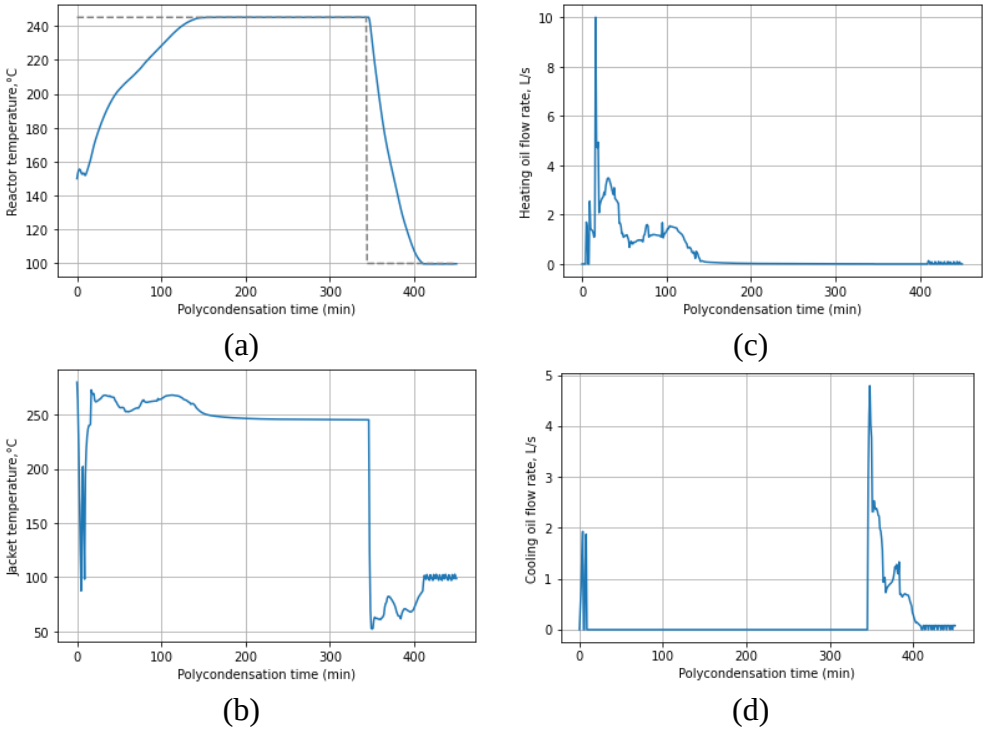

Figure 3-51 (a) Reactor temperature (°C), (b) Jacket temperature (°C), (c) Flow rate of heating oil (L/s), (d) Flow rate of cooling oil (L/s) in polycondensation process under 200 neuron NNMPC control

doi:10.6342/NTU202302309

3.4.3 White noise case

Table 3-10 IAE performance criteria and simulation time under various NNMPC controller in esterification and polycondensation processes

	NNMPC				MPC
	20	**50**	**100**	**200**	
Esterification process					
IAE	2690.58	2490.93	2536.45	3225.23	2472.37
Time (s)	15.91	21.40	21.15	32.30	364.61
Polycondensation process					
IAE	9465.43	7299.60	8012.91	10863.01	6806.14
Time (s)	18.82	25.95	25.89	72.10	121.62

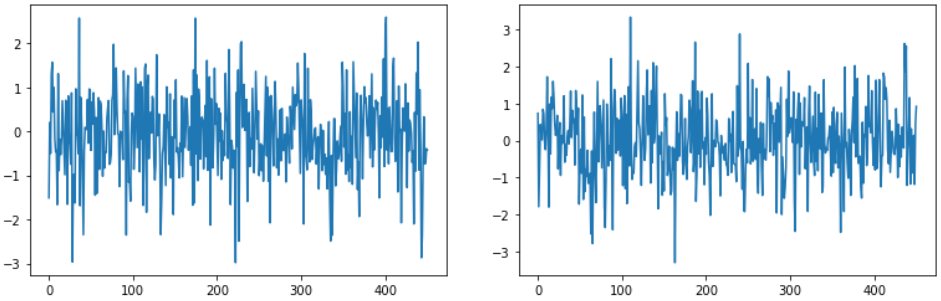

(a) (b)

Figure 3-52 (a) The set of white noise interferes with the reactor temperature, (b)The set of white noise interferes with the jacket temperature

In the simulation with noise interference, the two sets of white noise were randomly generated at all time steps (450 minutes) with zero mean and a standard deviation of 1, resulting in a maximum deviation of roughly ±3°C from the actual value in order to corrupt the measurement of the reactor and jacket temperature as shown in Figures 3-52a and 3-52b.

The temperature control of the esterification process demonstrated a significant advancement in robustness when subjected to interference from white noise upon the implementation of NNMPC control. The control action of each valve under NNMPC exhibited a less aggressive action during maintaining the reactor temperature isothermally

doi:10.6342/NTU202302309

compared to MPC control, resulting in a potential increase in utility usage efficiency through the use of NNMPC. The esterification process under 50 neuron NNMPC is shown in Figure 3-58, achieving an IAE value of 2490.93, equivalent to the MPC controller which exhibited the lowest IAE value across all controllers, as shown in Table 3-10.

For the polycondensation process, it was found that only the 50 neuron NNMPC demonstrated the necessary proficiency to effectively manage the effects of noise interference while maintaining isothermal reactor temperature control. As a result, this particular neural network structure exhibited the lowest IAE value when compared against other NN configurations tested. Although the 100 and 200 neuron NNMPC controllers were able to control temperature to the synthesis setpoint of 245°C, their control action was notably aggressive as shown in Figures 3-64 and 3-68, leading to inefficient dynamic response. Specifically, the 100 neuron NNMPC was able to provide good performance in the nominal case, but when white noise corrupted the temperature measurement, it regulated aggressively in raising reactor temperature that wasting energy usage and poor dynamic. This reflects the NN model complexity impacts the robustness of the controller.

The 20 neuron NNMPC has the lowest complexity of the varied NN structure, this relatively simple structure proved to be not a limiting factor, as it has ability to learn the dynamic changes of the polycondensation process from the provided data. The simulation revealed that the optimal manipulated variables computed by the 20 neuron NN model, could manage the noise interference and maintain isothermal control at the setpoints throughout the operation as shown in Figure 3-56.

doi:10.6342/NTU202302309

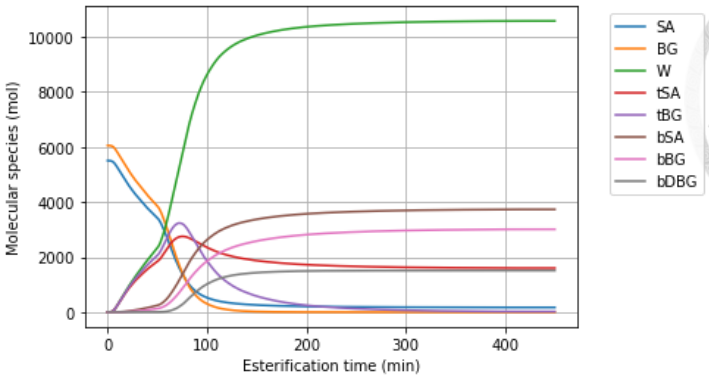

Figure 3-53 Molecular species profile in esterification process under 20 neuron NNMPC control with white noise

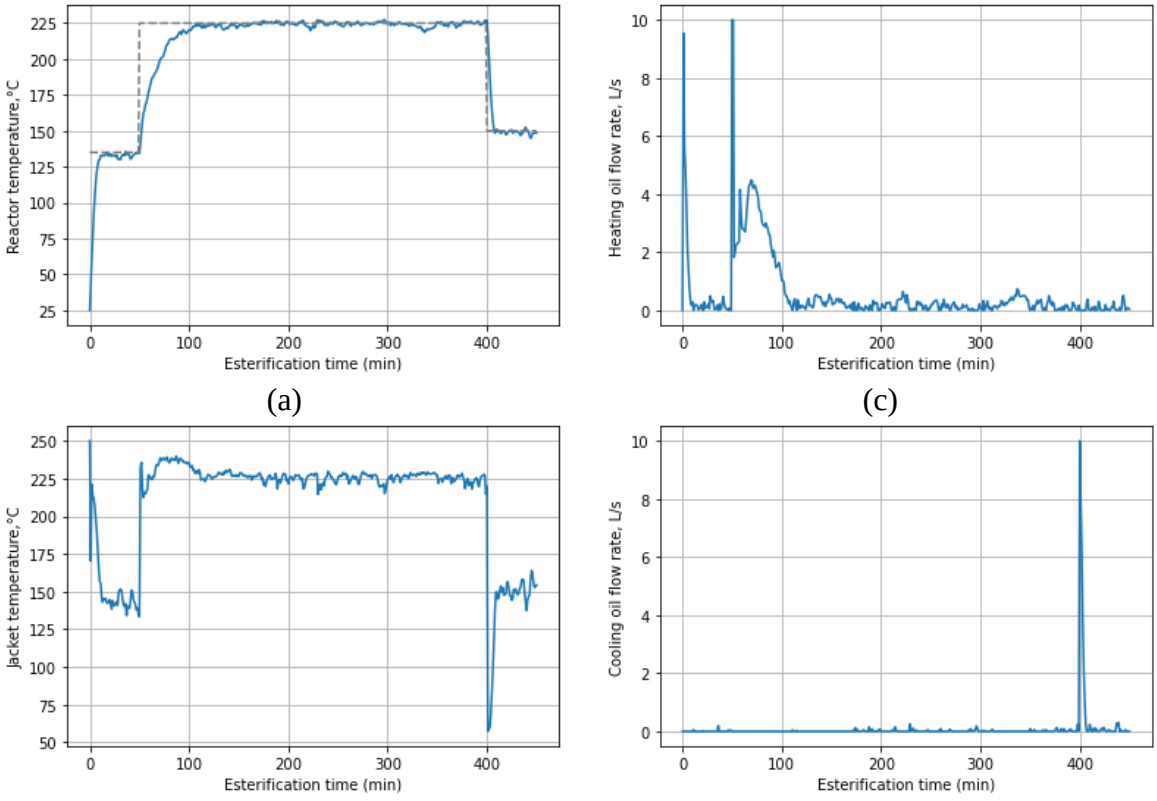

Figure 3-54 Molecular specie profile in esterification process under 20 neuron NNMPC control with white noise

doi:10.6342/NTU202302309

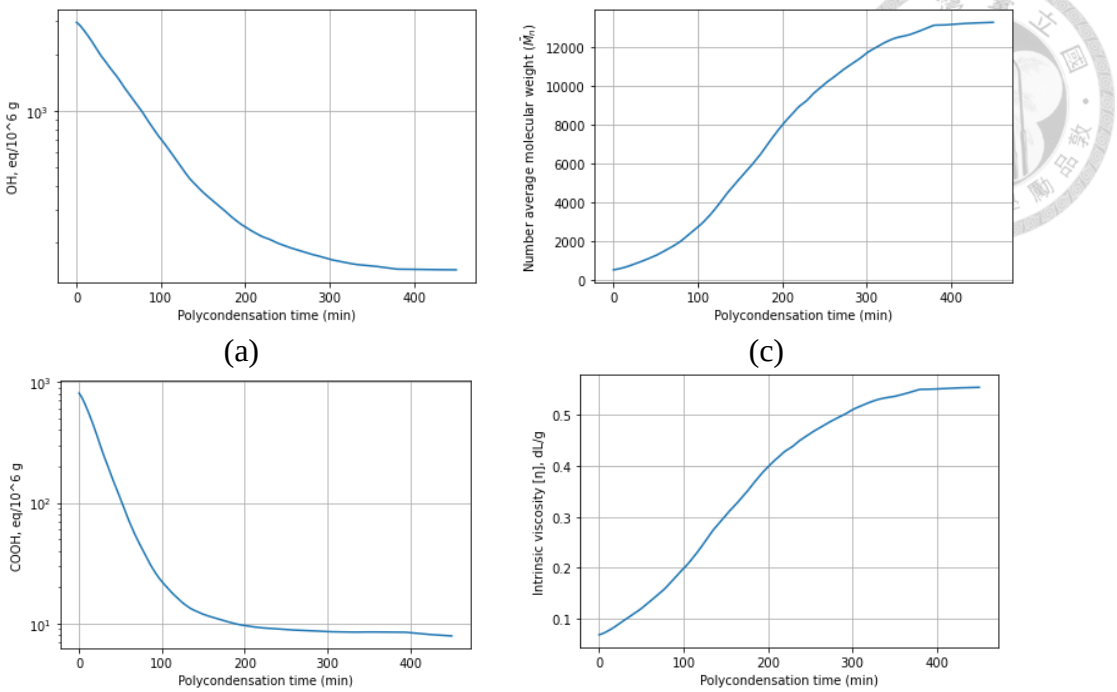

Figure 3-55 (a) OH end group (eq/10^6 g), (b) COOH end group (eq/10^6 g), (c) Number average molecular weight ($\bar{M}_n$), (d) Intrinsic viscosity (dL/g) during polycondensation process under 20 neuron NNMPC control with white noise

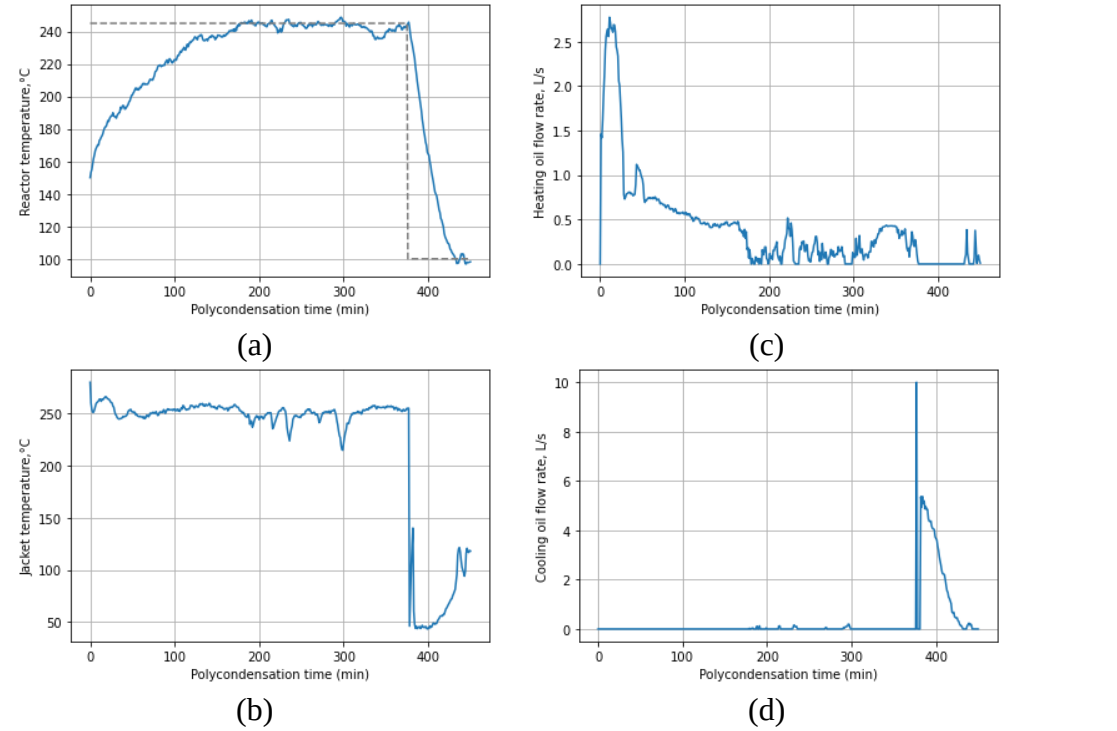

Figure 3-56 (a) Reactor temperature (°C), (b) Jacket temperature (°C), (c) Flow rate of heating oil (L/s), (d) Flow rate of cooling oil (L/s) in polycondensation process under 20 neuron NNMPC control with white noise

doi:10.6342/NTU202302309

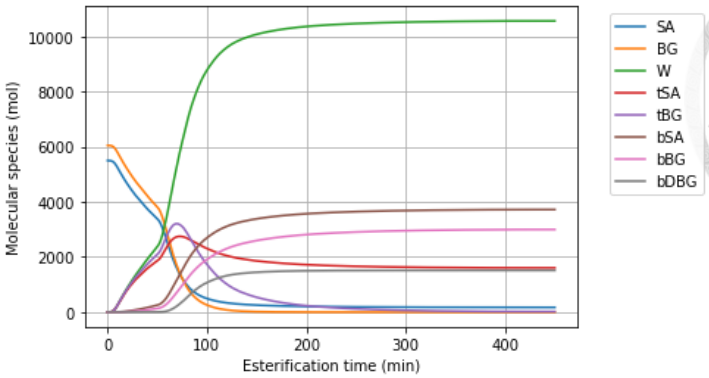

Figure 3-57 Molecular species profile in esterification process under 50 neuron NNMPC control with white noise

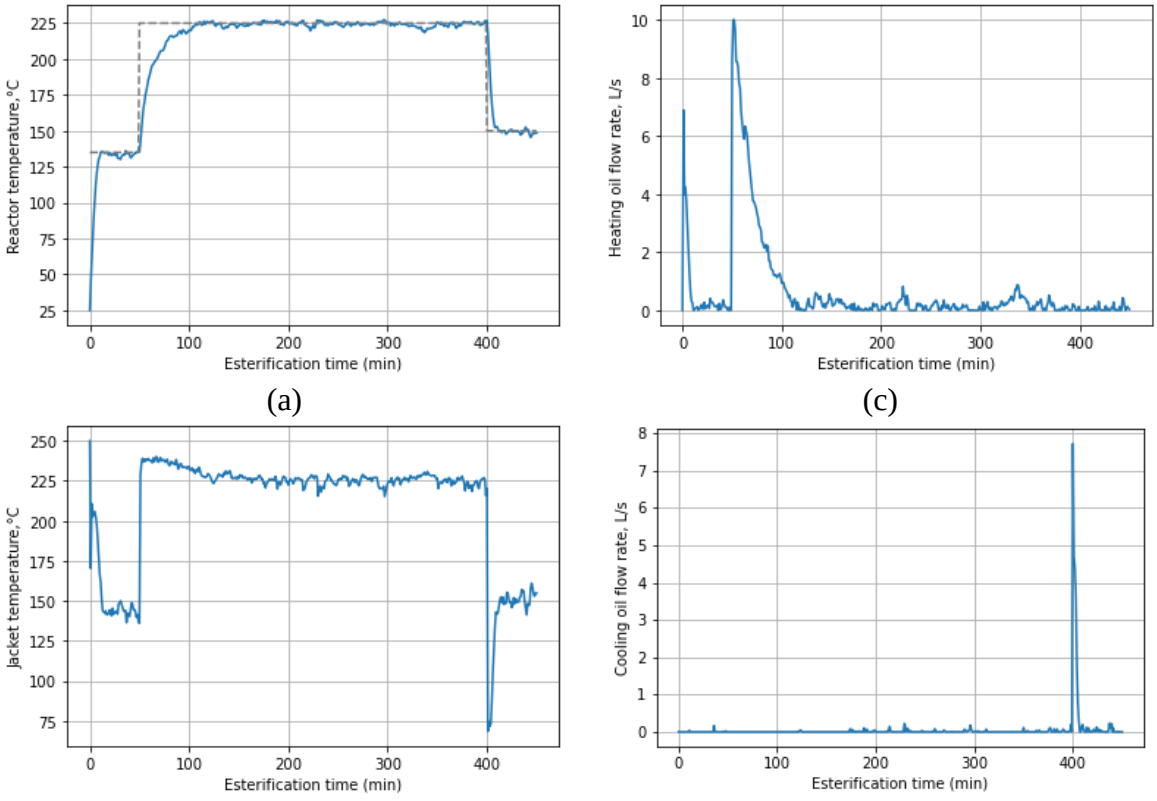

Figure 3-58 (a) Reactor temperature (°C), (b) Jacket temperature (°C), (c) Flow rate of heating oil (L/s), (d) Flow rate of cooling oil (L/s) in esterification process under 50 neuron NNMPC control with white noise

doi:10.6342/NTU202302309

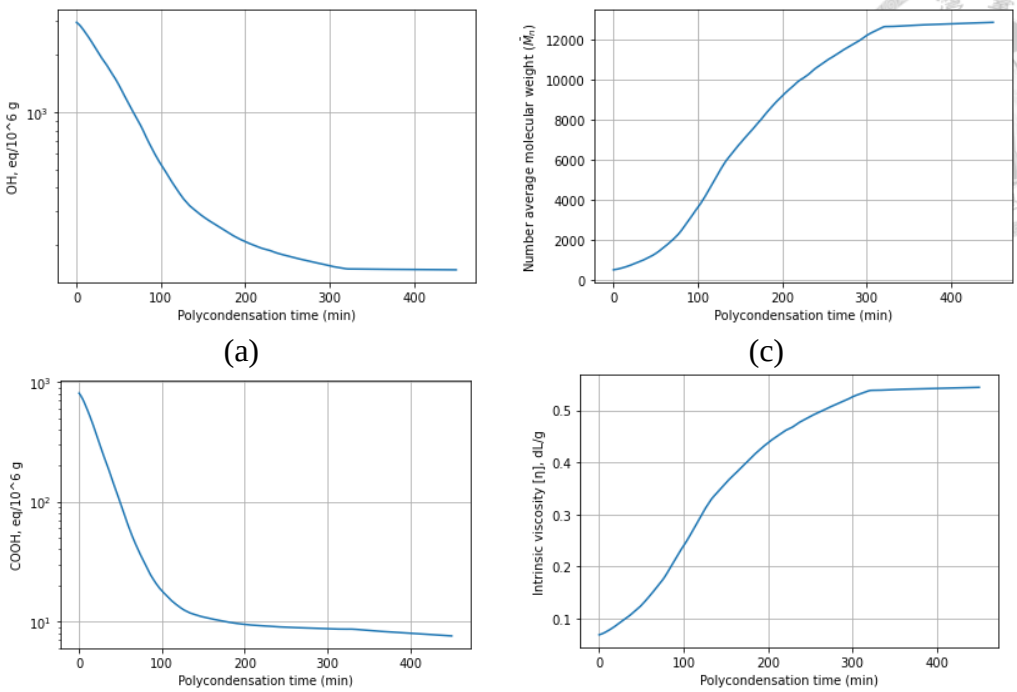

Figure 3-59 (a) OH end group (eq/10^6g), (b) COOH end group (eq/10^6g), (c) Number average molecular weight ($\bar{M}_n$), (d) Intrinsic viscosity (dL/g) during polycondensation process under 50 neuron NNMPC control with white noise

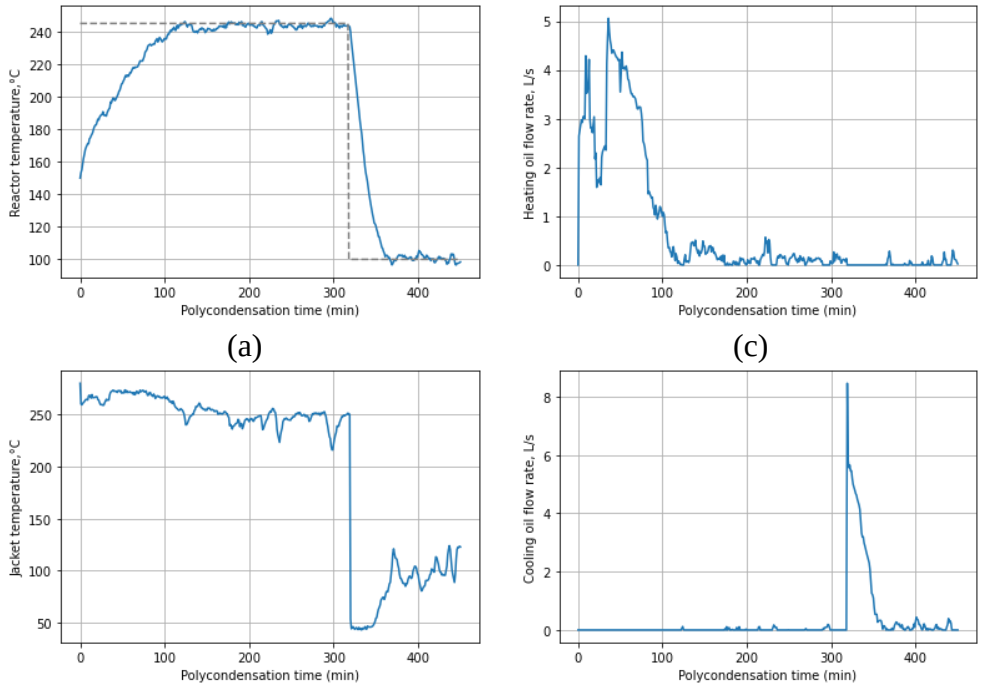

Figure 3-60 (a) Reactor temperature (°C), (b) Jacket temperature (°C), (c) Flow rate of heating oil (L/s), (d) Flow rate of cooling oil (L/s) in polycondensation process under 50 neuron NNMPC control with white noise

doi:10.6342/NTU202302309

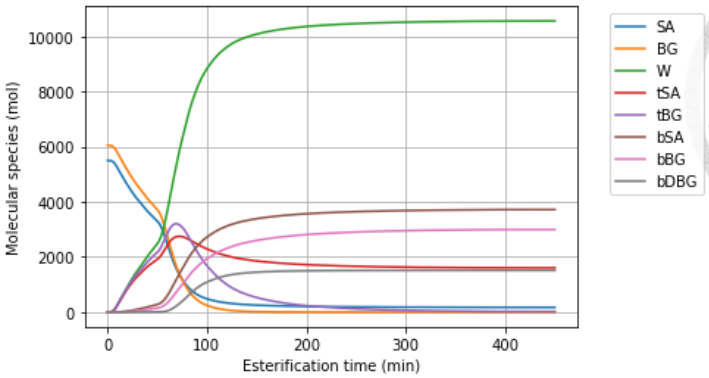

Figure 3-61 Molecular species profile in esterification process under 100 neuron NNMPC control with white noise

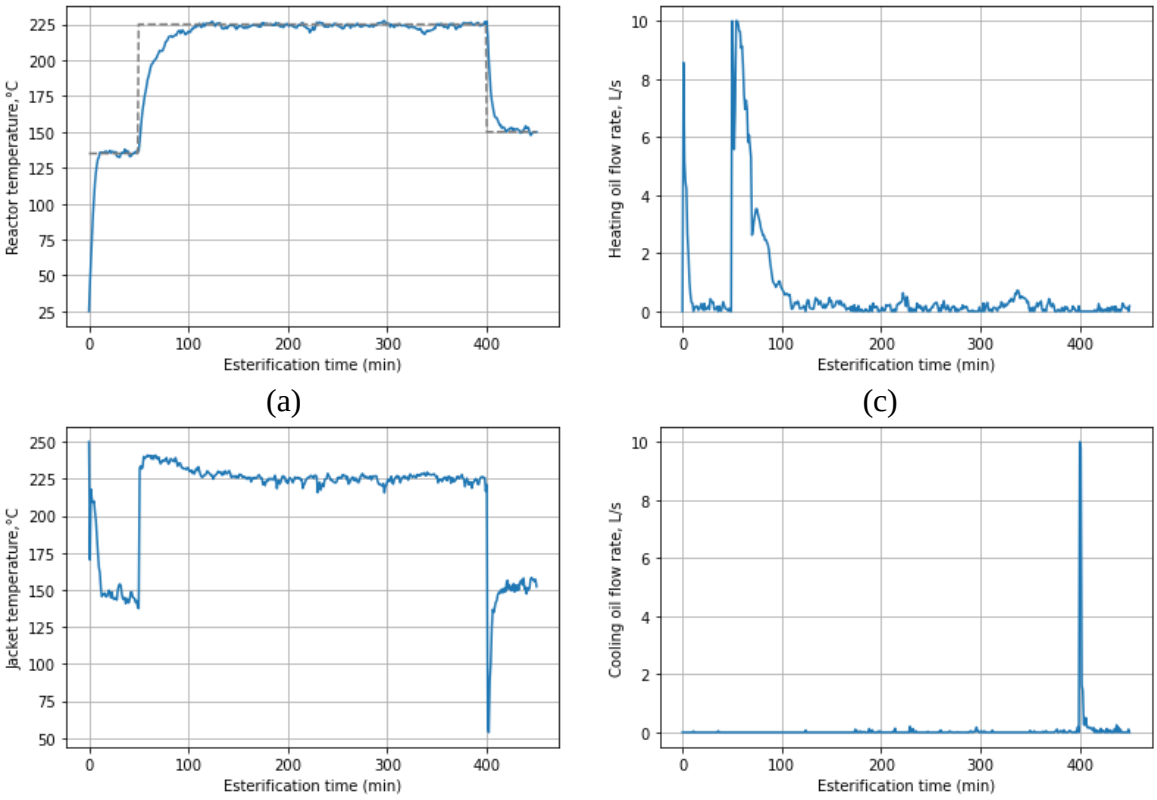

Figure 3-62 (a) Reactor temperature (°C), (b) Jacket temperature (°C), (c) Flow rate of heating oil (L/s), (d) Flow rate of cooling oil (L/s) in esterification process under 100 neuron NNMPC control with white noise

doi:10.6342/NTU202302309

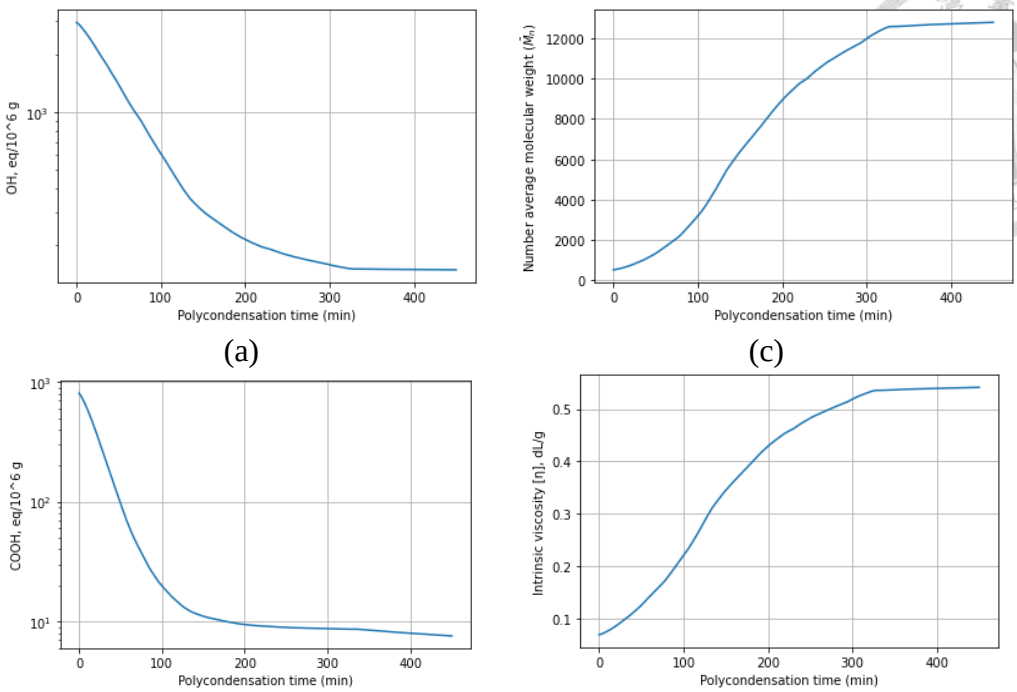

Figure 3-63 (a) OH end group (eq/10^6g), (b) COOH end group (eq/10^6g), (c) Number average molecular weight ($\bar{M}_n$), (d) Intrinsic viscosity (dL/g) during polycondensation process under 100 neuron NNMPC control with white noise

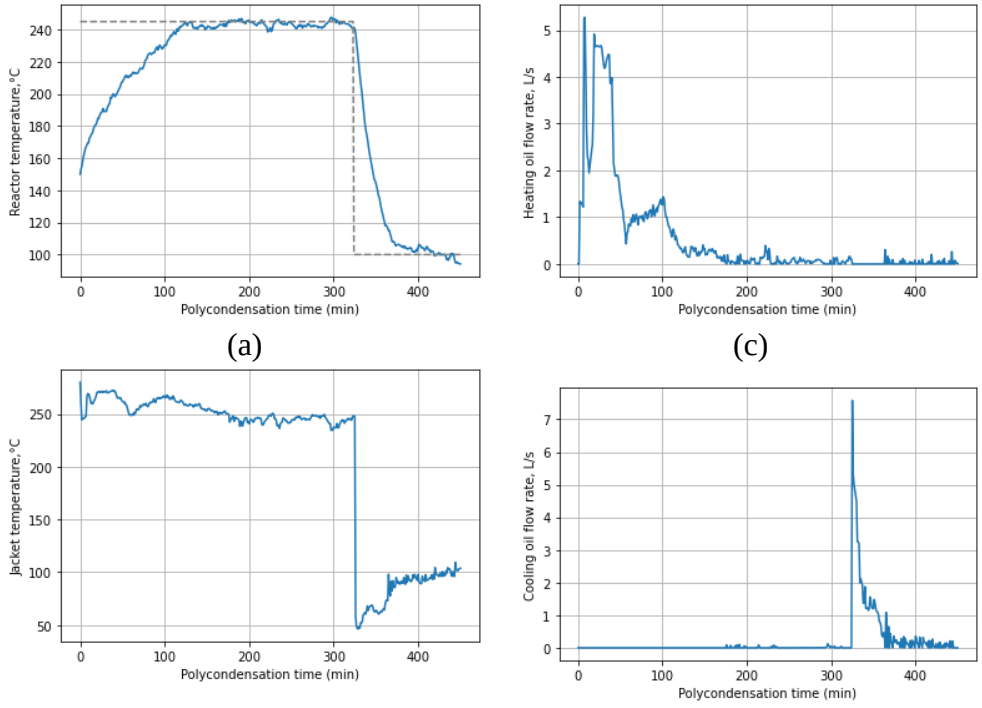

Figure 3-64 (a) Reactor temperature (°C), (b) Jacket temperature (°C), (c) Flow rate of heating oil (L/s), (d) Flow rate of cooling oil (L/s) in polycondensation process under 100 neuron NNMPC control with white noise

doi:10.6342/NTU202302309

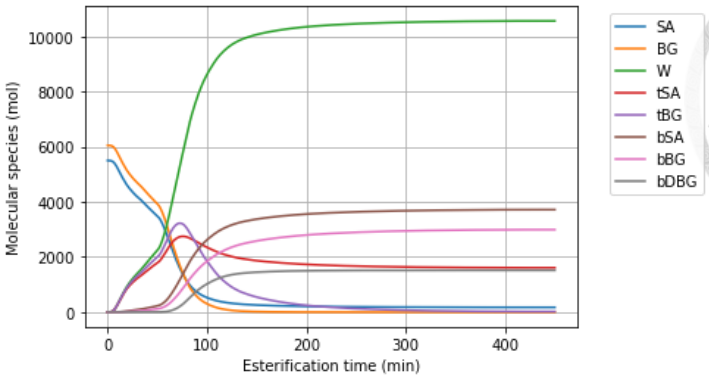

Figure 3-65 Molecular species profile in esterification process under 200 neuron NNMPC control with white noise

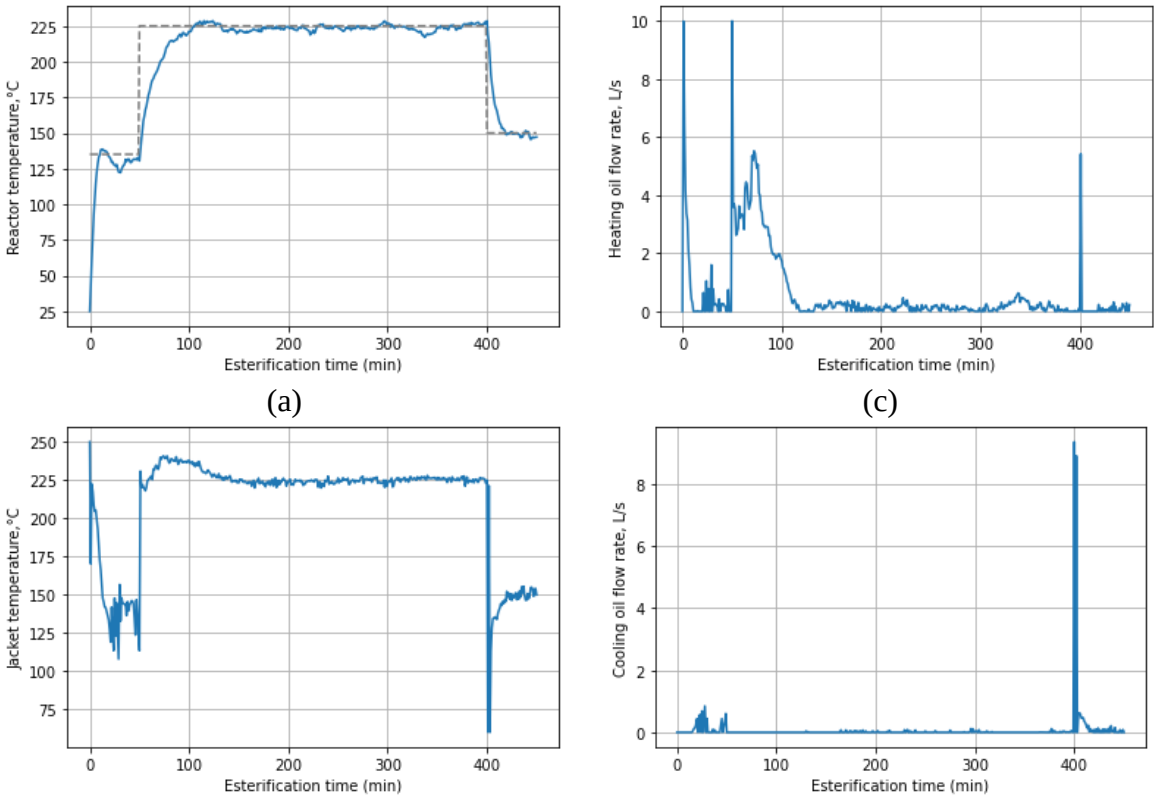

Figure 3-66 (a) Reactor temperature (°C), (b) Jacket temperature (°C), (c) Flow rate of heating oil (L/s), (d) Flow rate of cooling oil (L/s) in esterification process under 200 neuron NNMPC control with white noise

doi:10.6342/NTU202302309

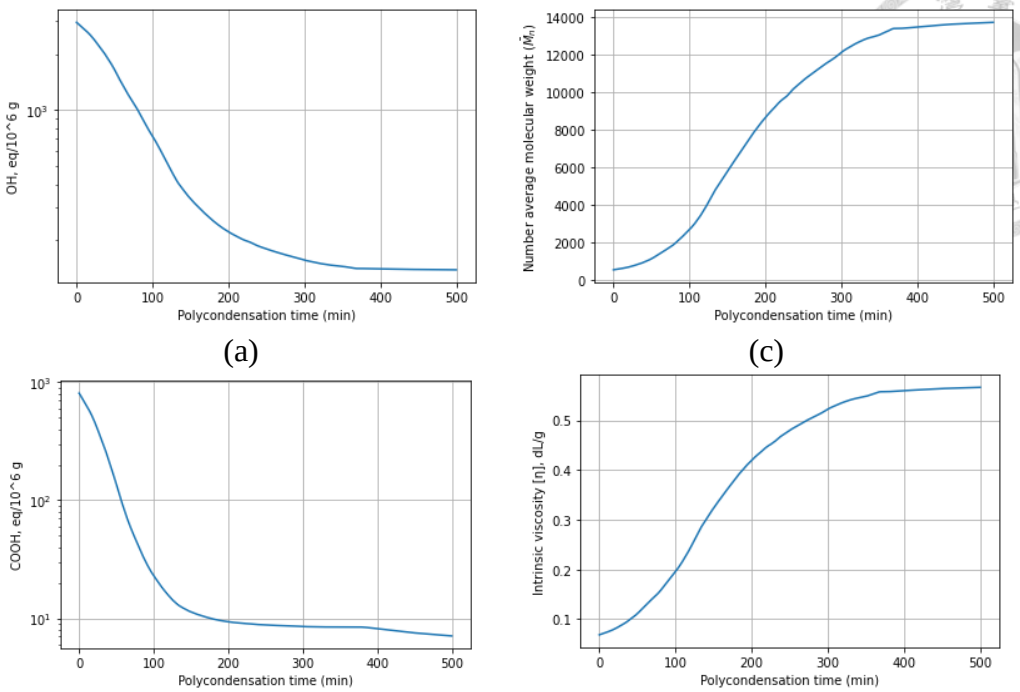

Figure 3-67 (a) OH end group (eq/10^6 g), (b) COOH end group (eq/10^6 g), (c) Number average molecular weight ($\bar{M}_n$), (d) Intrinsic viscosity (dL/g) during polycondensation process under 200 neuron NNMPC control with white noise

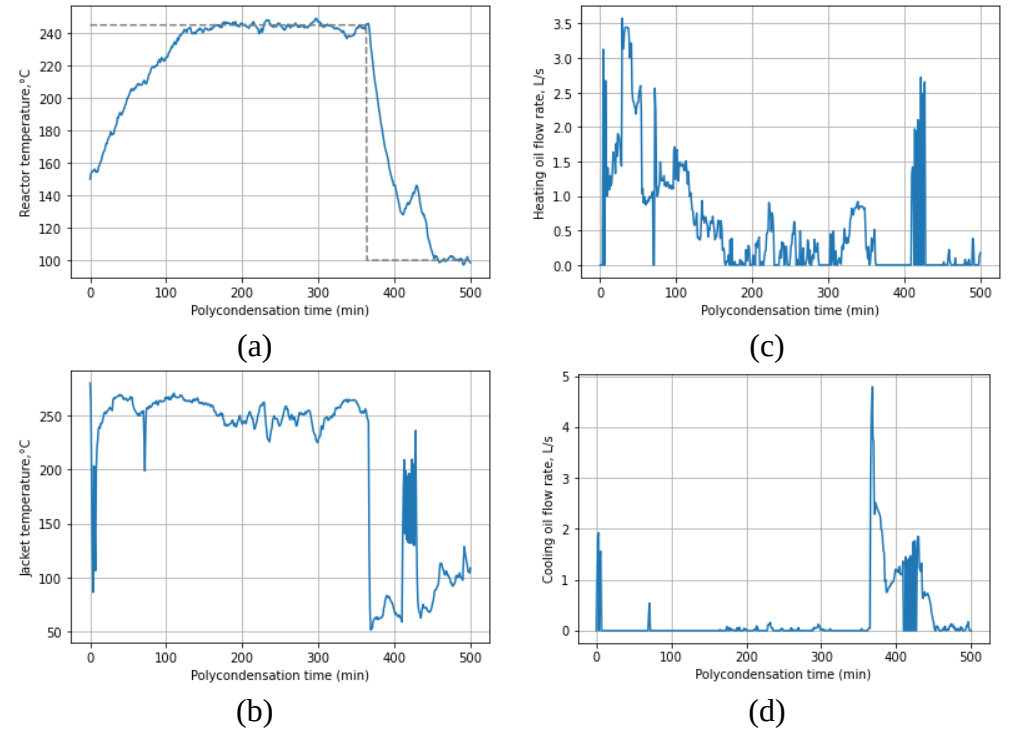

Figure 3-68 (a) Reactor temperature (°C), (b) Jacket temperature (°C), (c) Flow rate of heating oil (L/s), (d) Flow rate of cooling oil (L/s) in polycondensation process under 200 neuron NNMPC control with white noise

doi:10.6342/NTU202302309

3.4.4 Model mismatch case

Table 3-11 IAE performance criteria and simulation time under various NNMPC controller in esterification and polycondensation processes with model mismatch

	NNMPC				MPC
	20	**50**	**100**	**200**	
Esterification process					
IAE	3143.89	2892.41	3088.79	3745.34	3009.59
Time (s)	14.63	18.25	21.49	28.53	128.74
Polycondensation process					
IAE	11623.74	9795.90	10902.57	11504.63	10160.21
Time (s)	19.79	22.48	25.26	39.86	53.88

When the process encountered a model mismatch scenario, the dynamic response of temperature control for the model mismatch case takes a longer time to reach the setpoint because of the lower heat transfer capability of the process, thus, a higher IAE compared to the nominal case is obtained. The implementation of neural network model within MPC was simulated and it proved to be a significant improvement over the mathematic model MPC in terms of control performance.

The optimal manipulated variables were computed by NNMPC, driving the temperature to the desired setpoint faster than temperature control under MPC. Despite a large difference between the overall heat transfer coefficient of the process and the model, the controller still showed efficient control performance. Specifically, the esterification process under 50 neuron NNMPC control as shown in Figure 3-74 reveals that the heating oil fed into the jacket was a moderately high flow rate and the control action was not extremely aggressive resulting in the minimum IAE value of 2892.41 compared to the MPC's control performance, which yielded an IAE value of 3009.59. This can be attributed to the fact that the neural network models were trained using a wide range of data, enhancing the ability to adapt its prediction and offer improved control performance

doi:10.6342/NTU202302309

in uncertain events.

The other NN structure arrangements provide reasonable performance, the lowest complexity model consisting of 20 neurons provided good control action with an IAE of 3143.89. However, the heating oil flow rate was not sufficient to achieve a faster increase in temperature as shown in Figure 3-70. On the other hand, the high complexity NN model of 100 and 200 neurons shows highly aggressive actions in manipulating the oil valves for certain durations resulting in unreasonable waste of utility supply as illustrated in Figures 3-78 and 3-82. The overfitting of the model led to lower prediction accuracy that impacted the energy usage efficiency.

In polycondensation process, synthesis temperature and time are the main factors that impact the polymer properties. When the process encounters with model mismatch scenario, the temperature slowly rises to the setpoint and it takes a longer time in the synthesis process due to fouling in the reactor, thus the polymer properties exceed the specifications than the nominal case. From the simulations, the polycondensation process under 50 neuron NNMPC shows that the number average molecular weight rose up to 14,483 at the end of the process as a result of the optimal manipulated variable of heating oil flow rate being insufficient leading to the temperature slowly reached the setpoint of 245°C at around 220 minutes of the operation as shown in Figure 3-76.

doi:10.6342/NTU202302309

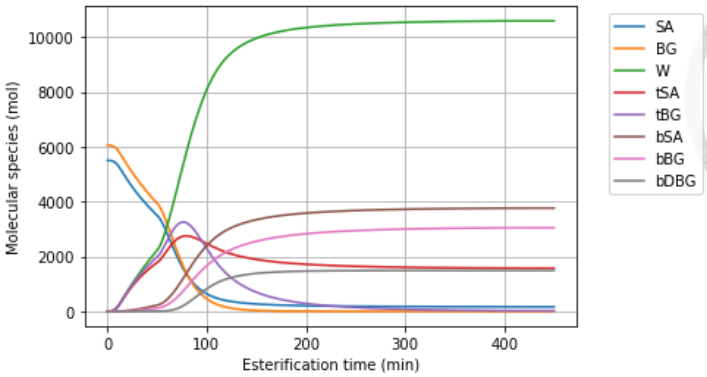

Figure 3-69 Molecular species profile in esterification process under 20 neuron NNMPC control with model mismatch

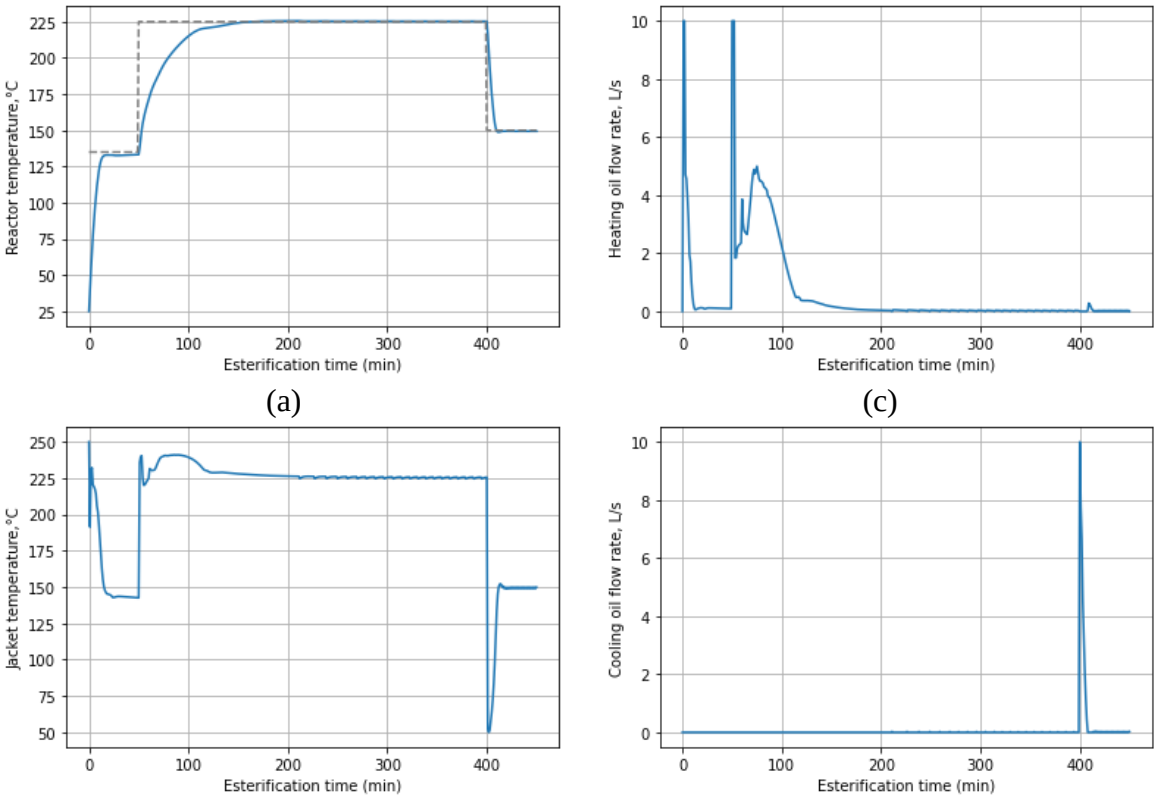

Figure 3-70 (a) Reactor temperature (°C), (b) Jacket temperature (°C), (c) Flow rate of heating oil (L/s), (d) Flow rate of cooling oil (L/s) in esterification process under 20 neuron NNMPC control with model mismatch

doi:10.6342/NTU202302309

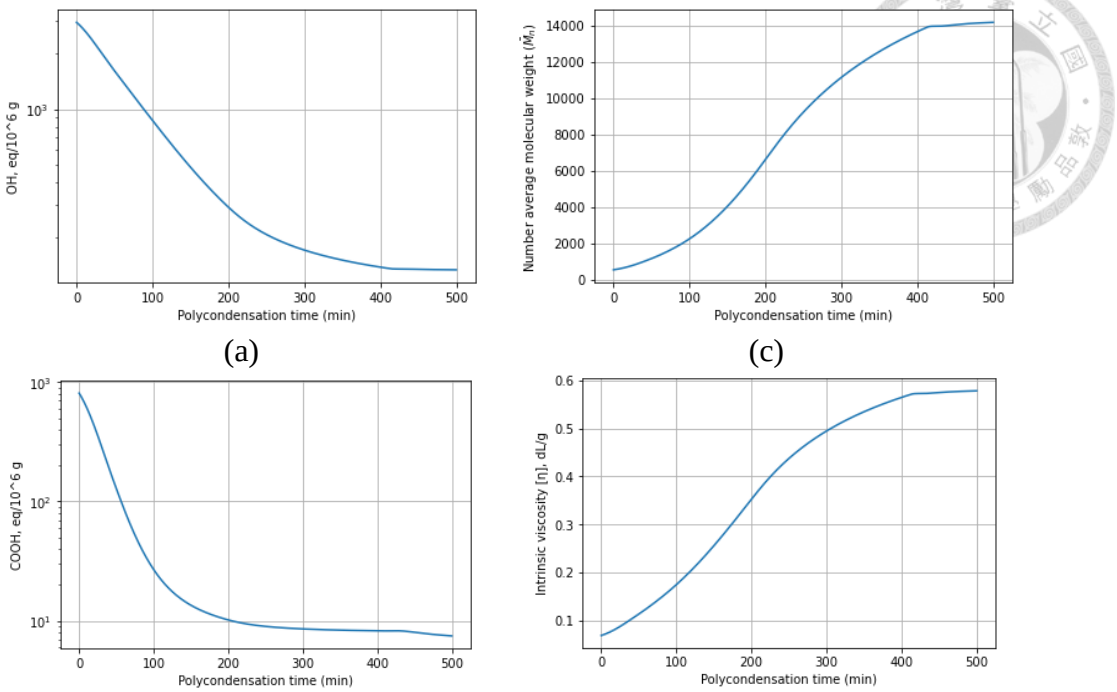

Figure 3-71 (a) OH end group (eq/10^6 g), (b) COOH end group (eq/10^6 g), (c) Number average molecular weight ($\bar{M}_n$), (d) Intrinsic viscosity (dL/g) during polycondensation process under 20 neuron NNMPC control with model mismatch

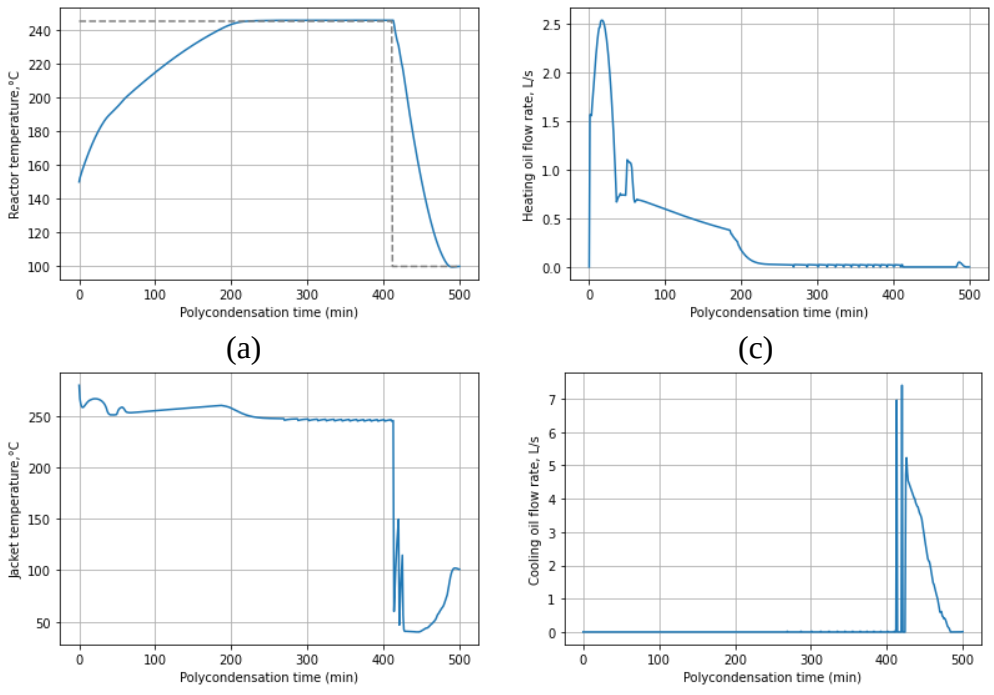

Figure 3-72 (a) Reactor temperature (°C), (b) Jacket temperature (°C), (c) Flow rate of heating oil (L/s), (d) Flow rate of cooling oil (L/s) in polycondensation process under 20 neuron NNMPC control with model mismatch

doi:10.6342/NTU202302309

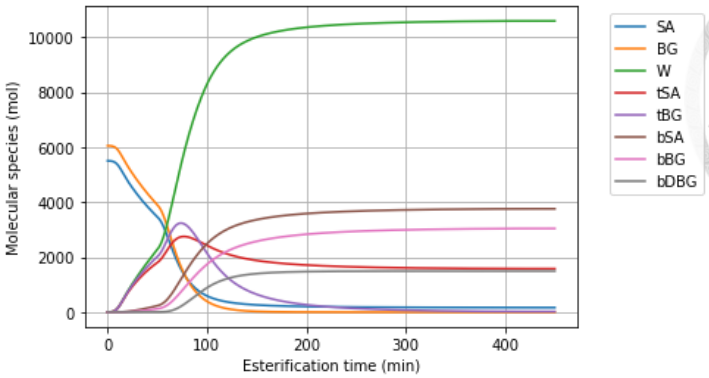

Figure 3-73 Molecular species profile in esterification process under 50 neuron NNMPC control with model mismatch

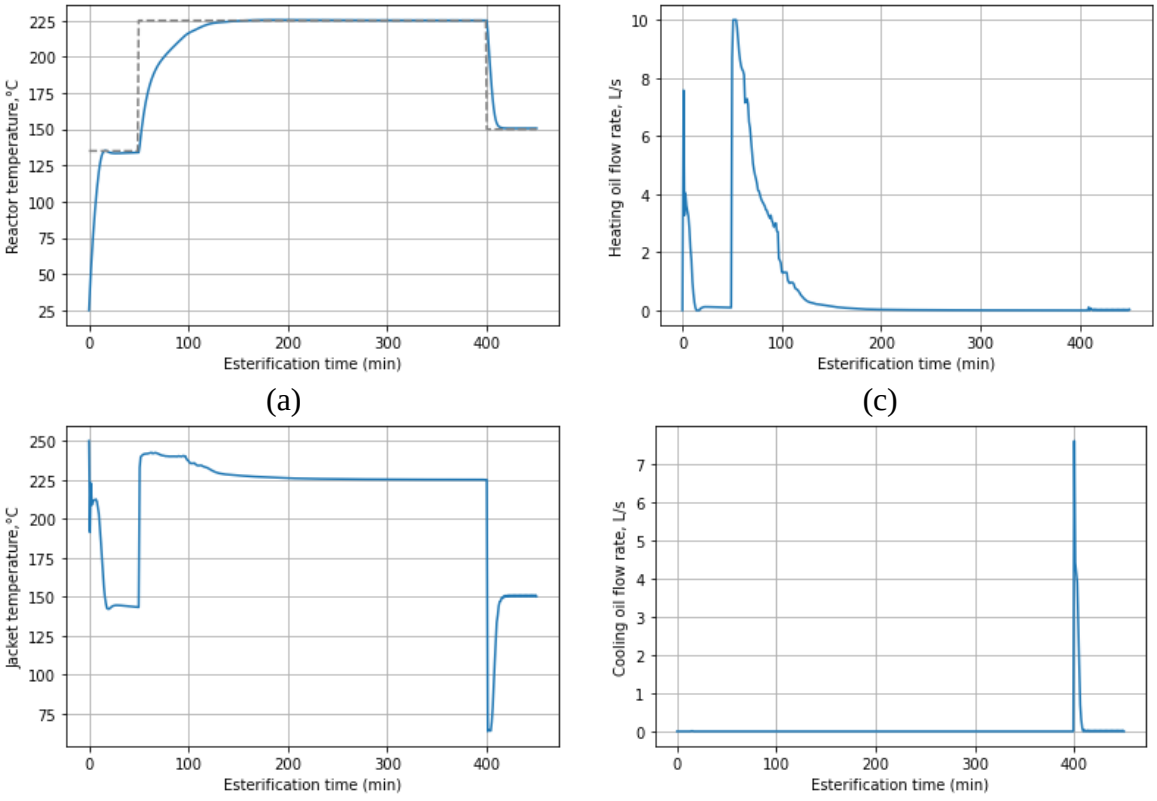

Figure 3-74 (a) Reactor temperature (°C), (b) Jacket temperature (°C), (c) Flow rate of heating oil (L/s), (d) Flow rate of cooling oil (L/s) in esterification process under 50 neuron NNMPC control with model mismatch

doi:10.6342/NTU202302309

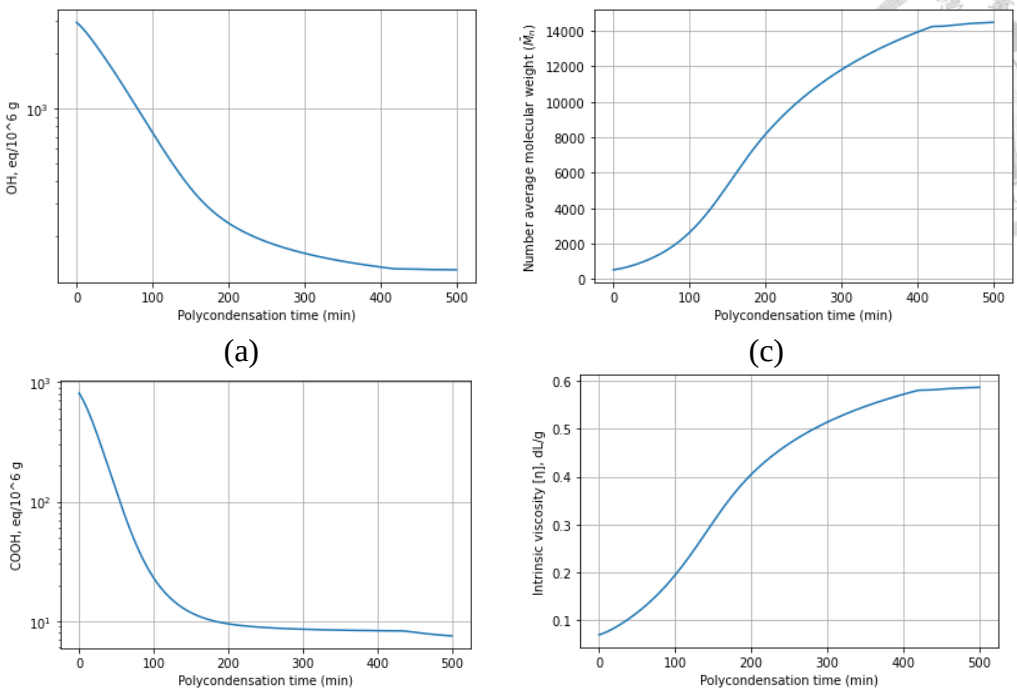

Figure 3-75 (a) OH end group (eq/10^6g), (b) COOH end group (eq/10^6g), (c) Number average molecular weight ($\bar{M}_n$), (d) Intrinsic viscosity (dL/g) during polycondensation process under 50 neuron NNMPC control with model mismatch

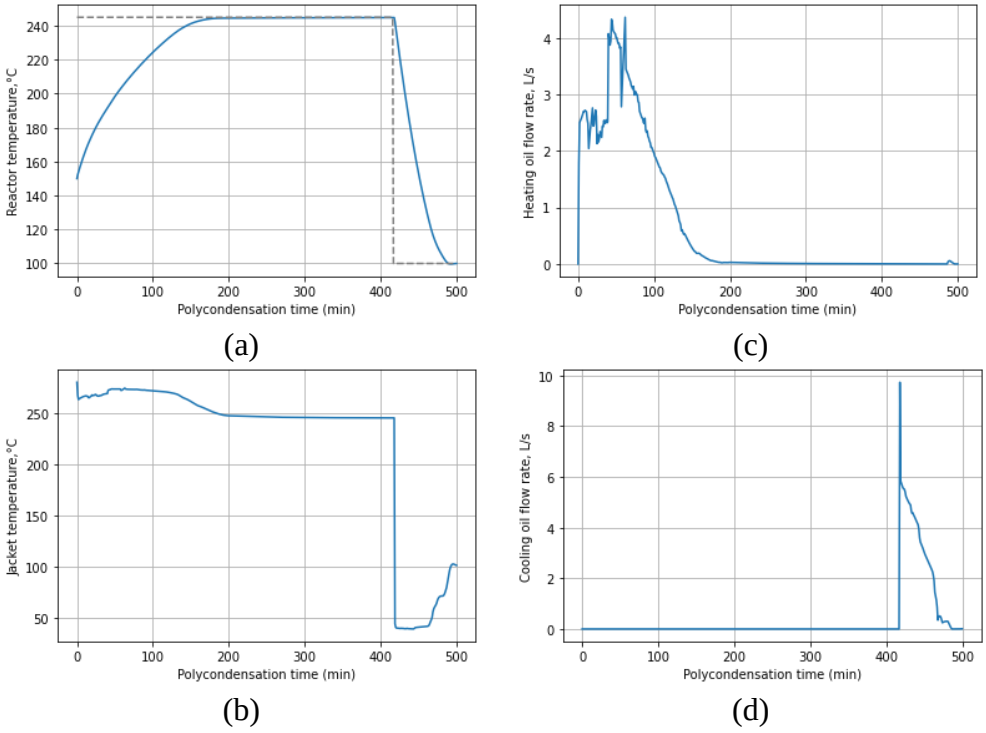

Figure 3-76 (a) Reactor temperature (°C), (b) Jacket temperature (°C), (c) Flow rate of heating oil (L/s), (d) Flow rate of cooling oil (L/s) in polycondensation process under 50 neuron NNMPC control with model mismatch

doi:10.6342/NTU202302309

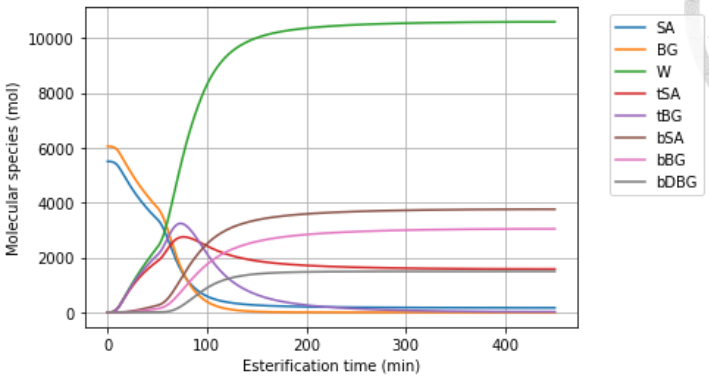

Figure 3-77 Molecular species profile in esterification process under 100 neuron NNMPC control with model mismatch

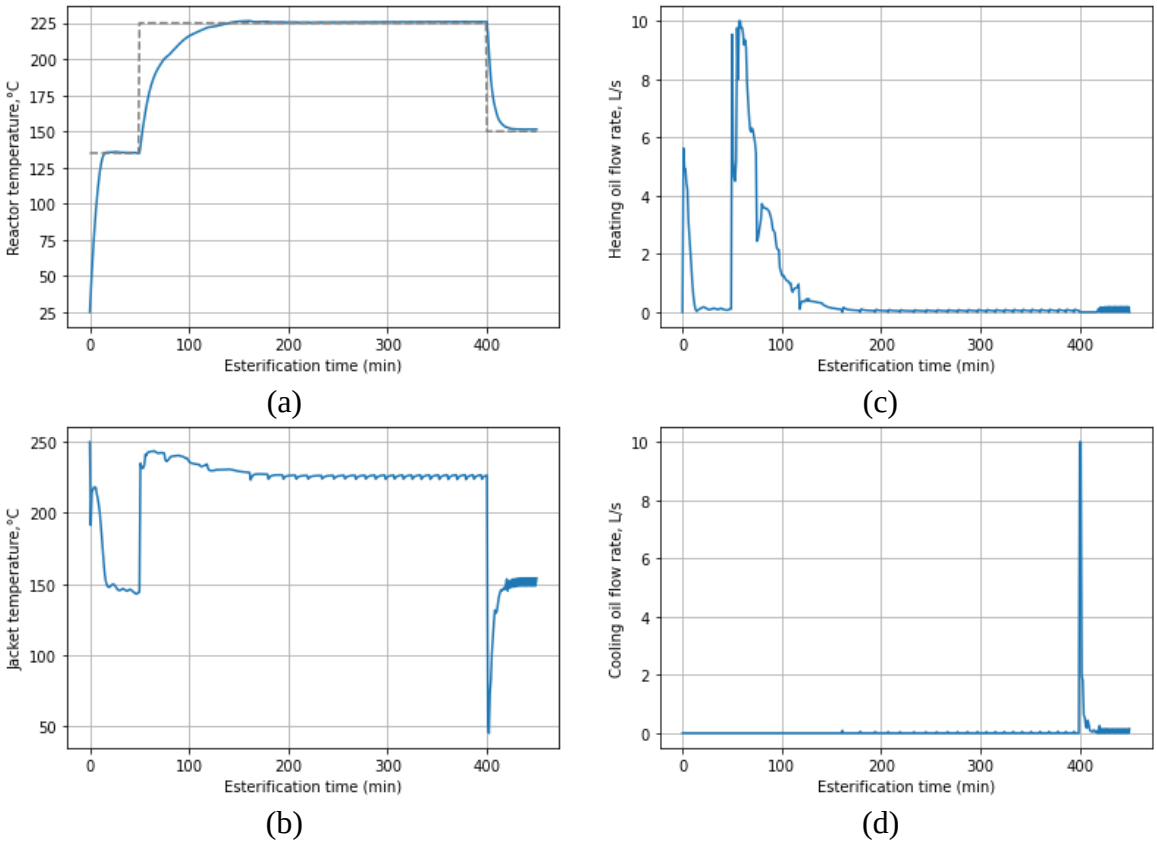

Figure 3-78 (a) Reactor temperature (°C), (b) Jacket temperature (°C), (c) Flow rate of heating oil (L/s), (d) Flow rate of cooling oil (L/s) in esterification process under 100 neuron NNMPC control with model mismatch

doi:10.6342/NTU202302309

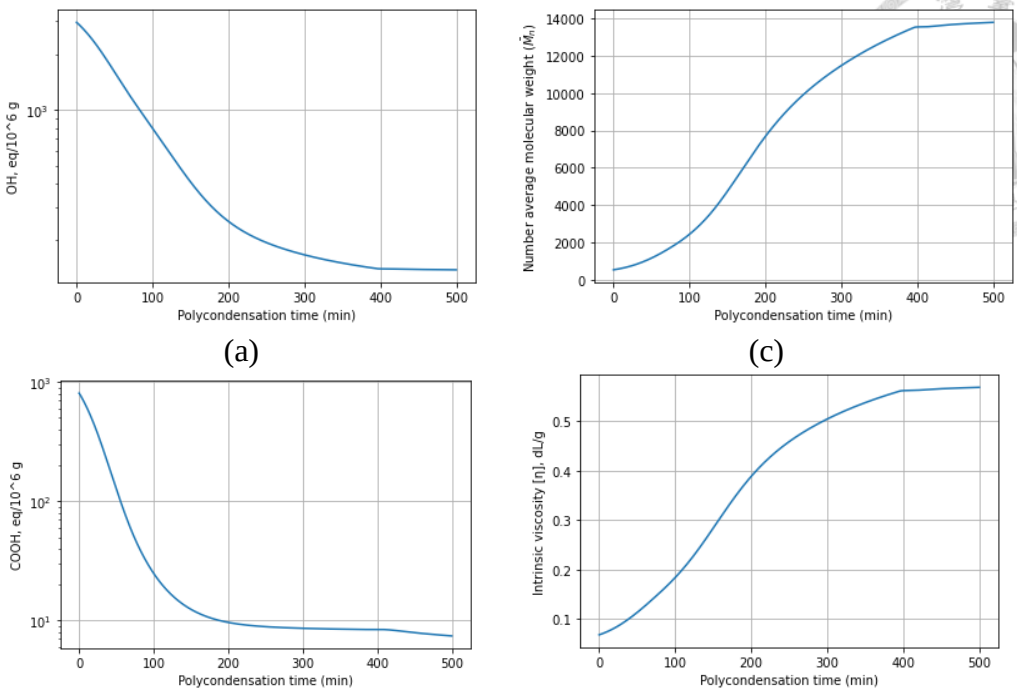

Figure 3-79 (a) OH end group (eq/10^6g), (b) COOH end group (eq/10^6g), (c) Number average molecular weight ($\bar{M}_n$), (d) Intrinsic viscosity (dL/g) during polycondensation process under 100 neuron NNMPC control with model mismatch

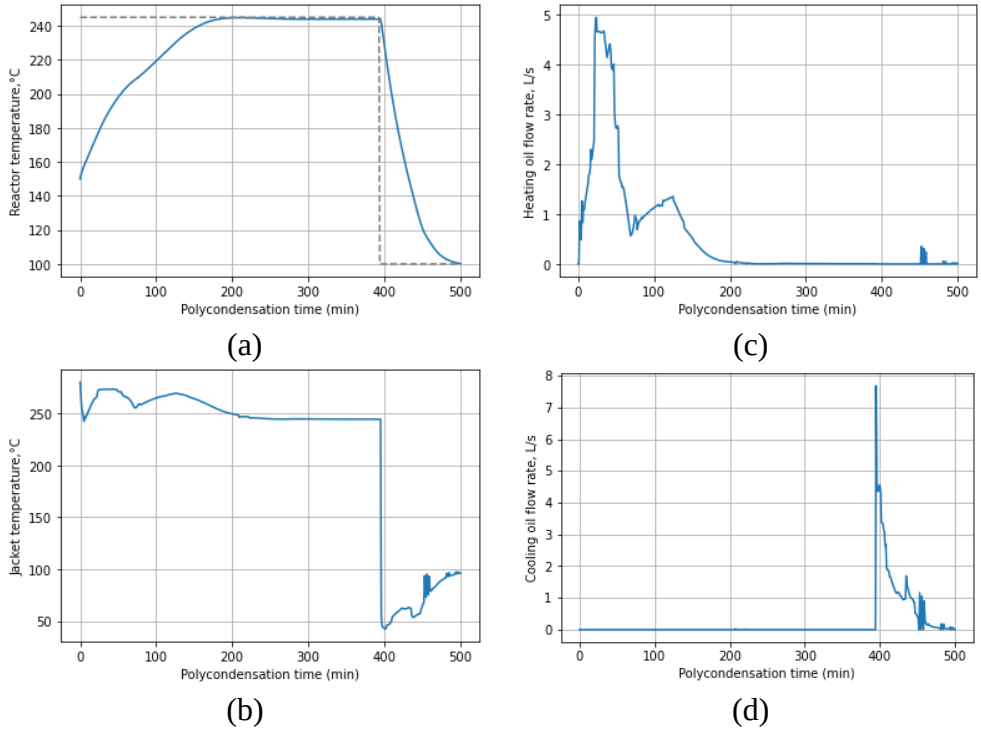

Figure 3-80 (a) Reactor temperature (°C), (b) Jacket temperature (°C), (c) Flow rate of heating oil (L/s), (d) Flow rate of cooling oil (L/s) in polycondensation process under 100 neuron NNMPC control with model mismatch

doi:10.6342/NTU202302309

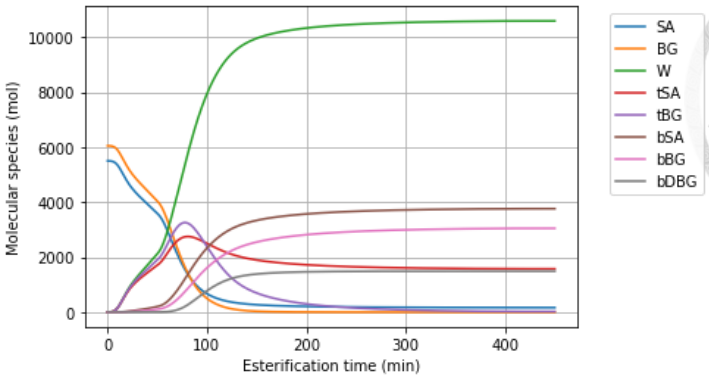

Figure 3-81 Molecular species profile in esterification process under 200 neuron NNMPC control with model mismatch

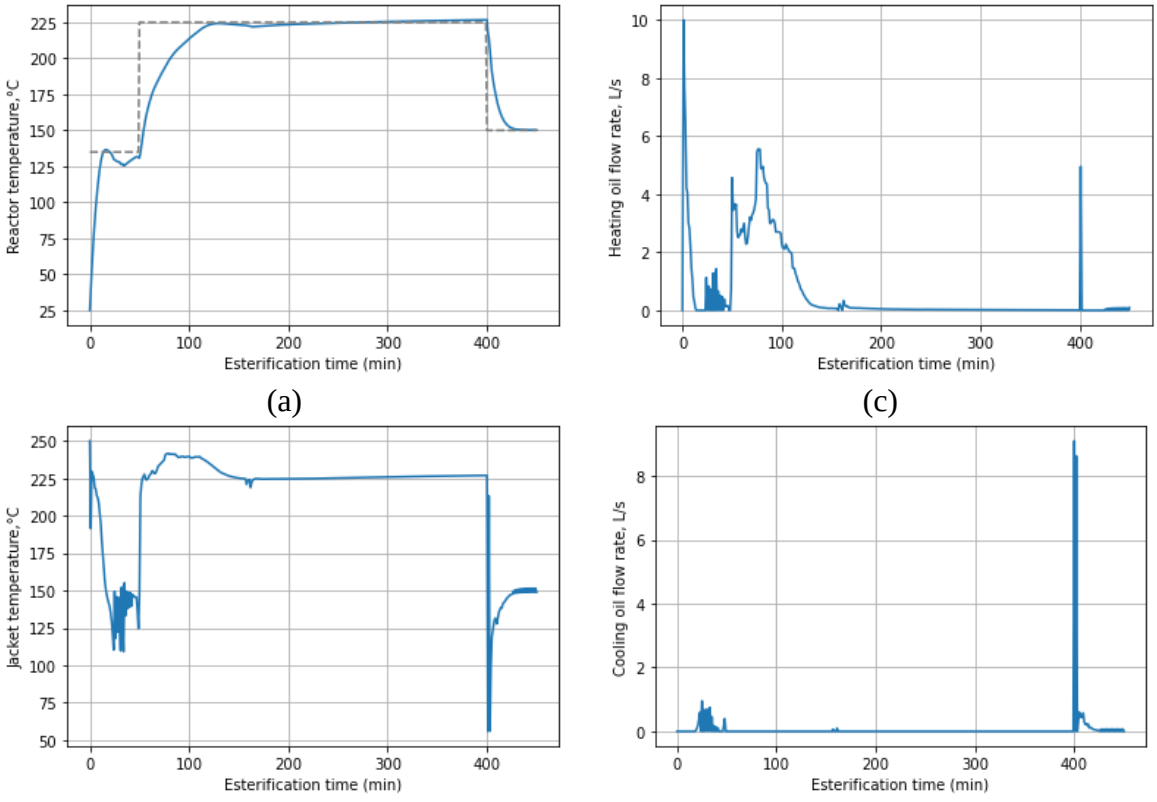

Figure 3-82 (a) Reactor temperature (°C), (b) Jacket temperature (°C), (c) Flow rate of heating oil (L/s), (d) Flow rate of cooling oil (L/s) in esterification process under 200 neuron NNMPC control with model mismatch

doi:10.6342/NTU202302309

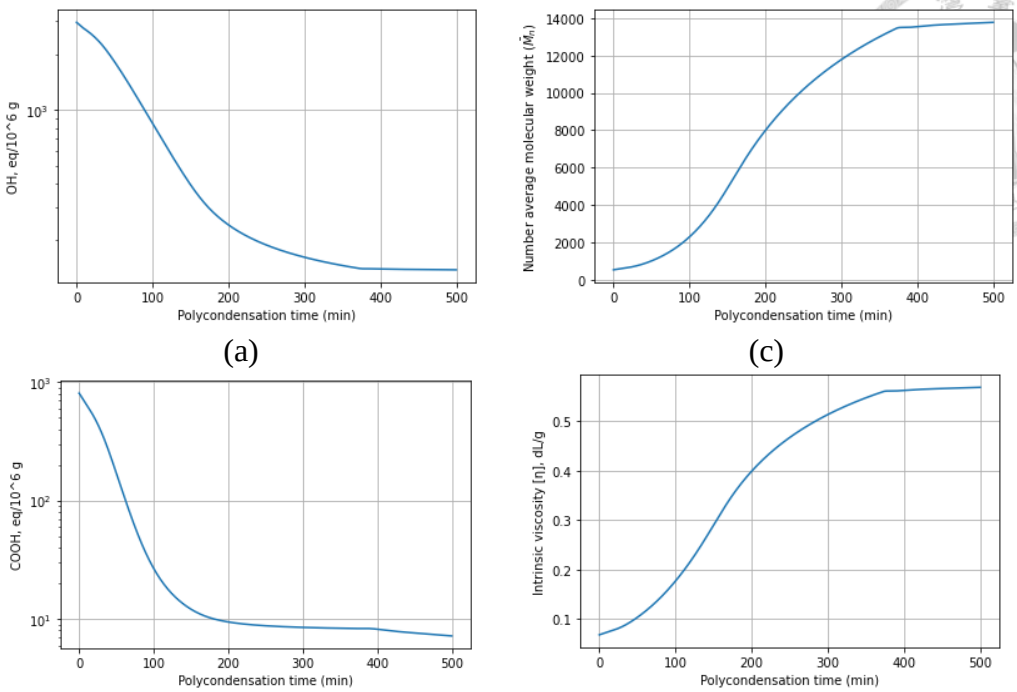

Figure 3-83 (a) OH end group (eq/10^6g), (b) COOH end group (eq/10^6g), (c) Number average molecular weight ($\bar{M}_n$), (d) Intrinsic viscosity (dL/g) during polycondensation process under 200 neuron NNMPC control with model mismatch

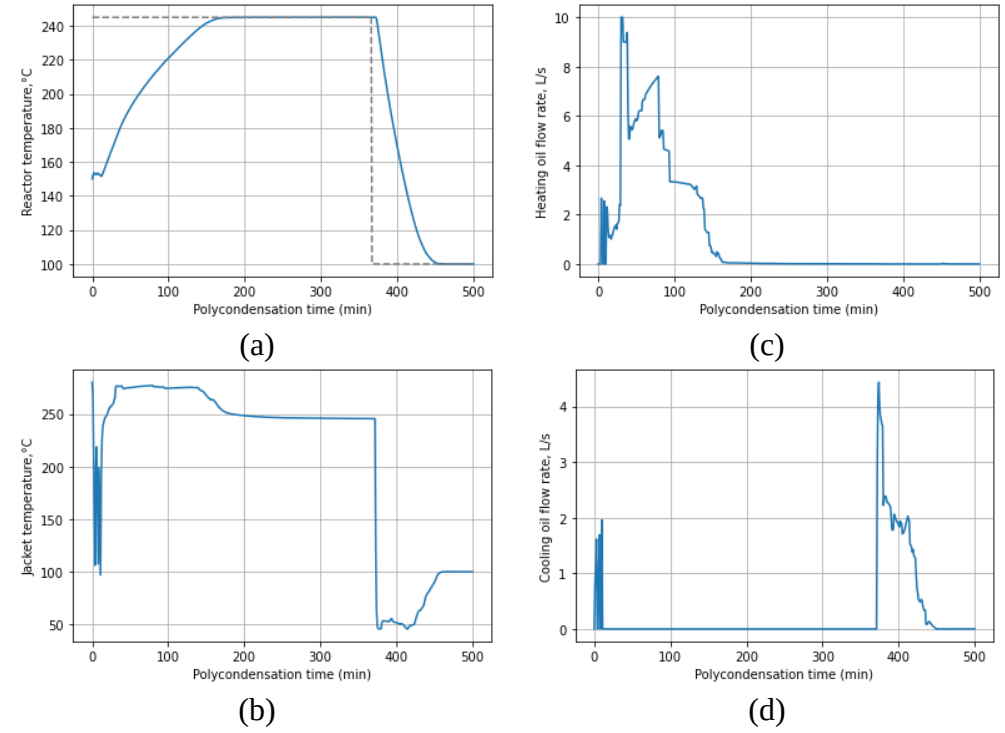

Figure 3-84 (a) Reactor temperature (°C), (b) Jacket temperature (°C), (c) Flow rate of heating oil (L/s), (d) Flow rate of cooling oil (L/s) in polycondensation process under 200 neuron NNMPC control with model mismatch

doi:10.6342/NTU202302309

3.5 Multi-NNMPC control

Multiple neural network model based predictive control (Multi-NNMPC). This method aims to improve the performance of the previous control method which was based on a single neural network model. The single MM model was not able to learn the dynamic behavior of the entire polymerization process accurately due to the complexity of the process. To overcome this issue, the single model was divided into three models, with lower complexity, to handle different parts of the process including esterification and polycondensation. By doing so, the control performance can be improved, and the simulation time can be shortened.

The NN models were designed with two hidden layers, and the number of neurons in each layer varied by two different configurations. One with 10 neurons per layer, and the other with 20 neurons per layer. These models were deployed in MPC to control the polymerization processes, and their control performance was compared to a single model with 50 neurons and a standard MPC control.

In the optimization procedure, the similar objective function as the first principle MPC is implemented in the reactor temperature control procedure, and each neural network model is assigned for a particular duration. For the esterification process, the preheating NN model (model 1-1) is used for the first 100 minutes, followed by the heating NN model (model 1-2) is in charge from 100 to 300 minutes, and the cooling NN model (model 1-3) is activated towards the end of the operation. In the polycondensation process, the heating NN model (model 2-1) controls the process from 0 to 150 minutes, then the isothermal control NN model (model 2-2) for 150 to 300 minutes, and finally, the cooling model (model 2-3) takes over from 300 minutes until the temperature reaches the final setpoint. The tuning parameters of Multi-NNMPC, including horizons, and

doi:10.6342/NTU202302309

weight matrices, remain the same as previous simulations.

3.5.1 Nominal case

Table 3-12 IAE performance criteria and simulation time under various Multi-NNMPC controller in esterification and polycondensation processes

	Multi-NNMPC		NNMPC	MPC
	10	**20**	**50**	
Esterification process				
IAE	2140.08	2030.52	2104.77	1880.69
Time (s)	8.75	10.13	16.61	122.22
Polycondensation process				
IAE	6652.24	6952.12	7239.28	6425.58
Time (s)	5.03	10.91	19.05	45.44

In esterification process, 20 neuron Multi-NNMPC performed the best and achieved precise temperature control to the setpoints without overshoot or offset, with an IAE value of 2030.52 as indicated in Table 3-12. The implementation of reduced NN models of 10 neurons shows a slightly lower performance that provided a higher IAE of 2140.08, this reflects the improvement of the esterification process control ability through 20 neuron Multi-NNMPC beyond a single NN model predictive controller (50 neuron NNMPC) that gained IAE of 2104.77. From Figure 3-90c illustrates the controlled valve action under 20 neuron Multi-NNMPC, indicating that more heating oil volume was supplied during the heating procedure than the control under 10 neuron Multi-NNMPC as shown in Figure 3-86c. This resulted in a rapid increase in temperature up to the setpoint of 225°C.

The implementation of Multi-NNMPC into the polycondensation process shows more appropriate usage of reduced complexity of NN model because the number of inputs is lesser than the prior process, thus, 10 neurons per hidden layer are sufficient for

doi:10.6342/NTU202302309

dynamic prediction in particular durations. The control action of heating oil flow under 10 neuron Multi-NNMPC, it is clear that the controller performed the heating oil supply with a highly smooth action and provided a higher efficiency (IAE=6652.24) as illustrated in Figure 3-88c. While 20 neuron NNMPC performed highly aggressive control action at heating and cooling oil valve movement because the lesser amount of training data led to a higher overfitting probability of NN model.

The reduced model shows a remarkable improvement in simulation time when compared to a single neural network model with high complexity implemented in NNMPC. This improvement is attributed to the reduced model's ability to easily compute outputs which is highly beneficial during the optimization procedure.

The results in Table 3-12 show that the esterification and polycondensation processes took significantly less time to simulate using the reduced model with 10 neurons, compared to the larger neural network model with 50 neurons implemented in NNMPC. Specifically, the esterification process took 8.75 seconds to complete the simulation under the 10 neuron Multi-NNMPC, while it took 16.61 seconds under the 50 neuron NNMPC. Similarly, the polycondensation process took 5.03 seconds to complete the simulation under the 10 neuron Multi-NNMPC, while it took 19.05 seconds under the 50 neuron NNMPC. This highlights the superior computational efficiency of the reduced model.

doi:10.6342/NTU202302309

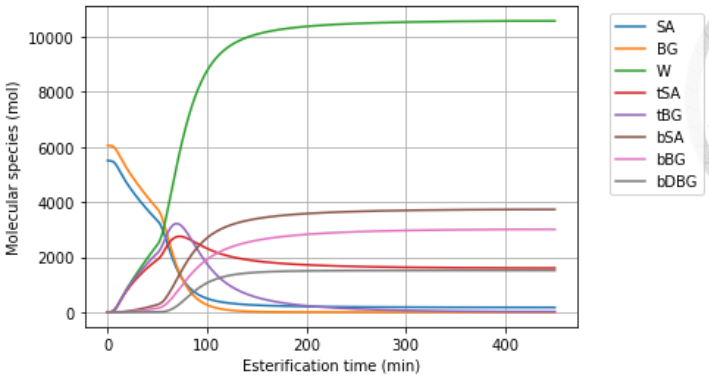

Figure 3-85 Molecular species profile in esterification process under 10 neuron Multi-NNMPC control

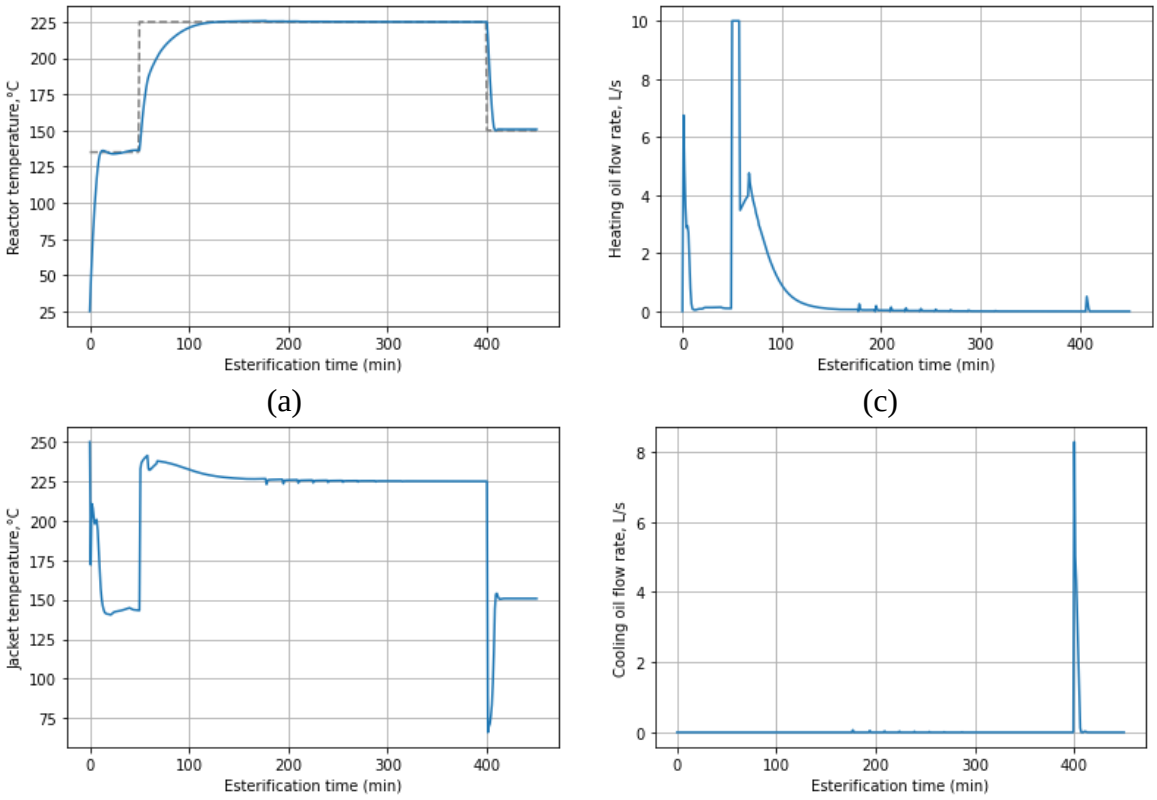

Figure 3-86 (a) Reactor temperature (°C), (b) Jacket temperature (°C), (c) Flow rate of heating oil (L/s), (d) Flow rate of cooling oil (L/s) in esterification process under 10 neuron Multi-NNMPC control

doi:10.6342/NTU202302309

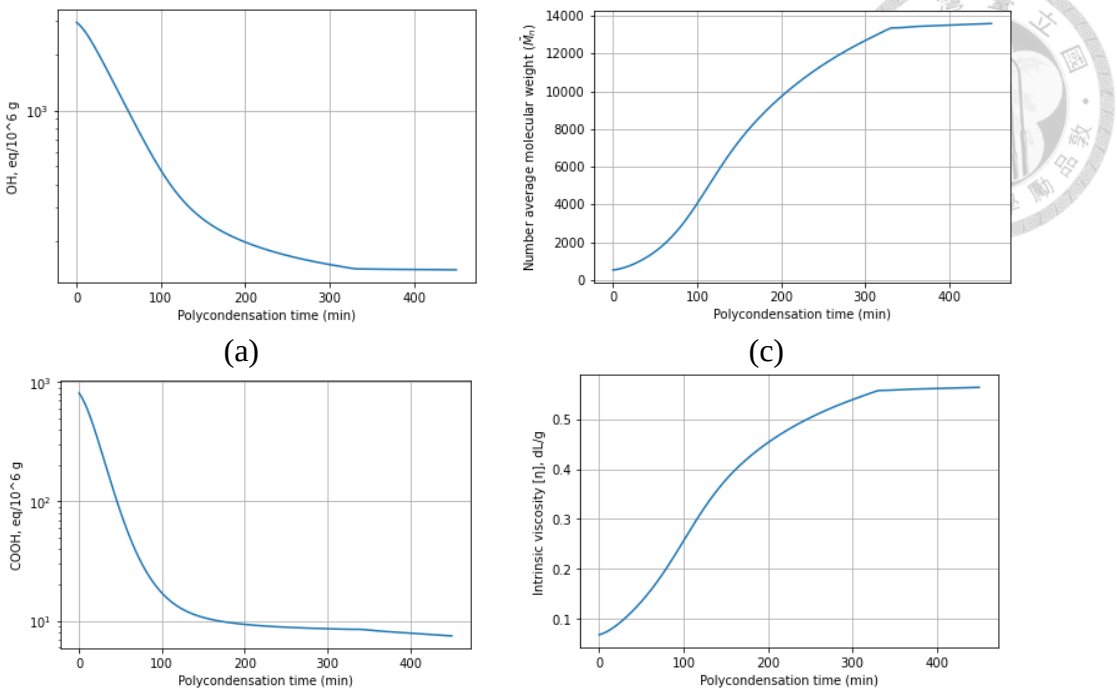

Figure 3-87 (a) OH end group (eq/10^6g), (b) COOH end group (eq/10^6g), (c) Number average molecular weight ($\bar{M}_n$), (d) Intrinsic viscosity (dL/g) during polycondensation process under 10 neuron Multi-NNMPC control

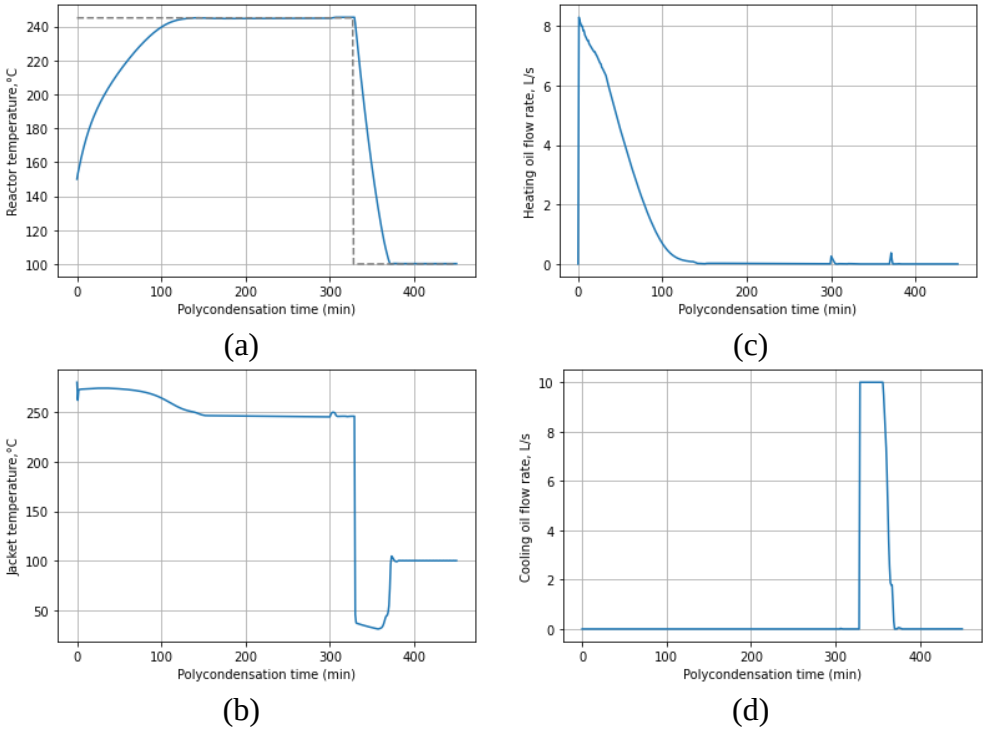

Figure 3-88 (a) Reactor temperature (°C), (b) Jacket temperature (°C), (c) Flow rate of heating oil (L/s), (d) Flow rate of cooling oil (L/s) in polycondensation process under 10 neuron Multi-NNMPC control

doi:10.6342/NTU202302309

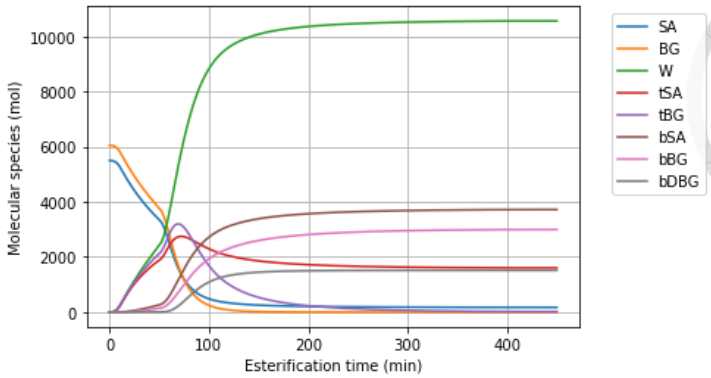

Figure 3-89 Molecular species profile in esterification process under 20 neuron Multi-NNMPC control

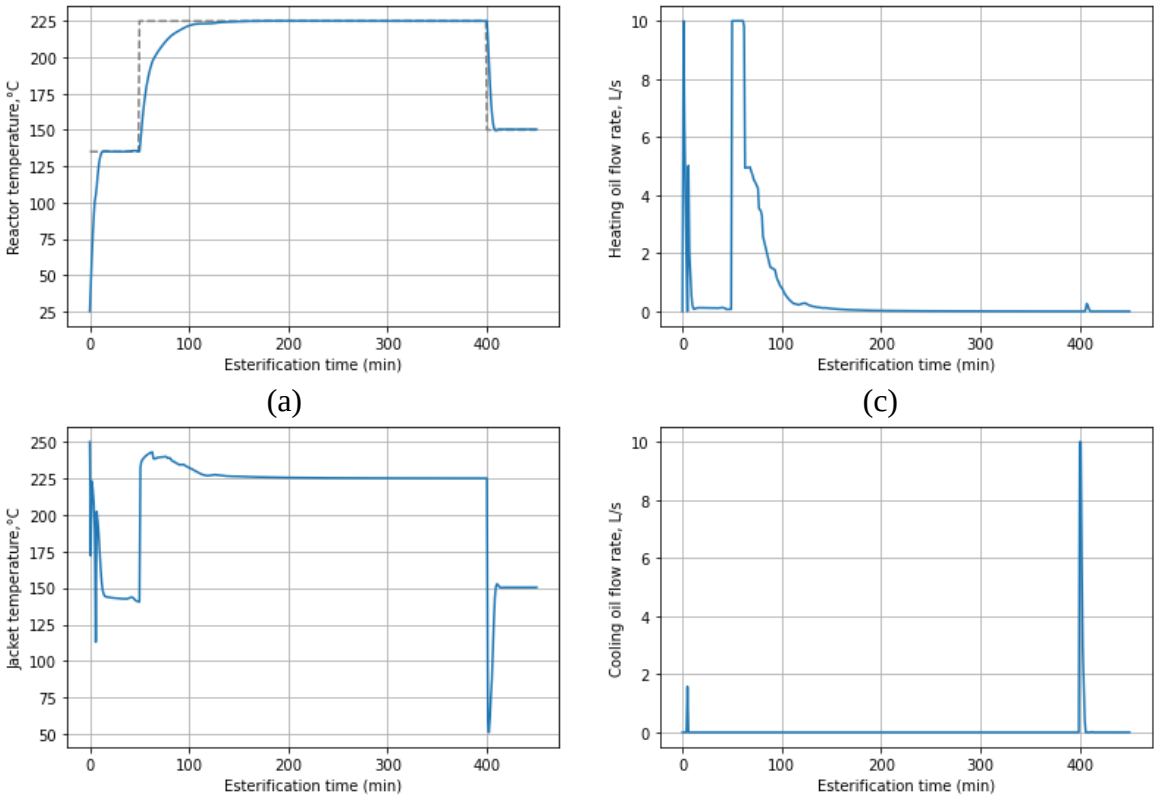

Figure 3-90 (a) Reactor temperature (°C), (b) Jacket temperature (°C), (c) Flow rate of heating oil (L/s), (d) Flow rate of cooling oil (L/s) in esterification process under 20 neuron Multi-NNMPC control

doi:10.6342/NTU202302309

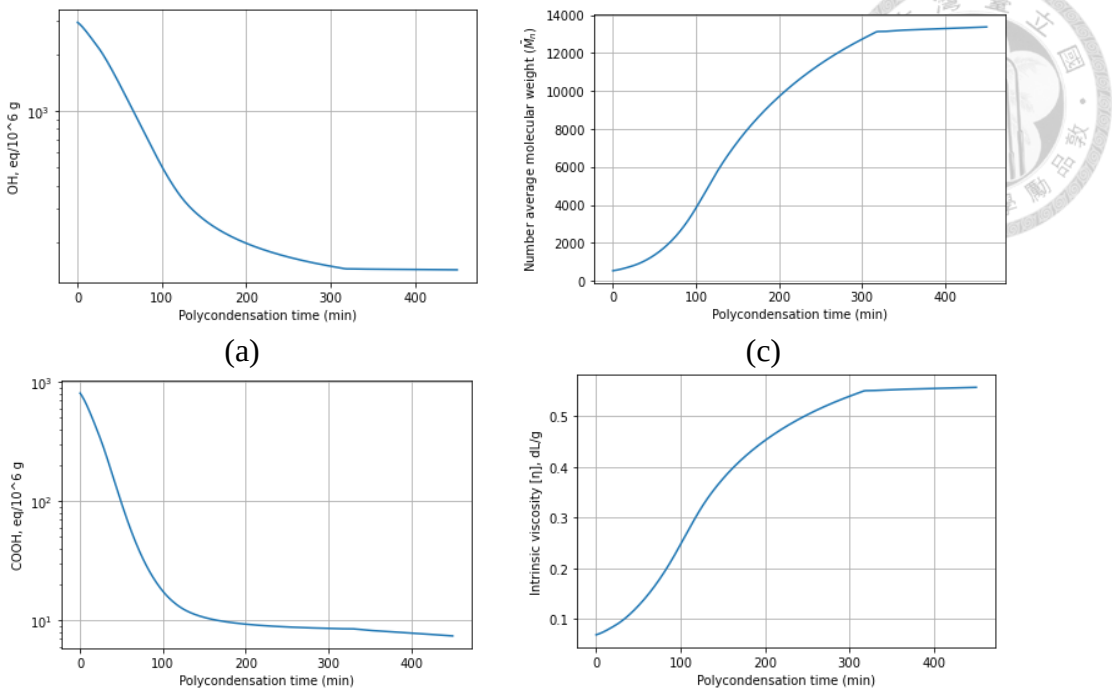

Figure 3-91 (a) OH end group (eq/10^6g), (b) COOH end group (eq/10^6g), (c) Number average molecular weight ($\bar{M}_n$), (d) Intrinsic viscosity (dL/g) during polycondensation process under 20 neuron Multi-NNMPC control

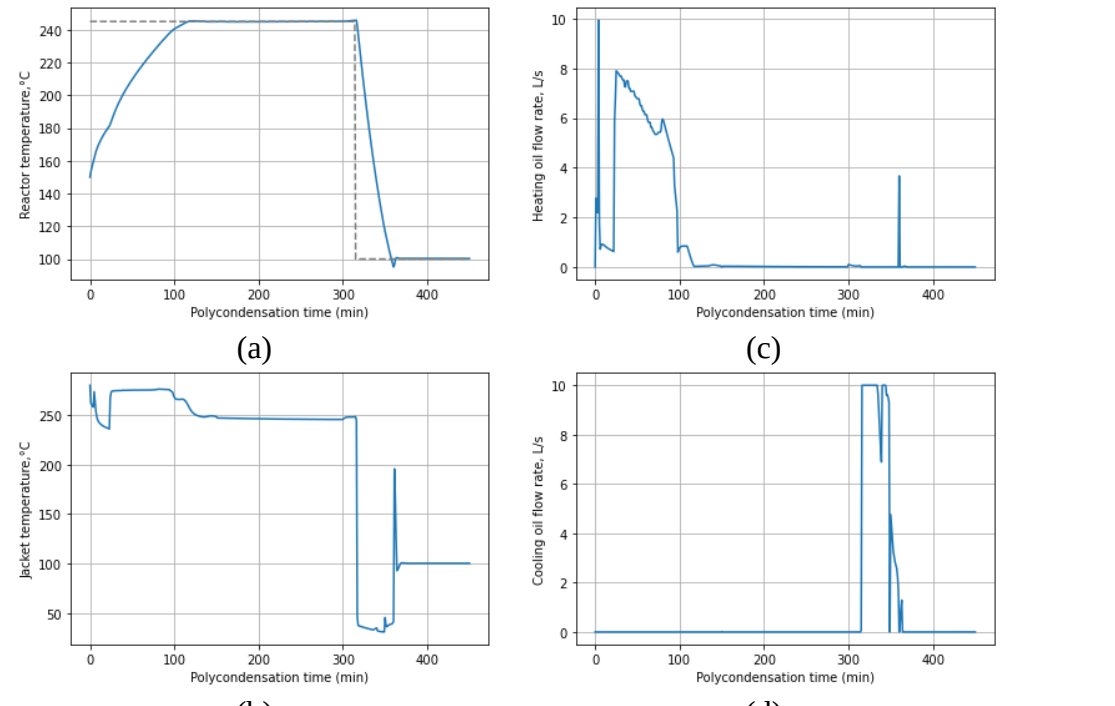

Figure 3-92 (a) Reactor temperature (°C), (b) Jacket temperature (°C), (c) Flow rate of heating oil (L/s), (d) Flow rate of cooling oil (L/s) in polycondensation process under 20 neuron Multi-NNMPC control

doi:10.6342/NTU202302309

3.5.2 White noise case

Table 3-13 IAE performance criteria and simulation time under various Multi-NNMPC controller in esterification and polycondensation processes with white noise

	Multi-NNMPC		NNMPC	MPC
	10	20	50	
Esterification process				
IAE	2497.98	2457.19	2490.93	2472.37
Time (s)	12.40	18.59	21.40	364.61
Polycondensation process				
IAE	6842.63	8325.03	7299.60	6806.14
Time (s)	7.97	26.25	25.95	121.62

The study found that the multiple neural network model predictive control was highly efficient in controlling reactor temperature, particularly in term of robustness, its ability to handle the interference from white noise during the esterification reaction. The reactor temperature control under Multi-NNMPC with 10 and 20 neuron structure could handle the noise and performed highly stable temperature control throughout the operation, as illustrated in Figures 3-94 and 3-98. This improved control performance with the utilization of 20 neuron Multi-NNMPC provided the IAE value of 2457.19. Meanwhile, the 10 neuron Multi-NNMPC provided a slightly higher IAE value of 2497.98 but its reduced NN structure offered a significantly shorter simulation time of only 12.40 seconds.

The excellent performance of the 10 neuron Multi-NNMPC in controlling reactor temperature was found during the polycondensation process. The control efficiency is demonstrated in Figure 3-96, where it can be observed that the 10 neuron Multi-NNMPC maintains the synthesis setpoint of 245°C with a remarkably low IAE value of 6842.63, outperforming all other neural network models tested. In addition, the 10 neuron Multi-

doi:10.6342/NTU202302309

NNMPC exhibits high-speed optimization ability, with the entire simulation completed in only 7.97 seconds, indicating its potential for efficient and rapid control in polycondensation processes.

The application of the 20 neuron Multi-NNMPC in the nominal case of the polycondensation process exhibited aggressive control action, while the temperature reach to the setpoint of 245°C. However, when the process was subjected to white noise, overfitting of the NN model became an issue, resulting in an inability to maintain the target temperature. Specifically, due to the overfitting, the heating oil flow rate supplied into the jacket was exceeded, leading to an undesirable increase in the reactor temperature up to 265°C as illustrated in Figure 3-100. This highlights the potential impact of NN model overfitting on the robustness of the controller.

The simulation demonstrated that the performance of the 20 neuron Multi-NNMPC in controlling the polycondensation process was significantly affected by the presence of white noise. When temperature measurements were corrupted by noise, the control system failed, resulting in a substantial increase in both the number average molecular weight and intrinsic viscosity of the product. Figure 3-99 provides a clear illustration of the extent of this effect, with the number average molecular weight and intrinsic viscosity rising to 16451.50 and 0.63 dL/g, respectively.

doi:10.6342/NTU202302309

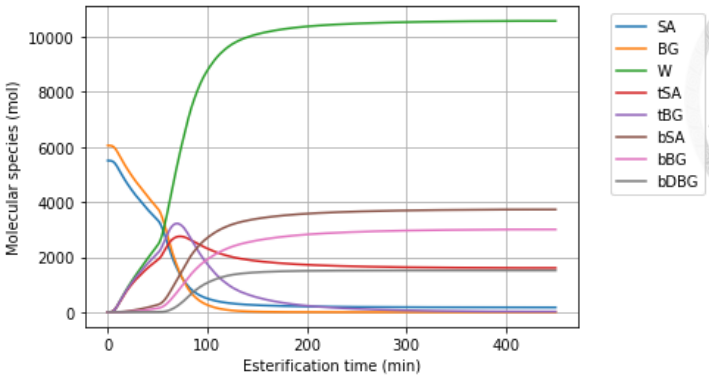

Figure 3-93 Molecular species profile in esterification process under 10 neuron Multi-NNMPC control with white noise

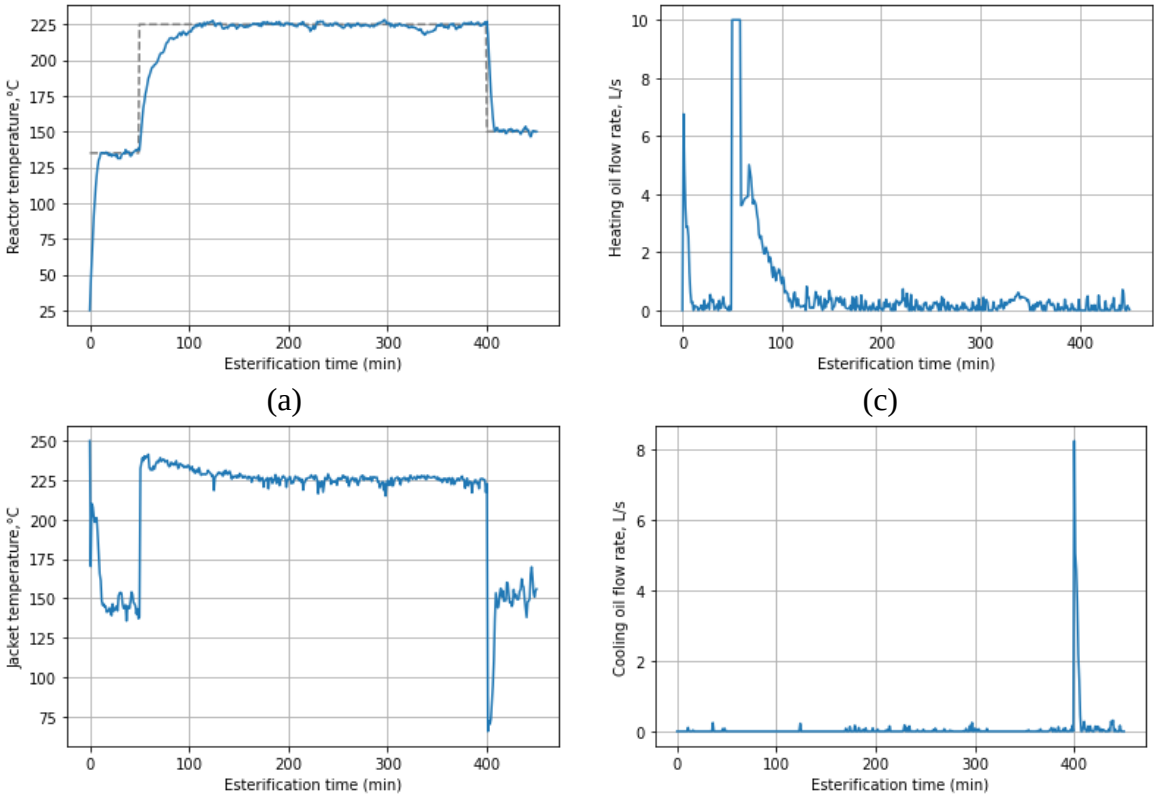

Figure 3-94 (a) Reactor temperature (°C), (b) Jacket temperature (°C), (c) Flow rate of heating oil (L/s), (d) Flow rate of cooling oil (L/s) in esterification process under 10 neuron Multi-NNMPC control with white noise

doi:10.6342/NTU202302309

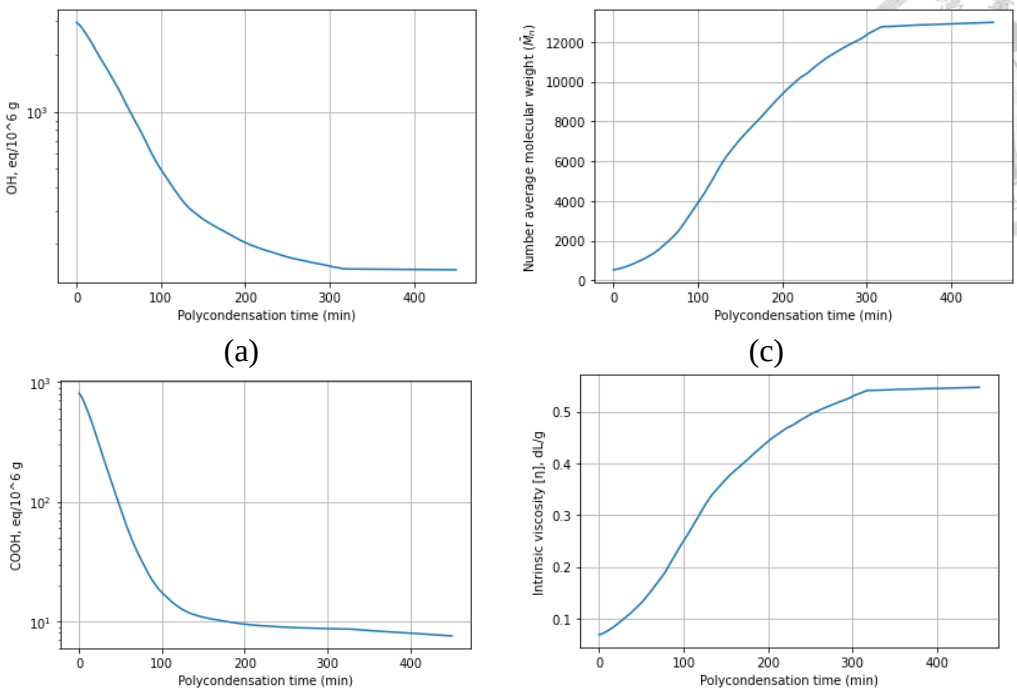

Figure 3-95 (a) OH end group (eq/10^6g), (b) COOH end group (eq/10^6g), (c) Number average molecular weight ($\bar{M}_n$), (d) Intrinsic viscosity (dL/g) during polycondensation process under 10 neuron Multi-NNMPC control with white noise

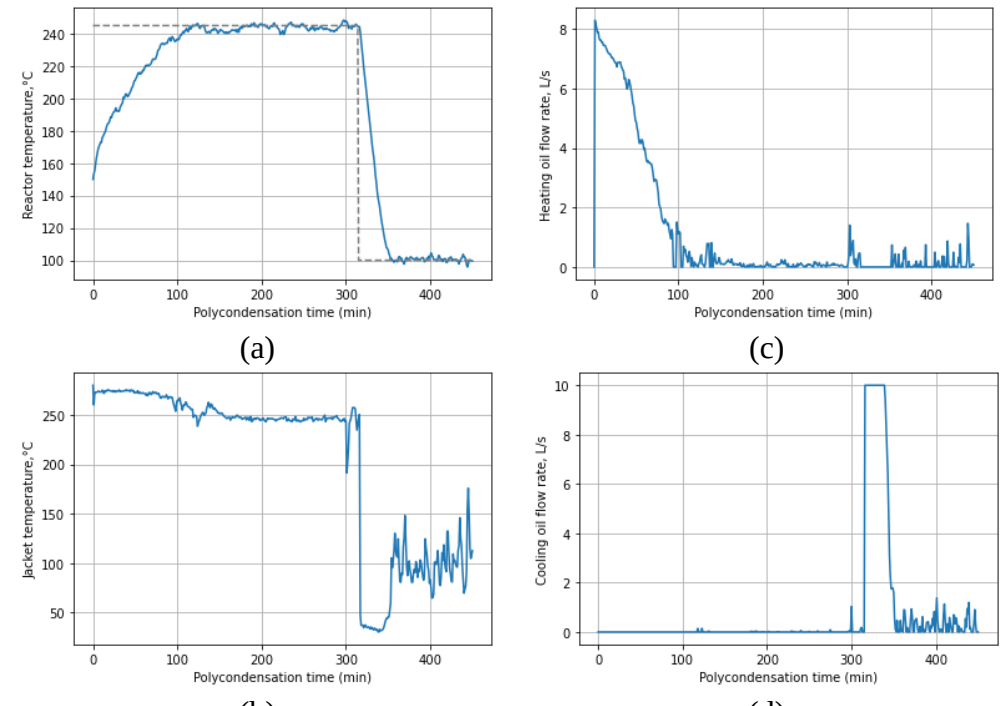

Figure 3-96 (a) Reactor temperature (°C), (b) Jacket temperature (°C), (c) Flow rate of heating oil (L/s), (d) Flow rate of cooling oil (L/s) in polycondensation process under 10 neuron Multi-NNMPC control with white noise

doi:10.6342/NTU202302309

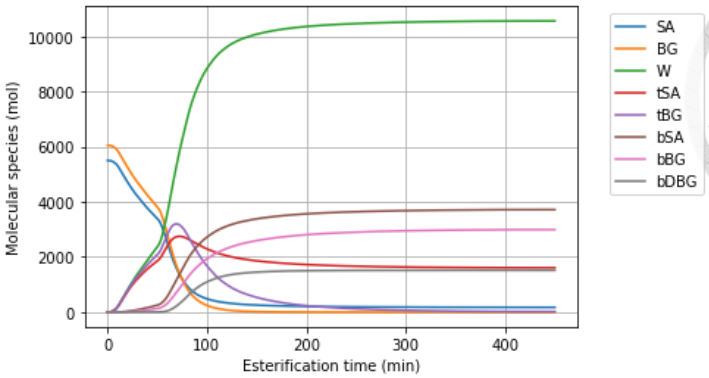

Figure 3-97 Molecular species profile in esterification process under 20 neuron Multi-NNMPC control with white noise

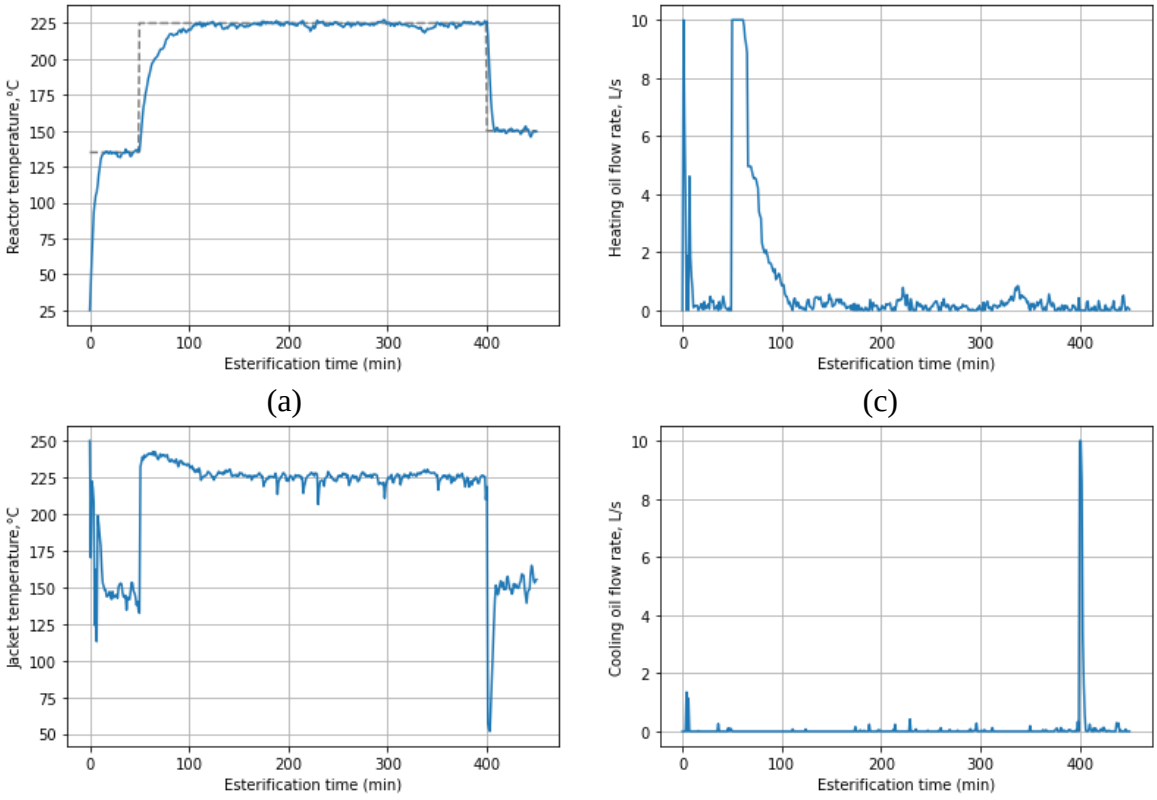

Figure 3-98 (a) Reactor temperature (°C), (b) Jacket temperature (°C), (c) Flow rate of heating oil (L/s), (d) Flow rate of cooling oil (L/s) in esterification process under 20 neuron Multi-NNMPC control with white noise

doi:10.6342/NTU202302309

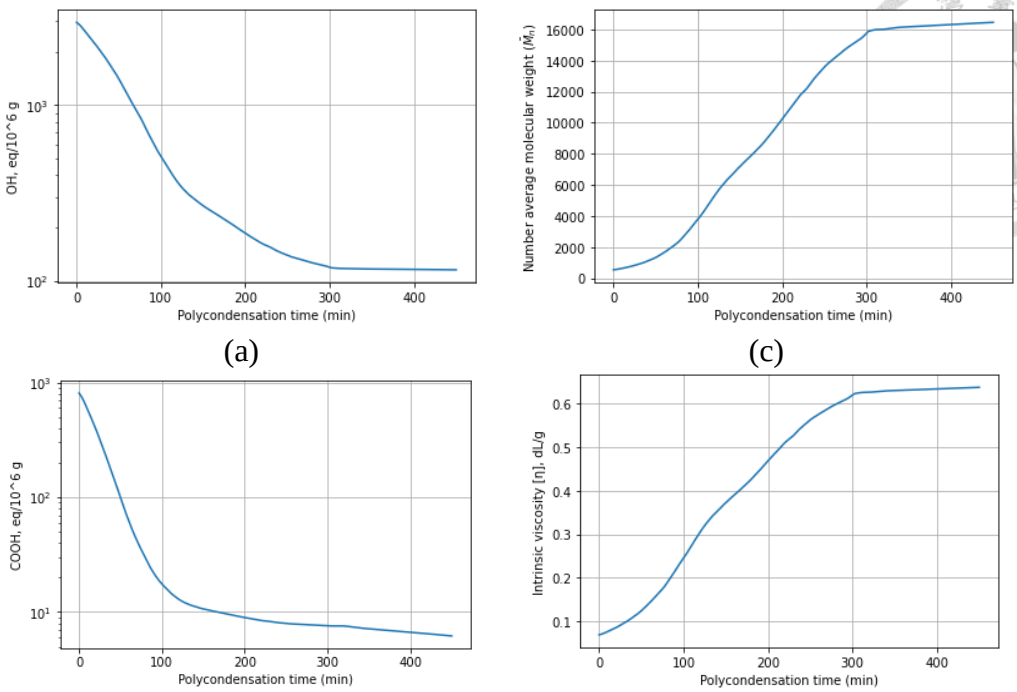

Figure 3-99 (a) OH end group (eq/10^6g), (b) COOH end group (eq/10^6g), (c) Number average molecular weight ($\bar{M}_n$), (d) Intrinsic viscosity (dL/g) during polycondensation process under 20 neuron Multi-NNMPC control with white noise

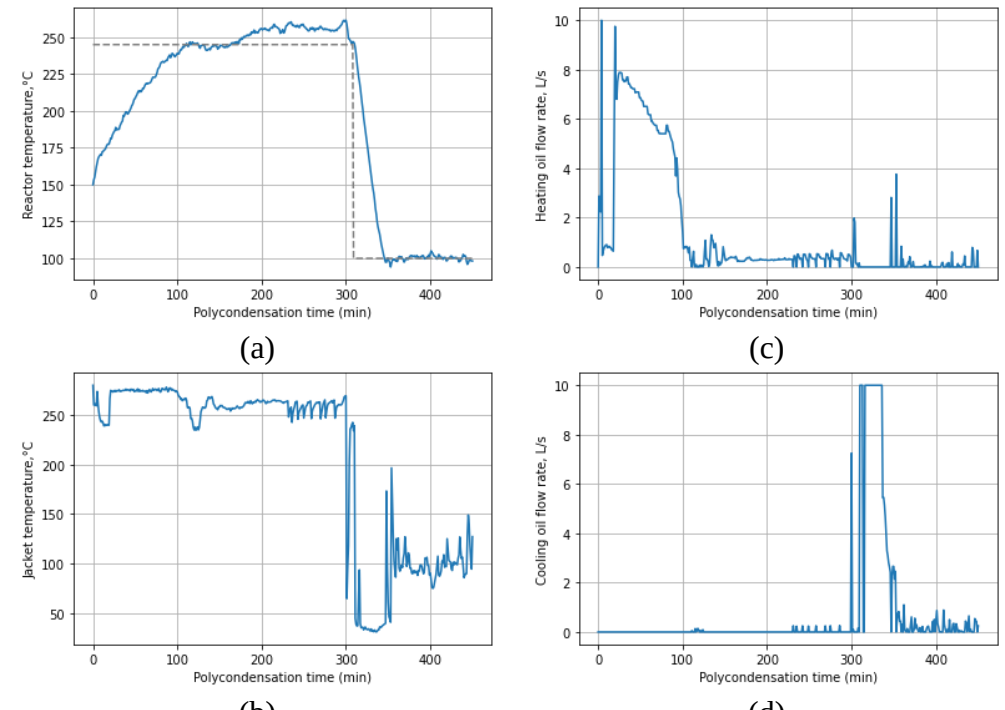

Figure 3-100 (a) Reactor temperature (°C), (b) Jacket temperature (°C), (c) Flow rate of heating oil (L/s), (d) Flow rate of cooling oil (L/s) in polycondensation process under 20 neuron Multi-NNMPC control with white noise

doi:10.6342/NTU202302309

3.5.3 Model mismatch case

Table 3-14 IAE performance criteria and simulation time under various Multi-NNMPC controller in esterification and polycondensation processes with white noise

	Multi-NNMPC		NNMPC	MPC
	10	**20**	**50**	
Esterification process				
IAE	2886.75	2795.99	2892.41	3009.59
Time (s)	7.90	9.98	18.25	128.74
Polycondensation process				
IAE	9226.62	9277.59	9795.90	10160.21
Time (s)	5.39	11.66	22.48	53.88

NNMPC has proven to be an exceptional control strategy, demonstrate remarkable proficiency in managing model mismatch scenarios that surpasses mathematic based MPC techniques. The advanced technique of NNMPC, particularly the Multi-NNMPC, exhibits the next level of improvement in the control performance, delivering rapid setpoint tracking capabilities while demonstrating higher levels of robustness.

In esterification process, all NN configuration of Multi-NNMPC provided a better control performance than 50 neuron NNMPC. Both of Multi-NNMPC with 10 and 20 neurons performed the temperature control to the setpoints within a shorter duration than NNMPC, and resulting in a substantially lower IAE of 2886.75 and 2795.99, respectively.

The polycondensation process, the synthesis temperature was driven to the setpoint of 245°C by using 10 neuron Multi-NNMPC. The temperature was successfully achieved within 147 minutes, representing a significant improvement over the control under 50 neuron NNMPC in model mismatch condition that reached the setpoint at 217 minutes, as illustrated in Figure 3-104. A large difference in time required to achieve setpoint was

doi:10.6342/NTU202302309

a consequence of the 50 neuron NNMPC exhibited a protracted temperature ramp-up period, particularly in the range of 240-245°C where only increasing 5°C, taking a total of 72 minutes (from 145 to 217 minutes) to reach the setpoint.

The performance of 20 neuron Multi-NNMPC was comparable to other approaches as shown in Figure 3-108, but it exhibited highly aggressive control action during the final stages of the operation, leading to substantial jacket temperature fluctuations and energy wastage. This issue was attributed to overfitting of the neural network model.

The application of Multi-NNMPC with the proposed configuration has proven to be highly effective in mitigating the issue of a prolonged temperature ramp-up when model mismatch occurs, leading to faster and more efficient attainment of the target reactor temperature and superior control performance. By leveraging advanced machine learning techniques and neural networks, Multi-NNMPC is able to accurately predict system behavior and adapt in real-time to changing conditions, enabling precise and effective control even in challenging operating environments.

doi:10.6342/NTU202302309

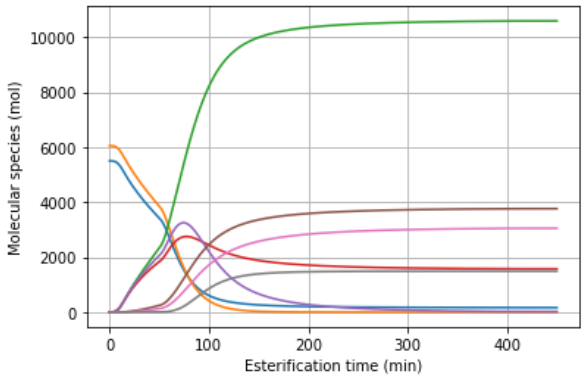

Figure 3-101 Molecular species profile in esterification process under 10 neuron Multi-NNMPC control with model mismatch

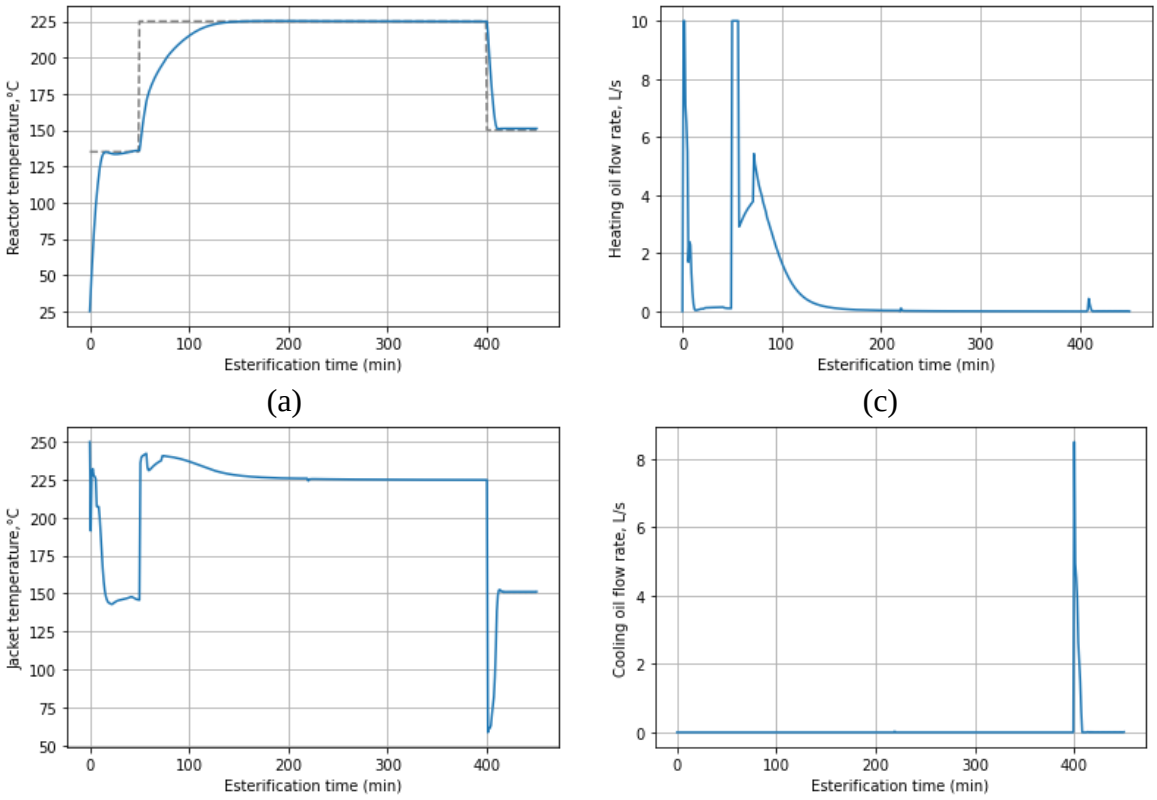

Figure 3-102 (a) Reactor temperature (°C), (b) Jacket temperature (°C), (c) Flow rate of heating oil (L/s), (d) Flow rate of cooling oil (L/s) in esterification process under 10 neuron Multi-NNMPC control with model mismatch

doi:10.6342/NTU202302309

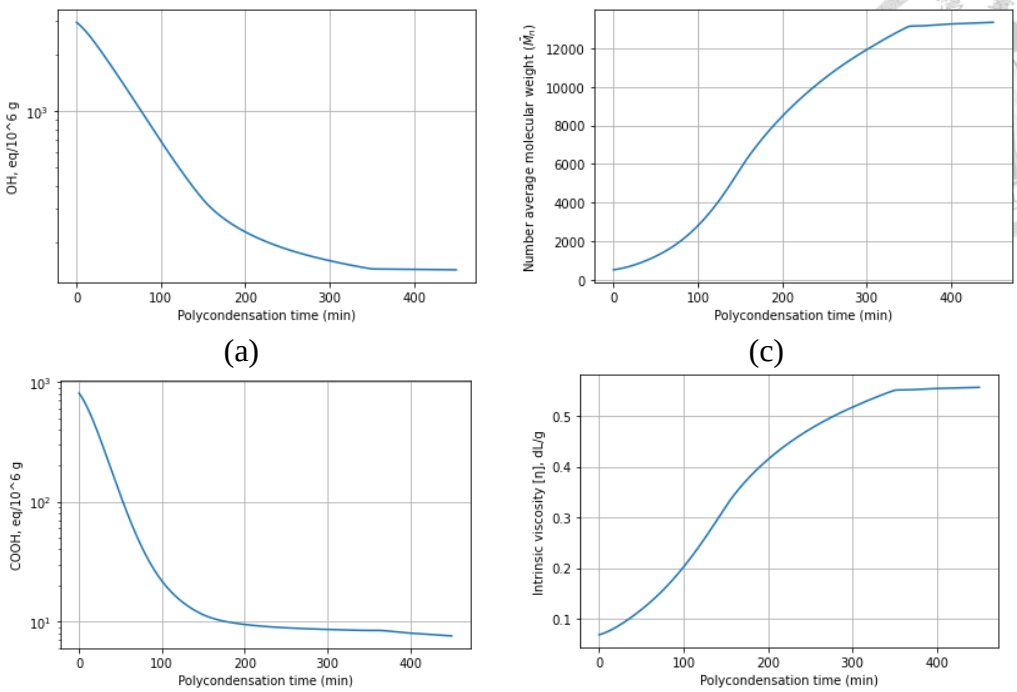

Figure 3-103 (a) OH end group (eq/10^6g), (b) COOH end group (eq/10^6g), (c) Number average molecular weight ($\bar{M}_n$), (d)Intrinsic viscosity (dL/g) during polycondensation process under 10 neuron Multi-NNMPC control with model mismatch

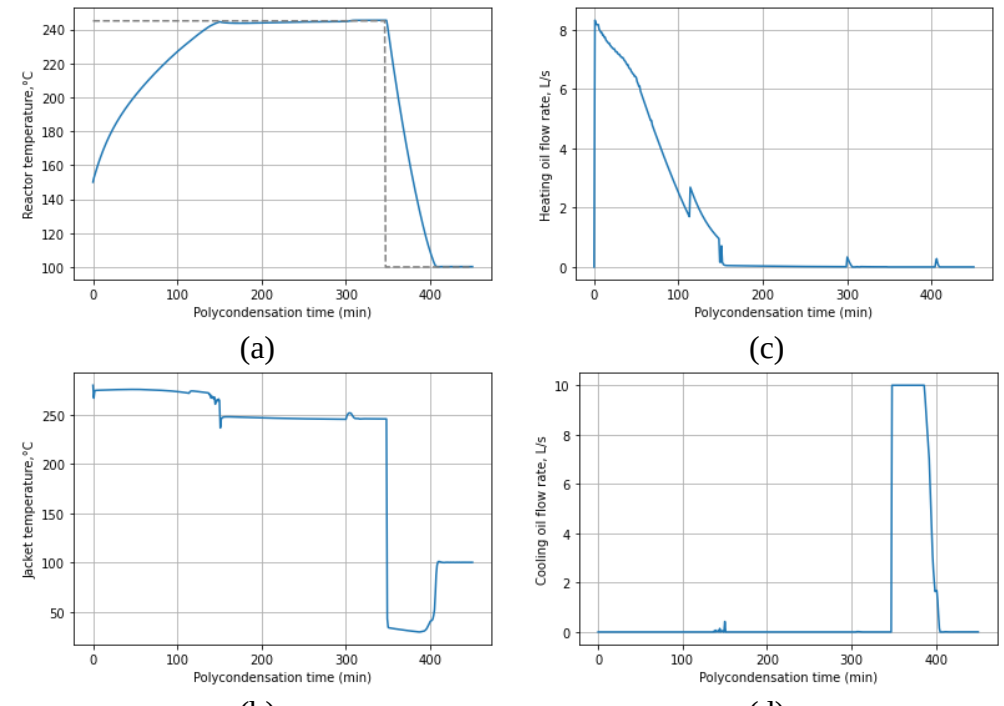

Figure 3-104 (a) Reactor temperature (°C), (b) Jacket temperature (°C), (c) Flow rate of heating oil (L/s), (d) Flow rate of cooling oil (L/s) in polycondensation process under 10 neuron Multi-NNMPC control with model mismatch

doi:10.6342/NTU202302309

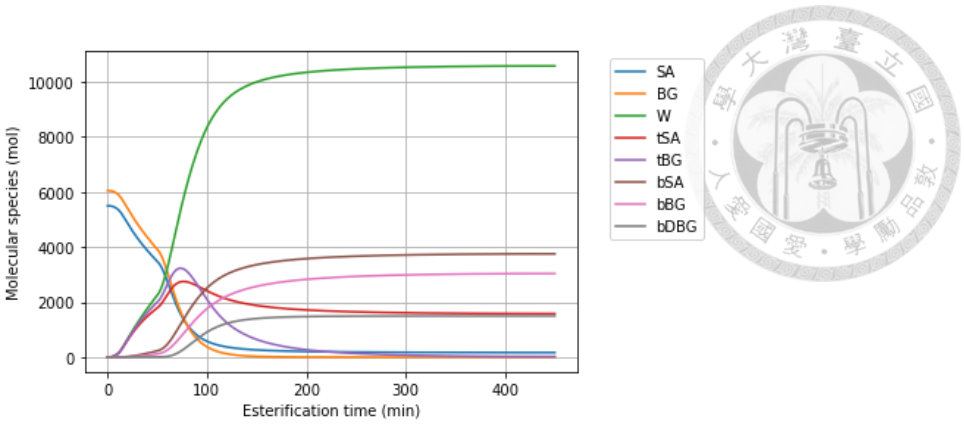

Figure 3-105 Molecular species profile in esterification process under 20 neuron Multi-NNMPC control with model mismatch

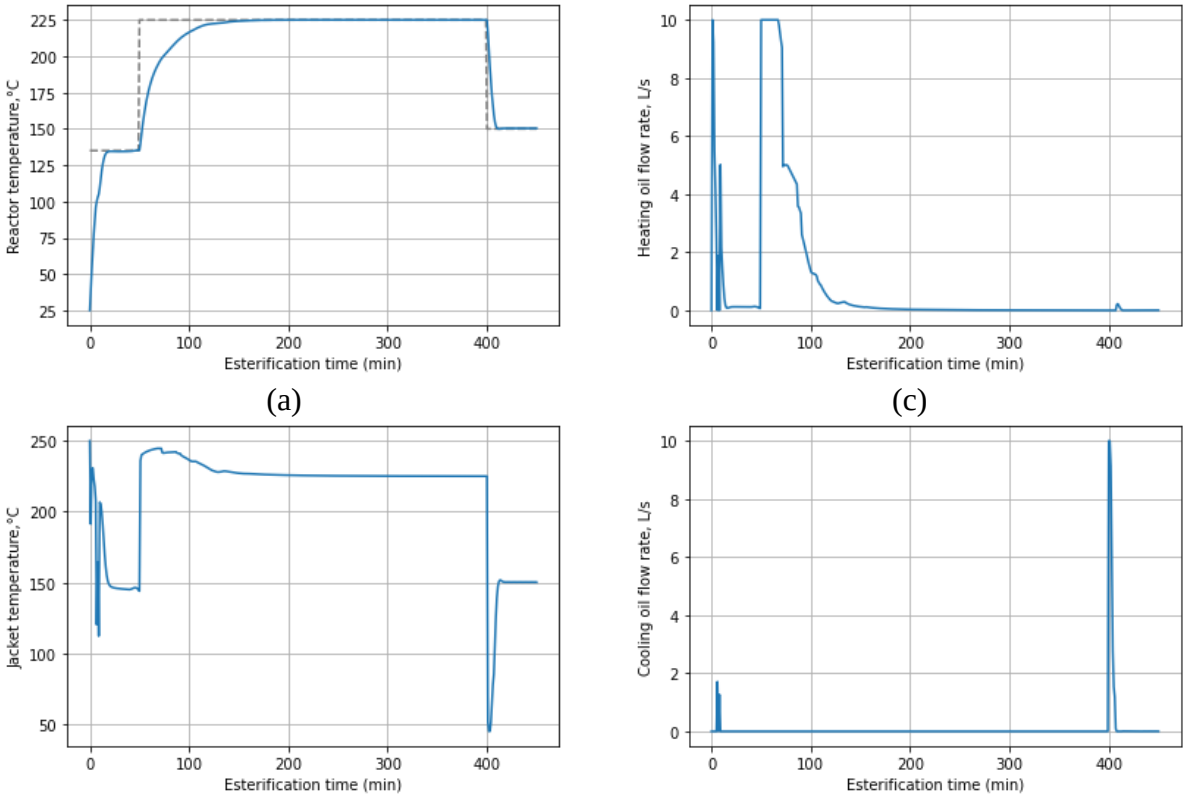

Figure 3-106 (a) Reactor temperature (°C), (b) Jacket temperature (°C), (c) Flow rate of heating oil (L/s), (d) Flow rate of cooling oil (L/s) in esterification process under 20 neuron Multi-NNMPC control with model mismatch

doi:10.6342/NTU202302309

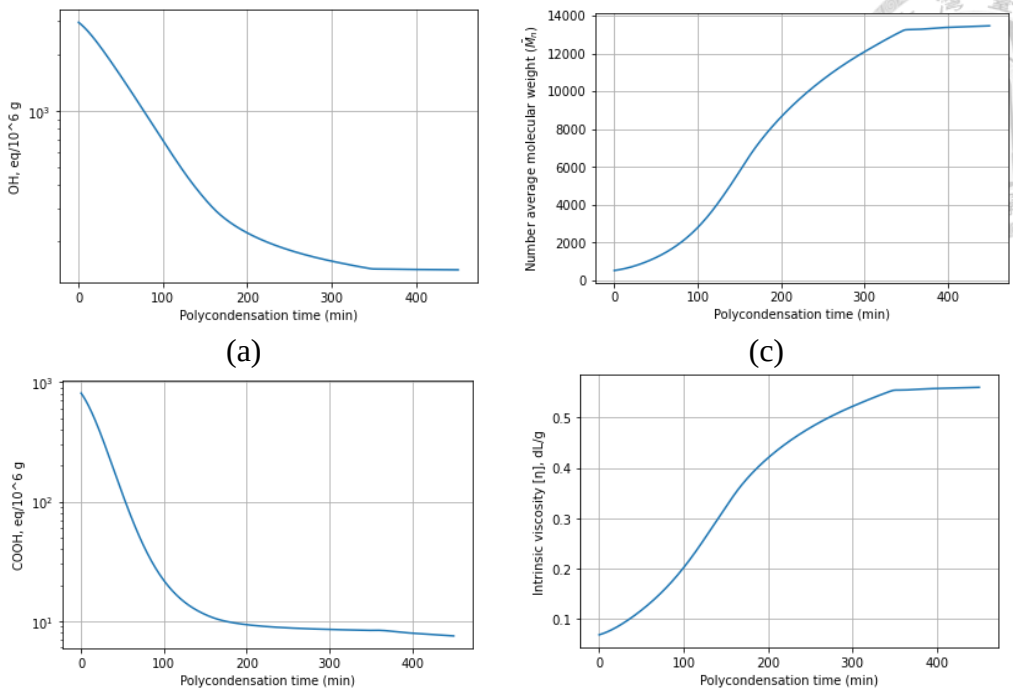

Figure 3-107 (a) OH end group (eq/10^6g), (b) COOH end group (eq/10^6g), (c) Number average molecular weight ($\bar{M}_n$), (d) Intrinsic viscosity (dL/g) during polycondensation process under 20 neuron Multi-NNMPC control with model mismatch

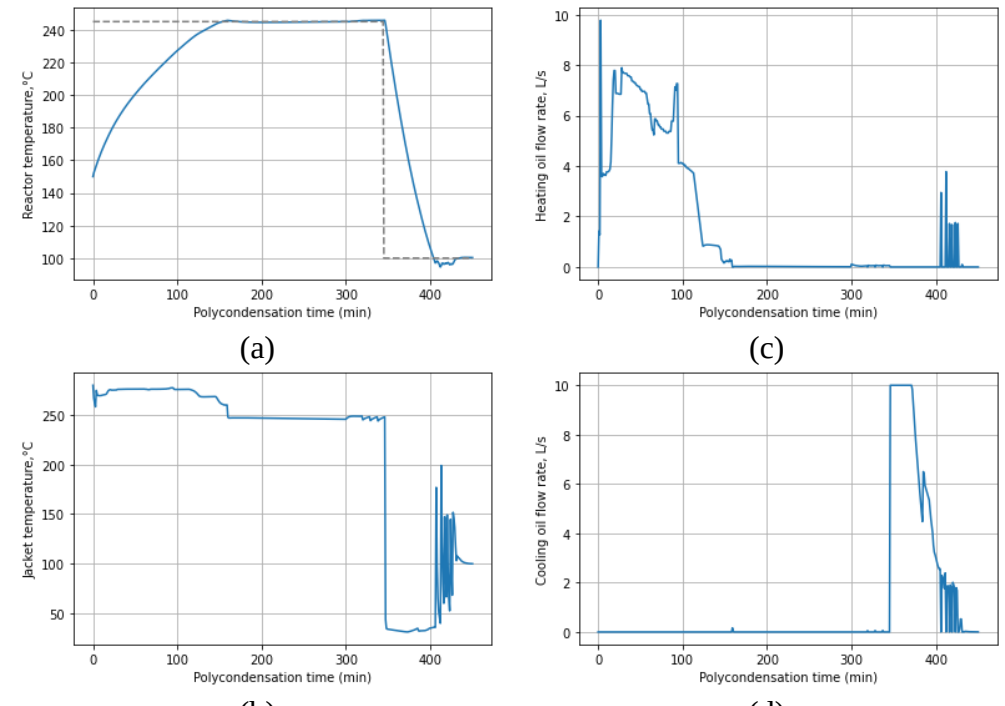

Figure 3-108 (a) Reactor temperature (°C), (b) Jacket temperature (°C), (c) Flow rate of heating oil (L/s), (d) Flow rate of cooling oil (L/s) in polycodensation process under 20 neuron Multi-NNMPC control with model mismatch

doi:10.6342/NTU202302309

Chapter 4 Conclusions

This research focuses on the use of data-driven technology for process control, specifically by implementing a neural network model in model predictive control for temperature control during the synthesis of polybutylene succinate (PBS) through esterification and polycondensation processes. The data-driven control techniques of NNMPC, and Multi-NNMPC control techniques were compared to split range PID in terms of their control performance and robustness under nominal and uncertain conditions, using integral absolute error (IAE) as a metric in the performance comparison.

The reactor temperature is designed to be controlled by direct feed heat transfer fluid of heat transfer oil into the jacket of the reactor, this technique has a huge utility consumption during the operation. In order to achieve both of a high level of control performance and efficient energy usage, it is crucial to ensure that each controller is sufficiently robust to handle a wide gap of setpoint tracking and interference of noise. This can be accomplished by sufficient robustness of each controller to reduce excessive utility consumption.

The split-range PID control method is employed with the sampling time of 1 minute. The simulation results indicate that the reactor temperature was successfully regulated with a large overshoot while reaching the setpoints, and the highly excess heating oil was fed into the jacket to raise the temperature up to the setpoints. The overshoot could be reduced by increasing the slope of the heating oil output line in order to increase sensitivity of the heating oil valve manipulation. However, highly aggressive control action was found when noise interfered during the operation, which reflects inefficient utility consumption under split-range PID control. This result highlights the tradeoff between the temperature control performance and robustness, as reducing overshoot

doi:10.6342/NTU202302309

results aggressive control action in response to noise corrupting the temperature measurement.

Neural network model predictive control (NNMPC) was implemented in both processes. Specifically, the feed-forward neural network architecture (FFNN) was chosen to deploy in model predictive controller. FFNN working principle is related to the process dynamic model, since the future state of a system for all time step in the operation through a model can be achieved by having all initial states and the system inputs without the influence of the previous outputs.

The feed-forward neural network models featuring a varying number of neurons in two hidden layers from 20, 50, 100, and 200 neurons were trained to study the process dynamic under different complexity. In the proposed neural network architectures of the processes, the inputs include all molecular species, the reactor and jacket temperatures, and the heating and cooling oil flow rates. Some variables are difficult to measure accurately in practical applications. Therefore, the implementation of this control technique in a real plant needs to incorporate an online state estimation technique into the controller, such as an extended Kalman filter. However, the model needs to be simplified to enhance the estimation performance but certain molecular species, particularly the monomer concentration, should be retained as inputs. This is due to the concentration is directly affected to the kinetic of the reaction, specifically the reaction rate, and the amount of heat released or absorbed during reaction proceed. Monomer concentration over time could be analyzed by Raman spectroscopy, this method offers a simple and accurate of process monitoring for semi-batch polymerization.

In the nominal operation, the study reveals that MPC proved to be efficient in temperature control due to the model is assumed to be matched the process 100%

doi:10.6342/NTU202302309

performed the IAE value of 1880.69, while NNMPC which has the NN model that was trained by using the wide range of process dynamic data from the conventional MPC. When the simulation proceeded without any uncertain event, the NNMPC with 50 neuron configuration performed outstanding control performance across all varying structures the process, the temperature could track the change of the setpoint efficiently without overshoot or offset provided the IAE value of 2104.77. However, it was observed that the 200 neuron NNMPC demonstrated more aggressive control action, likely due to overfitting of the neural network model, while the 20 neuron NNMPC model exhibited slight offset caused by insufficient neurons in the NN model.

The simulation included the interference of white noise to investigate control performance after the reactor and jacket temperature measurements were disturbed. 50 neuron NNMPC showed greater robustness than MPC, as the manipulated variables of heating and cooling oil flow rate were smoothly regulated to maintain isothermal temperature after the temperature fluctuated. Meanwhile, MPC exhibited aggressive control action, constantly switching both heating and cooling valves on and off throughout the operation, leading to excessive consumption of utility supply. However, MPC performed slightly better performance by obtaining a slightly lower IAE value than 50 neuron NNMPC (IAE: 50 neuron NNMPC = 2490.93 and MPC = 2472.37).

A scenario of model mismatch was simulated by the presence of fouling in the reactor, leading to a significant decline in heat transfer capability, this was achieved by reducing the overall heat transfer coefficient by 30%. The neural network models trained on nominal operation data were utilized to control the process with fouling. The NNMPC, consisting of 50 neurons, excelled in handling the mismatch event by driving the temperature to the setpoints faster than MPC after the valves were smoothly regulated.

doi:10.6342/NTU202302309

50 neuron NNMPC provided IAE value of 2892.41 while MPC was 3009.59. No overshoot or offset is observed, demonstrating its efficient ability to maintain isothermal control of the process. Furthermore, NNMPC exhibited a lower IAE value compared to MPC, the neural network model's adaptability in uncertain events, resulting in superior control performance. The control performance under model mismatch could be enhanced by data augmentation to cover various scenarios or events, leading to reduce the discrepancy between the model and process.

The neural network model enhanced optimization speed, with 50 neuron NNMPC model performed up to 5 times faster in optimization than the standard mathematical model under nominal conditions. Furthermore, utility consumption was significantly reduced compared to both split-range PID and MPC, even in cases where the processes encountered white noise or model mismatch scenarios. These results clearly highlight the benefits of incorporating a neural network model in the control strategy.

The synthesis of polybutylene succinate (PBS) is a complex and highly nonlinear chemical process, exhibiting distinct dynamic responses during each of its operational periods. Therefore, multiple NN models were developed, with each model specifically address the unique characteristics of three particular operational periods for better in describing the chemical processes or well duplicate the control action of MPC. To compare the models' performance, each neural network model was trained with reduced complexity of 10 and 20 neurons, the esterification process under 20 neurons Multi-NNMPC showed a slightly higher control performance than 50 neuron NNMPC in all scenarios with 2 times reduced simulation time. In the polycondensation process under Multi-NNMPC, the deployed neural network models with 10 neuron structure exhibited the most appropriate control action. This is because it has a lesser number of inputs, thus,

doi:10.6342/NTU202302309

10 neurons in each hidden layer are sufficient to precisely learn the dynamic data without causing model overfitting. The simpler NN structure achieved 3 times faster optimization procedure beyond 50 neuron NNMPC. Moreover, the protracted temperature ramp-up period problem when temperature almost reaches the setpoints was resolved.

This study presents a useful method for obtaining highly precise chemical process models without having to derive mathematical models or specifically black box models. This method reflects the effectiveness of data-driven technology in process control and highlights the potential of machine learning with improving control performance and robustness. The NNMPC approach could apply to control other processes that have complex kinetic and strong reactions. Furthermore, other chemical process equipment such as distillation column control that is related to a highly complex model because of deviating substance thermodynamic properties that can be defined by using NN model and employed in NNMPC to control the column temperature profile for obtaining desired purity.

doi:10.6342/NTU202302309

REFERENCES

1. Platnieks, O., et al., *Bio-based poly (butylene succinate): Recent progress, challenges and future opportunities.* European Polymer Journal, 2021. **161**: p. 110855.
2. Rafiqah, S.A., et al. *A Review on Properties and Application of Bio-Based Poly(Butylene Succinate)*. Polymers, 2021. **13**, DOI: 10.3390/polym13091436.
3. Bikiaris, D.N. and D.S. Achilias, *Synthesis of poly(alkylene succinate) biodegradable polyesters I. Mathematical modelling of the esterification reaction.* Polymer, 2006. **47**(13): p. 4851-4860.
4. Bikiaris, D.N. and D.S. Achilias, *Synthesis of poly(alkylene succinate) biodegradable polyesters, Part II: Mathematical modelling of the polycondensation reaction.* Polymer, 2008. **49**(17): p. 3677-3685.
5. Redchuk, A., et al. *Adoption Case of IIoT and Machine Learning to Improve Energy Consumption at a Process Manufacturing Firm, under Industry 5.0 Model*. Big Data and Cognitive Computing, 2023. **7**, DOI: 10.3390/bdcc7010042.
6. Shang, C. and F. You, *Data Analytics and Machine Learning for Smart Process Manufacturing: Recent Advances and Perspectives in the Big Data Era.* Engineering, 2019. **5**(6): p. 1010-1016.
7. Choi, Y., et al., *Data-driven modeling of multimode chemical process: Validation with a real-world distillation column.* Chemical Engineering Journal, 2023. **457**: p. 141025.
8. Jendoubi, I. and F. Bouffard, *Data-driven sustainable distributed energy resources' control based on multi-agent deep reinforcement learning.* Sustainable Energy, Grids and Networks, 2022. **32**: p. 100919.
9. Bonvin, D. and G. Francois, *Control and Optimization of Batch Chemical Processes*. 2017. p. 441-503.
10. Dyson, C., et al. *MPC Model-Plant-Mismatch Detection Through Slow Feature Analysis Preprocessing with Industrial Application*. in *2022 IEEE International Symposium on Advanced Control of Industrial Processes (AdCONIP)*. 2022.
11. Cao, Y. and R.B. Gopaluni, *Deep Neural Network Approximation of Nonlinear Model Predictive Control.* IFAC-PapersOnLine, 2020. **53**(2): p. 11319-11324.
12. Gütter, J., et al., *Impact of Training Set Size on the Ability of Deep Neural Networks to Deal with Omission Noise.* Frontiers in Remote Sensing, 2022. **3**: p. 932431.
13. Wang, Y. and S. Boyd, *Fast Model Predictive Control Using Online Optimization.* Control Systems Technology, IEEE Transactions on, 2010. **18**: p. 267-278.
14. Salzmann, T., et al., *Real-Time Neural MPC: Deep Learning Model Predictive Control for Quadrotors and Agile Robotic Platforms.* IEEE Robotics and Automation Letters, 2022. **8**: p. 2397-2404.
15. Tokiwa, Y., et al., *Biodegradability of Plastics.* International journal of molecular sciences, 2009. **10**: p. 3722-42.
16. Savitha, K.S., et al., *Polybutylene succinate, a potential bio-degradable polymer: synthesis, copolymerization and bio-degradation.* Polymer Chemistry,

doi:10.6342/NTU202302309

2022. **13**(24): p. 3562-3612.
17. xu, J., et al., *Morphological, barrier and mechanical properties of films from poly (butylene succinate) reinforced with nanocrystalline cellulose and chitin whiskers using melt extrusion.* Journal of Polymer Research, 2019. **26**.
18. Jin, T.-x., et al., *Effect of molecular weight on the properties of poly(butylene succinate).* Chinese Journal of Polymer Science, 2014. **32**(7): p. 953-960.
19. Jin, H.-J., et al., *Chain extension and biodegradation of poly(butylene succinate) with maleic acid units.* Journal of Polymer Science Part B: Polymer Physics, 2000. **38**(17): p. 2240-2246.
20. Peñas, M.I., et al. *A Review on Current Strategies for the Modulation of Thermomechanical, Barrier, and Biodegradation Properties of Poly (Butylene Succinate) (PBS) and Its Random Copolymers*. Polymers, 2022. **14**, DOI: 10.3390/polym14051025.
21. Zhu, Q.-Y., et al., *Synthesis and characterization of a novel multiblock copolyester containing poly(ethylene succinate) and poly(butylene succinate).* Materials Chemistry and Physics, 2011. **130**(3): p. 943-949.
22. Martins, F., *Tuning PID controllers using the ITAE criterion.* International Journal of Engineering Education, 2005. **21**.
23. Jibril, M., et al., *Comparison of PID and MPC controllers for continuous stirred tank reactor (CSTR) concentration control.* 2020. **02**: p. 133-140.
24. Rajalakshmi, M., P. Saranya, and P. Shanmugavadivu. *Pattern Recognition-Recognition of Handwritten Document Using Convolutional Neural Networks*. in *2019 IEEE International Conference on Intelligent Techniques in Control, Optimization and Signal Processing (INCOS)*. 2019.
25. Sako, K., B.N. Mpinda, and P.C. Rodrigues *Neural Networks for Financial Time Series Forecasting*. Entropy, 2022. **24**, DOI: 10.3390/e24050657.
26. Kamel, A., L. Rahmani, and R. Lebied, *New application of artificial neural network-based direct power control for permanent magnet synchronous generator.* Electrical Engineering & Electromechanics, 2021: p. 18-24.
27. Fényes, D., et al. *Robust Control Design for Autonomous Vehicles Using Neural Network-Based Model-Matching Approach*. Energies, 2021. **14**, DOI: 10.3390/en14217438.
28. Jiang, B., et al. *Neural Network Based Model Predictive Control for a Quadrotor UAV*. Aerospace, 2022. **9**, DOI: 10.3390/aerospace9080460.
29. Rowell, D. *State-Space Representation of LTI Systems*. October 2002.
30. Konakom, K., P. Kittisupakorn, and I.M. Mujtaba, *Neural network-based controller design of a batch reactive distillation column under uncertainty.* Asia-Pacific Journal of Chemical Engineering, 2012. **7**(3): p. 361-377.
31. Arpornwichanop, A., P. Kittisupakorn, and M.A. Hussain, *Model-based control strategies for a chemical batch reactor with exothermic reactions.* Korean Journal of Chemical Engineering, 2002. **19**(2): p. 221-226.
32. Antão, R., et al. *Model Predictive Control of Non-Linear Systems Using Tensor Flow-Based Models*. Applied Sciences, 2020. **10**, DOI: 10.3390/app10113958.
33. Hosen, M.A., M.A. Hussain, and F.S. Mjalli, *Control of polystyrene batch reactors using neural network based model predictive control (NNMPC): An experimental investigation.* Control Engineering Practice, 2011. **19**(5): p. 454-467.
34. Kittisupakorn, P., et al., *Neural network based model predictive control for a steel pickling process.* Journal of Process Control, 2009. **19**(4): p. 579-590.

doi:10.6342/NTU202302309

35. Han, J., et al. *Synthesis, Properties of Biodegradable Poly(Butylene Succinate-co-Butylene 2-Methylsuccinate) and Application for Sustainable Release*. Materials, 2019. **12**, DOI: 10.3390/ma12091507.
36. Perry, R.H. and D.W. Green, *Perry's chemical engineers' handbook*. 8th ed. ed. 2008, New York: McGraw-Hill.
37. Karayannidis, G.P., et al., *Study of various catalysts in the synthesis of poly(propylene terephthalate) and mathematical modeling of the esterification reaction.* Polymer, 2003. **44**(4): p. 931-942.
38. Park, S.S., H.W. Jun, and S.S. Im, *Kinetics of forming poly(butylene succinate) (PBS) oligomer in the presence of MBTO catalyst.* Polymer Engineering & Science, 1998. **38**(6): p. 905-913.
39. Masayuki Kamikawa, H.J., et al., *Device and method for producing polybutylene succinate*. 2013, Hitachi, Ltd., Tokyo (JP)
40. Achilias, D.S., *A Review of Modeling of Diffusion Controlled Polymerization Reactions.* Macromolecular Theory and Simulations, 2007. **16**(4): p. 319-347.
41. Nunes, R.W., J.R. Martin, and J.F. Johnson, *Influence of molecular weight and molecular weight distribution on mechanical properties of polymers.* Polymer Engineering & Science, 1982. **22**(4): p. 205-228.
42. Berkowitz, S., *Viscosity–molecular weight relationships for poly(ethylene terephthalate) in hexafluoroisopropanol–pentafluorophenol using SEC–LALLS.* Journal of Applied Polymer Science, 1984. **29**(12): p. 4353-4361.
43. Charlier, Q., et al., *Solution viscosity -molar mass relationships for poly(Butylene succinate) and discussion on molar mass analysis.* eXPRESS Polymer Letters, 2015. **9**: p. 424.
44. Fonseca, R.R., et al., *A fuzzy–split range control system applied to a fermentation process.* Bioresource Technology, 2013. **142**: p. 475-482.
45. Drgoňa, J., et al., *All you need to know about model predictive control for buildings.* Annual Reviews in Control, 2020. **50**: p. 190-232.
46. Lheureux, A. *Feed-forward vs feedback neural networks*. 2022; Available from: https://blog.paperspace.com/feed-forward-vs-feedback-neural-networks/.
47. Baheti, P. *Activation functions in neural networks (12 types & use cases)*. 2022; Available from: https://www.v7labs.com/blog/neural-networks-activation-functions.
48. Wu, G.-D. and S.-L. Lo, *Effects of data normalization and inherent-factor on decision of optimal coagulant dosage in water treatment by artificial neural network.* Expert Systems with Applications, 2010. **37**(7): p. 4974-4983.
49. Ahmad, Z. and J. Zhang. *A Nonlinear Model Predictive Control Strategy Using Multiple Neural Network Models*. in *Advances in Neural Networks - ISNN 2006*. 2006. Berlin, Heidelberg: Springer Berlin Heidelberg.

doi:10.6342/NTU202302309

APPENDIX A Simulation data

All state variables of the processes reflect the dynamic behavior of the process under the manipulation of heating and cooling oil flow rates throughout the operation, which was used to train the neural network. The 50 simulation datasets, including profiles of all molecular species, reactor and jacket temperatures, and heat transfer oil flow rates, are shown in the figures below. These datasets were collected by randomly setting the temperature setpoint in each phase within the range of 25 – 250°C for the esterification process and 25 - 280°C for the polycondensation process. The manipulated variables of heating and cooling oil valves were calculated using a mathematic MPC.

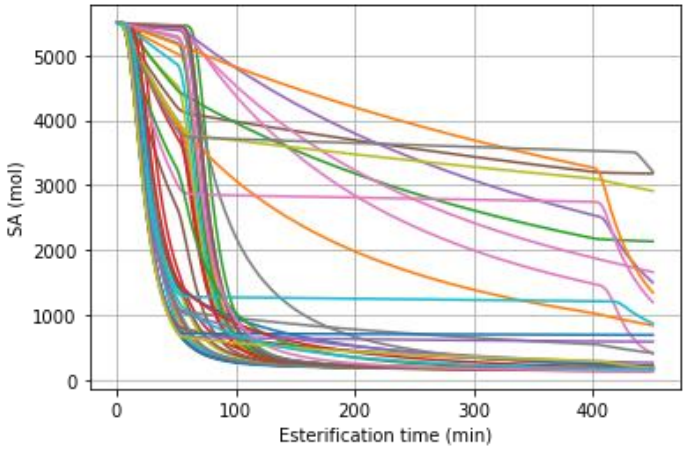

Figure A-1 Succinic acid simulation data

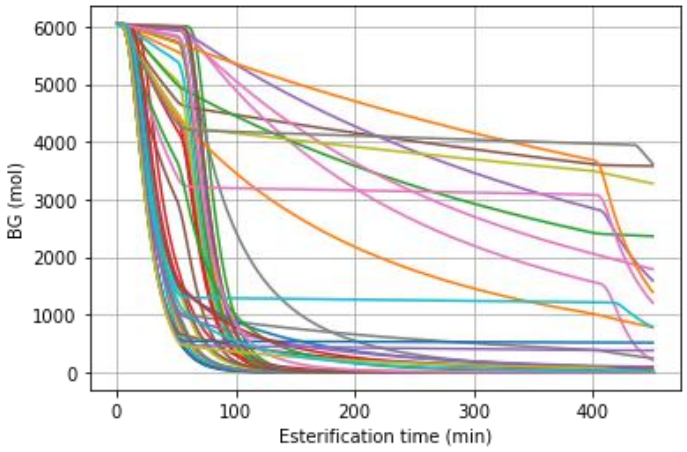

Figure A-2 Butylene glycol simulation data

doi:10.6342/NTU202302309

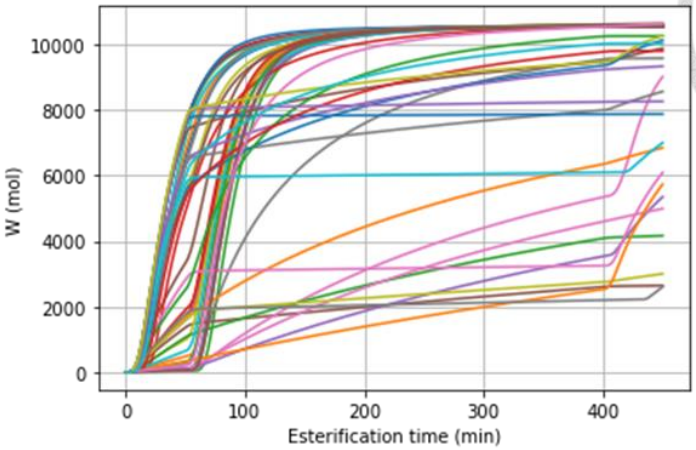

Figure A-3 Water simulation data

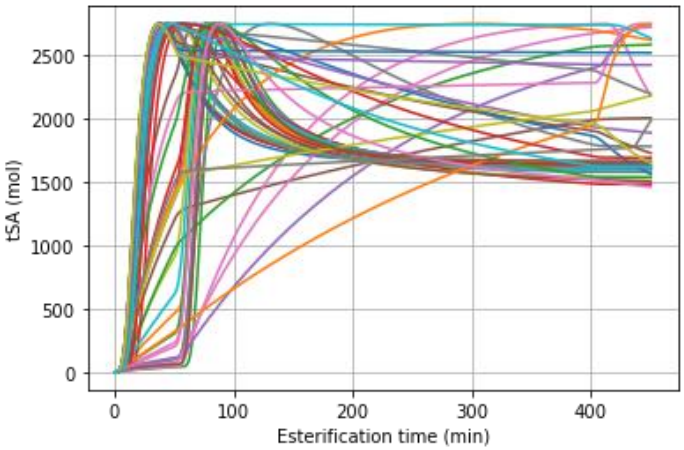

Figure A-4 Succinic acid end group simulation data

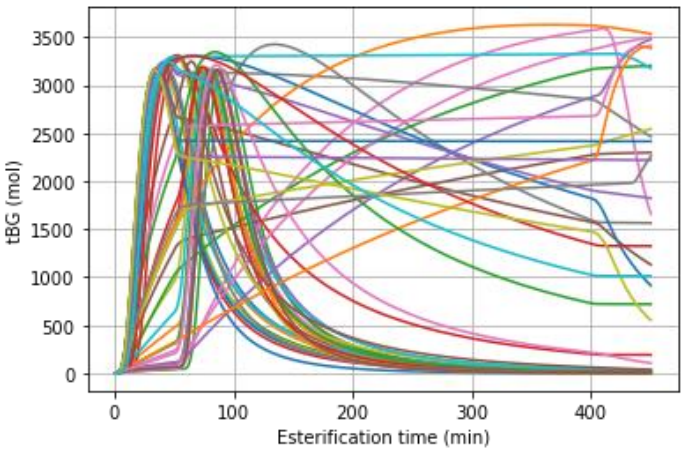

Figure A-5 Butylene glycol end group simulation data

doi:10.6342/NTU202302309

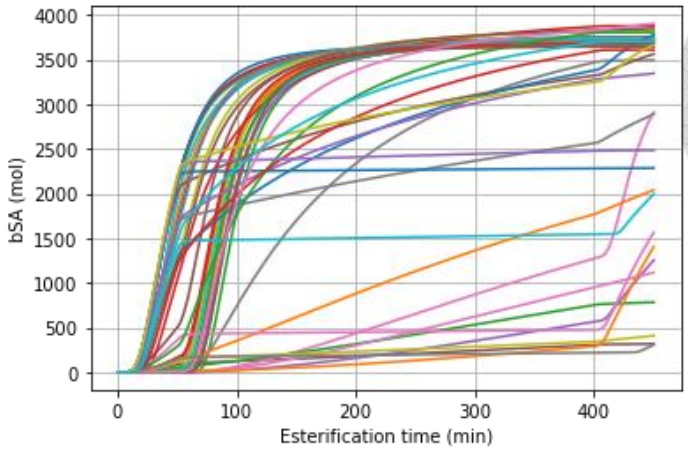

Figure A-6 Succinic acid repeating unit simulation data

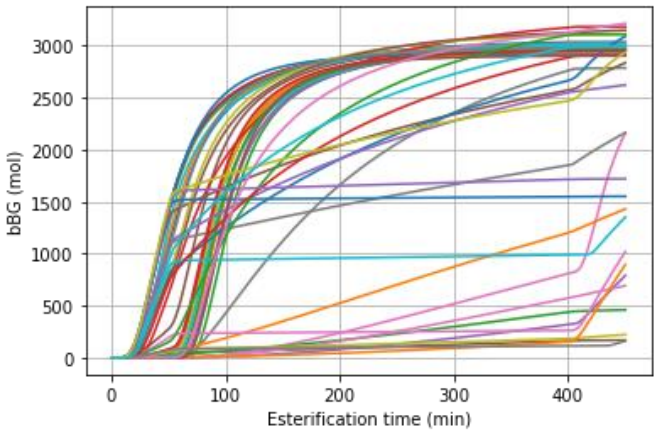

Figure A-7 Butylene glycol repeating unit simulation data

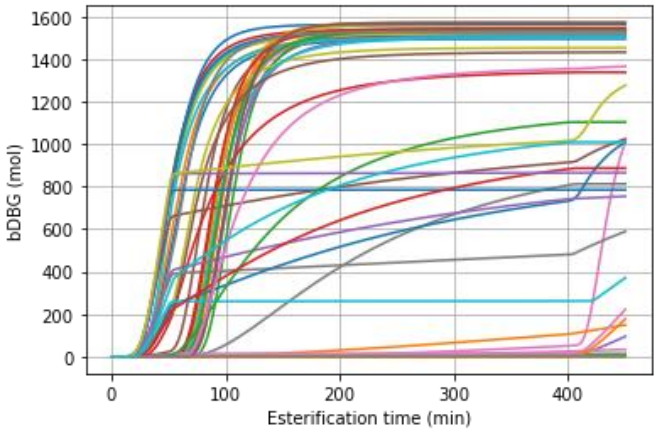

Figure A-8 Dibutylene glycol repeating unit simulation data

doi:10.6342/NTU202302309

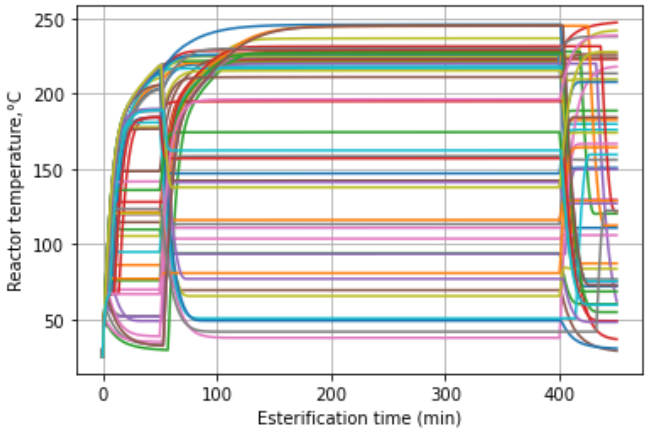

Figure A-9 Reactor temperature of esterification process simulation data

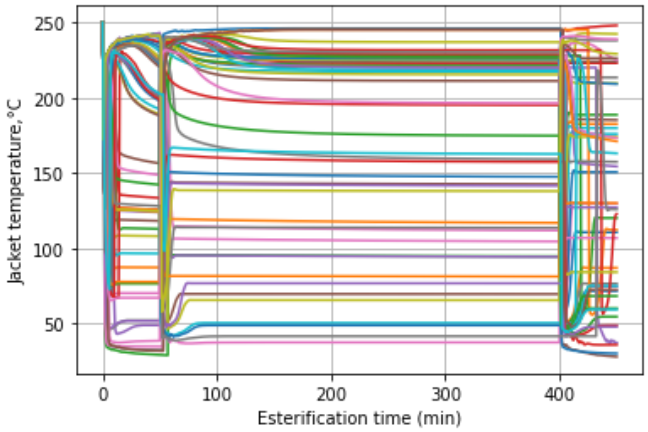

Figure A-10 Jacket temperature of esterification process simulation data

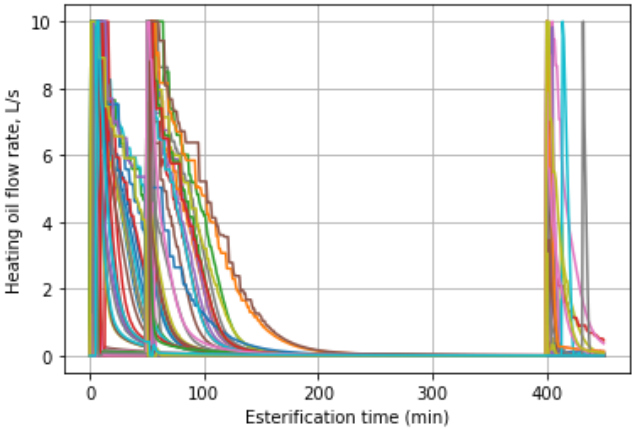

Figure A-11 Heating oil flow rate of esterification process simulation data

doi:10.6342/NTU202302309

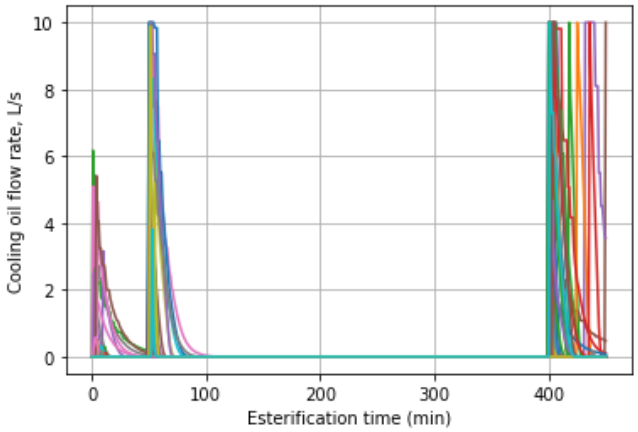

Figure A-12 Cooling oil flow rate of esterification process simulation data

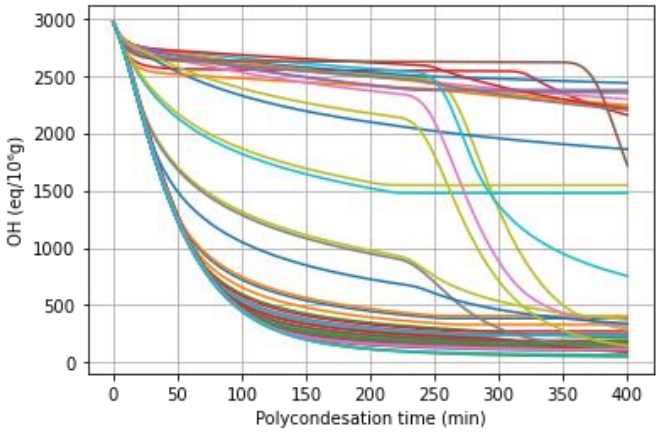

Figure A-13 Hydroxyl end group simulation data

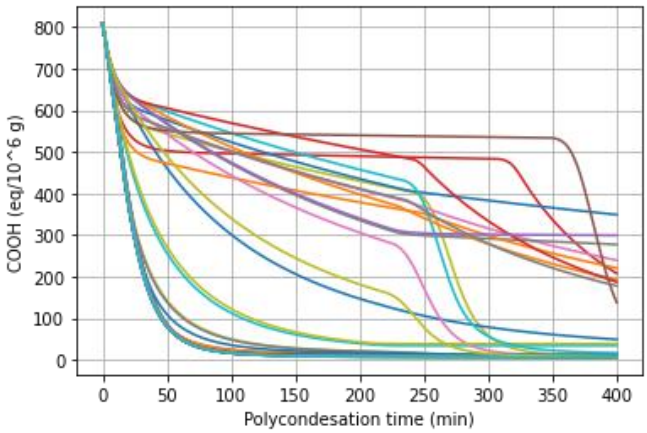

Figure A-14 Carboxyl end group simulation data

doi:10.6342/NTU202302309

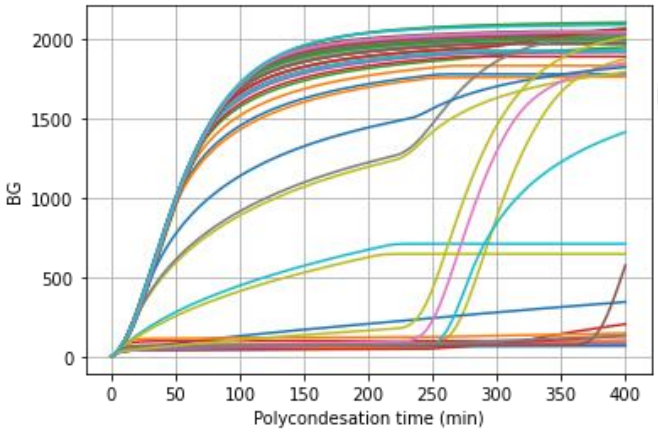

Figure A-15 Butylene glycol simulation data

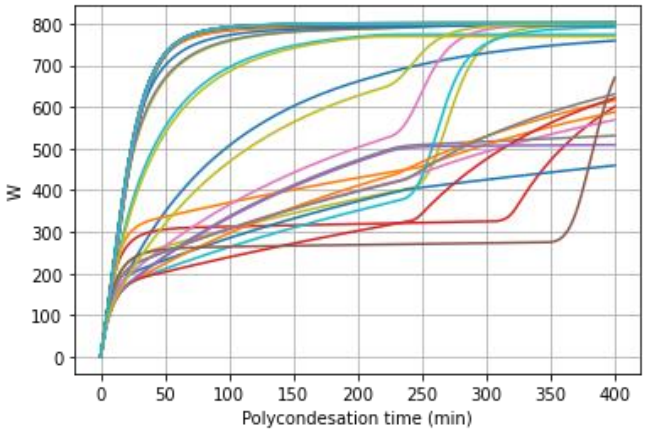

Figure A-16 Water simulation data

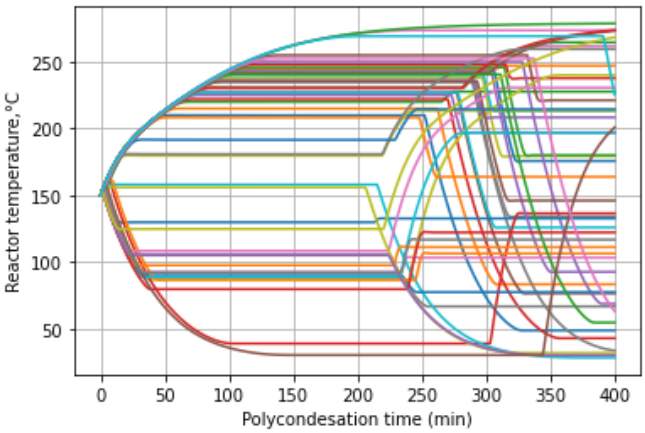

Figure A-17 Reactor temperature of polycondensation process simulation data

doi:10.6342/NTU202302309

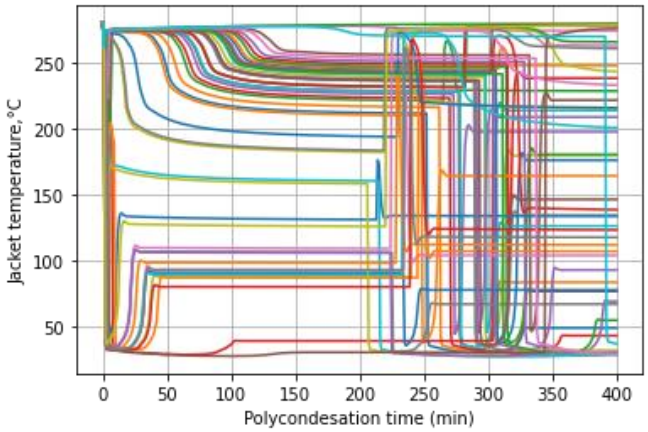

Figure A-18 Jacket temperature of polycondensation simulation data

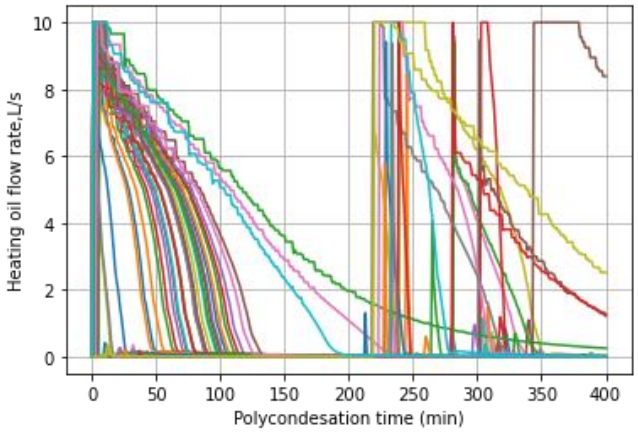

Figure A-19 Heating oil flow rate of polycondensation process simulation data

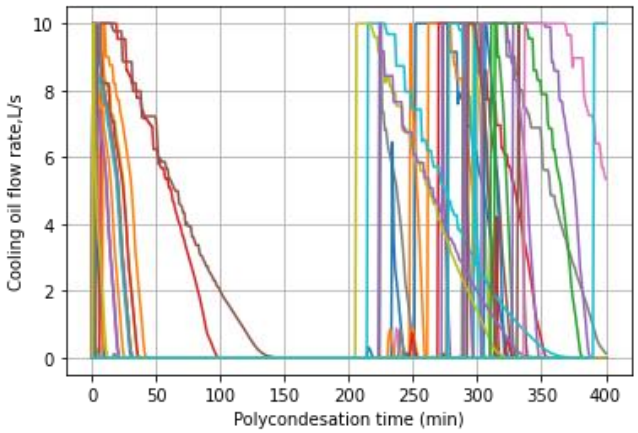

Figure A-20 Cooling oil flow rate of polycondensation process simulation data

doi:10.6342/NTU202302309